

SIMULATION OF THE CHEMICAL ENVIRONMENT
OF A NUCLEAR EXPLOSION BY
EXPLODING WIRE TECHNIQUES

by 45

OLIVER ULFERT JOHN BLOCK
B.S., University of Nebraska, 1965

A MASTER'S THESIS

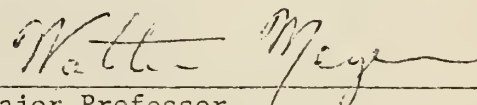
submitted in partial fulfillment of the
requirements for the degree

MASTER OF SCIENCE

Department of Nuclear Engineering
KANSAS STATE UNIVERSITY
Manhattan, Kansas

1969

Approved by:


Major Professor

LD
2648
74
1969
855

CONTENTS

1.0	INTRODUCTION.	1
2.0	LITERATURE SURVEY	3
	2.1 Mechanism of Wire Explosion - Physical Description .	3
	2.2 Parameters Affecting a Wire Explosion.	8
3.0	THEORY.	14
4.0	EXPERIMENTAL.	27
	4.1 Apparatus.	27
	4.2 Calibration Procedure.	30
	4.3 Exploding Wire Measurements.	34
5.0	RESULTS AND DISCUSSION.	41
	5.1 General Considerations of Exploding Wire Results .	41
	5.2 Estimate of Error in Exploding Wire Results.	71
	5.3 Aluminum Wire Results.	78
	5.4 Copper Wire Results.	79
	5.5 Iron Wire Results.	88
	5.6 Nickel-Chromium Wire Results	90
	5.7 Summary of Bare Wire Results	91
	5.8 Results of Wire Explosions in Sample Cell.	96
6.0	CONCLUSIONS.	101
	ACKNOWLEDGEMENTS.	107
	LITERATURE CITED.	108
	APPENDICES.	113
	APPENDIX A: Measurement and Calibration of Circuit Parameters.	113
	APPENDIX B: Description and Explanation of IBM-1410 Computer Program for Calculating Capacitance of Discharge Circuit.	125

CONTENTS (continued)

APPENDIX C:	Description and Explanation of IBM-1410 Computer Program for Calculating Extraneous Circuit Resistance and for Calculating the Calibration of the Current Measuring Circuit.	132
APPENDIX D:	Description and Explanation of IBM-1410 Computer Program for Calibration of the Current Derivative Measuring Circuit	138
APPENDIX E:	Description and Explanation of IBM 360/50 Computer Program for Calculating Physical Quantities Associated with an Exploding Wire.	144
APPENDIX F:	Energy Losses by Conduction and Convection from Exploding Wires	155
APPENDIX G:	Skin Effect and Magnetic Pressure.	159

LIST OF TABLES

I.	Data taken for exploding wires.	36
II.	Calculated experimental results of exploding wires. . .	70
III.	Material properties and energy densities to melt, vaporize, and ionize wire material used for exploding wire experiments.	72
IV.	Maximum estimated temperature of exploding wires. . . .	95
B-1.	Symbols used in the IBM-1410 computer program for calculating capacitance of discharge circuit.	127
C-1.	Symbols used in the IBM-1410 computer program for calculating the extraneous circuit resistance and for calculating the calibration of the current measuring circuit	133
D-1.	Symbols used in the IBM-1410 computer program for calculating the calibration of the current derivative measuring circuit	139
E-1.	Symbols used in the IBM 360/50 computer program for calculating physical quantities associated with an exploding wire.	146
F-1.	Estimates of maximum energy losses from exploding wires by conduction and convection.	158
G-1.	Time intervals at which the ratio of the current at a wire center to the steady state current equals .95 for wires used in this study.	160

LIST OF FIGURES

1.	Curves for typical fast and slow wire explosions. . . .	5
2.	Temperature distributions in a cylindrical thermal spike at various times.	22
3.	Energy per unit length as a function of wire temperature for the first few ionization levels for 10 mil copper, 14 mil iron, and 32 mil aluminum wire.	23
4.	Rate of radiative energy losses from wire as a function of temperature. Product of the emissivity and wire diameter used as a parameter	25
5.	Maximum theoretical power that can be delivered to a constant resistive load from an RLC circuit as a function of potential with which the capacitor is charged. C/L used as a parameter	26
6.	Schematic diagram of measuring circuits	28
7.	Schematic of sample cell geometry.	38
8.	Curves for 32 mil x 1 inch aluminum wire exploded at 8 μ F and 11 kV.	42
9.	Curves for 32 mil x 1 inch aluminum wire exploded at 8 μ F and 15 kV	43
10.	Curves for 20 mil x 1/2 inch copper wire exploded at 8 μ F and 11 kV	44
11.	Curves for 20 mil x 1 inch copper wire exploded at 8 μ F and 11 kV	45
12.	Curves for 20 mil x 2 inch copper wire exploded at 8 μ F and 11 kV	46
13.	Curves for 20 mil x 1/2 inch copper wire exploded at 8 μ F and 15 kV	47
14.	Curves for 20 mil x 1 inch copper wire exploded at 8 μ F and 15 kV	48
15.	Curves for 20 mil x 2 inch copper wire exploded at 8 μ F and 15 kV	49
16.	Curves for 20 mil x 3 inch copper wire exploded at 8 μ F and 15 kV	50

LIST OF FIGURES (Continued)

17.	Curves for 10 mil x 1 inch copper wire exploded at 4 μ F and 11 kV.	51
18.	Curves for 10 mil x 1 inch copper wire exploded at 4 μ F and 15 kV.	52
19.	Curves for 10 mil x 1 inch copper wire exploded at 8 μ F and 8 kV.	53
20.	Curves for 10 mil x 1 inch copper wire exploded at 8 μ F and 11 kV.	54
21.	Curves for 10 mil x 3 inch copper wire exploded at 8 μ F and 11 kV.	55
22.	Curves for 10 mil x 1 inch copper wire exploded at 8 μ F and 15 kV.	56
23.	Curves for 10 mil x 3 inch copper wire exploded at 8 μ F and 15 kV.	57
24.	Curves for 14 mil x 1 inch iron wire exploded at 4 μ F and 11 kV.	58
25.	Curves for 14 mil x 1 inch iron wire exploded at 4 μ F and 15 kV.	59
26.	Curves for 14 mil x 1 inch iron wire exploded at 8 μ F and 8 kV.	60
27.	Curves for 14 mil x 1 inch iron wire exploded at 8 μ F and 11 kV.	61
28.	Curves for 14 mil x 3 inch iron wire exploded at 8 μ F and 11 kV.	62
29.	Curves for 14 mil x 1 inch iron wire exploded at 8 μ F and 15 kV.	63
30.	Curves for 28 mil x 1 inch nickel-chromium wire exploded at 8 μ F and 11 kV.	64
31.	Curves for 28 mil x 1 inch nickel-chromium wire exploded at 8 μ F and 15 kV.	65
32.	Curves for 14 mil x 1 inch iron wire exploded in sample cell geometry at 8 μ F and 11 kV.	66

LIST OF FIGURES (Continued)

33.	Curves for 20 mil x 1 inch copper wire exploded in sample cell geometry at 8 μ F and 11 kV.	67
34.	Peak power as a function of wire length	81
35.	Energy deposition profiles for 20 mil diameter copper wires of various lengths.	82
36.	Deposited energy density for 20 mil diameter copper wires of various lengths.	84
37.	Logic diagram for capacitance of discharge circuit computer program.	131
38.	Logic diagram for extraneous circuit resistance and current calibration computer program.	137
39.	Logic diagram for current derivative calibration computer program.	143
40.	Logic diagram for physical quantities of an exploding wire computer program	154
41.	Sketch of magnetic pinch sample cell.	161

NOMENCLATURE

A	surface area of wire (in. ²)
A _n	vertical distance from zeroline to n th current peak as measured on photographs (in.)
a	defined by $a = -(1/C)$, (farads ⁻¹)
B	defined by $B = R/2L$, (sec ⁻¹)
C _{int}	capacitance of RC integrator used in current measuring circuit (farads)
C _p	heat capacity (joules/gram. ^o K)
c	velocity of light (meters/sec)
E	energy deposited in exploding wire (joules)
E _{co}	initial energy stored in capacitor bank (joules)
E _m	increase in energy density above standard conditions needed to melt wire material (eV/atom)
E _s	estimated integration error by Simpson's rule
E _v	increase in energy density above standard conditions needed to vaporize wire material (eV/atom)
I ₁	energy density required to ionize electrons from wire material (eV/atom)
I	current calibration (kA/photo division)
i	current (kA)
J ₀ (x)	Bessel function of the first kind of order zero
J ₁ (x)	Bessel function of the first kind of order one
K	defined by $K = V_o(C/L)^{1/2}$, (ampere)
K _n	defined by equation (F-11)
k	thermal conductivity (joules/meter·sec. ^o K)
L	inductance of discharge circuit (henries)
P	power (rate of energy deposited in wire), (megawatts)

NOMENCLATURE (continued)

p	pressure (dyne/cm ²)
Q	rate of conductive and convective heat losses from wire (joules/sec)
Q'	energy deposited per unit length of wire (joules/in.)
R	resistance of discharge circuit (ohms)
R_{cal}	calibrating resistance (ohms)
R_e	extraneous circuit resistance (ohms)
R_{int}	resistance of RC integrator used in current measuring circuit (ohms)
R_w	resistance of wire (ohms)
r	radial distance from center of wire (in.)
r_o	radius of wire (in.)
T	absolute temperature (^o K)
t	time (sec)
t_j	time at end of j^{th} time interval after initiation of discharge (sec)
t_m	maximum time interval of interest during a wire explosion (sec)
U	internal energy of exploding wire (joules)
$u(x-x_o)$	unit step function
V_c	voltage on capacitor bank (volts)
V_{L_p}	volt/cm setting on amplifier L_p (see Figure 6)
V_{L_s}	volt/cm setting on amplifier L_s (see Figure 6)
V_o	initial charging voltage on capacitor (volts)
W	hydrodynamic energy of the wire (joules)

NOMENCLATURE (continued)

w_n	weight of n^{th} value (used for averaging)
X_n	defined by equation A-10 (dimensionless ratio)
Y_m	defined by equation A-24 (dimensionless ratio)
y_i	value of function at end of i^{th} time interval
Z	atomic number
z	defined by $z = \ln V(t)$
α	thermal diffusivity ($\text{in.}^2/\text{sec}$)
Δt	time interval between measured points in measuring voltage across calibrated resistor (sec)
ΔU_j	internal energy change at j^{th} transition (joules)
ϵ	emissivity
$\theta(r,t)$	temperature variable defined by equation (F-2)
μ	permeability ($\text{mho}\cdot\text{m}^{-1}$)
π	3.141592654
ρ	density
σ	electrical conductivity ($\text{ohm}^{-1}\cdot\text{m}^{-1}$)
σ	Stefan-Boltzmann constant = $5.7 \times 10^{-5} \text{ erg/sec}\cdot\text{cm}^2\cdot\text{°K}^4$
$\sigma(x)$	estimated standard deviation of single observation for variable x
$\sigma^2(x)$	estimated variance of single observation for variable x
$\sigma(\bar{x})$	estimated standard deviation of mean for variable x
$\sigma^2(\bar{x})$	estimated variance of mean for variable x
τ	period of oscillation of discharge circuit (sec)
ϕ	ratio of current at wire center to steady state current (defined by equation G-1)
ω	frequency, $\omega = (1/LC)^{1/2}$, (sec^{-1})

1.0 Introduction

Exploding wires have been used for many practical purposes as well as being studied because of basic scientific interest in the phenomena itself. Examples of practical applications are high temperature sources for chemical reactions, metal forming explosives, and as initiators of (a) explosive devices, (b) shock waves, and (c) short duration intense light sources. In addition, some research has been aimed at the possibility of initiating a fusion process with an exploding wire.¹

The high energy densities associated with an exploding wire indicate that they could be used to simulate a nuclear explosion. Peaceful applications of nuclear explosions include mining, excavation, energy sources, isotope production, and in contribution to basic scientific knowledge.²⁻⁷ However, the amount and the chemical form of the fallout resulting from a nuclear explosion, even a typical underground shot, prohibits their application as noted above. It is desirable for all applications of nuclear explosions to control the chemical form and the amount of radioactive fallout.

In a typical underground shot experimental evidence indicates that water vapor and radioactive gasses are vented from the cavity between thirty seconds and two minutes after the shot; this is the time interval of interest in simulating the chemical effects so that the radioactive products can be tied up in nonvolatile and insoluble form. Thus, the temperature for the simulation of the chemical environment that determines the volatile products of a nuclear explosion is a few thousand degrees and the pressure is about that of the

static soil load above the shot. It is under these conditions in the environment of the explosion that the chemical nature of the fallout materials is determined. Meyer and Svensson of the Lawrence Radiation Laboratory have shown through experimental work that exploding wires may be used to simulate the pressure and temperature conditions that are important in determining the chemistry of the nuclear explosion.⁸ However, suitable apparatus needs to be developed which will trap the pressure and heat energy released in the wire explosions to do meaningful work.

The objectives of the research reported here were to:

- 1) determine the characteristics of a capacitor bank discharge into an exploding wire including
 - (a) the effect of wire size and composition on energy delivered and the rate of energy delivery.
 - (b) the effect of circuit parameters - capacitance, inductance, and charging voltage.
 - (c) designing of adequate fast switching circuitry.
- 2) determine the amount of energy and rate of deposition of energy needed to produce temperatures and pressures analogous to those of a nuclear explosion.
- 3) design and determine the effect of a sample cell (including magnetic pinch) on the energy density.
- 4) determine the feasibility of simulating the chemical environment of a nuclear explosion by exploding wire techniques.
- 5) compare alternative possibilities for simulating a nuclear explosion.

2.0 Literature Survey

2.1 Mechanism of Wire Explosion - Physical Description

The first paper on exploding wires was read before the Royal Society of London in 1773 by Edward Nairne.¹ At that time equipment was not available for detailed study of the microsecond phenomena. Significant quantitative research on exploding wires was not reported until after 1950, when microsecond measuring techniques were sufficiently developed. The development of these techniques made possible accurate and quantitative measurements of current, voltage, and other factors associated with this high speed phenomenon.

Since 1950 a large amount of interest has developed in exploding wires, sometimes as a means to an end and sometimes for the sake of the phenomena itself. Exploding wires are used in many different fields, some of which are commercial. Thus, although exploding wire phenomena is a relatively new area of quantitative scientific study, there is much information available in the literature on the characteristics of exploding wires.^{9,10}

A complete explanation is not available to describe the exploding wire mechanism. An equation of state is needed but the necessary data are not available to formulate one. It is generally agreed that the explosion of a wire is a complex phenomenon resulting from the deposition of a large amount of energy in a very short period of time (microseconds or less) into a piece of metal of small cross sectional area.

A rapidly increasing current, initially controlled by the RLC

circuit parameters, passes through the wire. After a brief heating interval the wire resistance is much greater than the resistance in the rest of the circuit. The heavy current density ($\approx 10^7$ - 10^{10} A/in.²) heats the wire material to its melting point (See Fig. 1). (The atmospheric melting point is usually taken to be the temperature at which the wire melts.¹¹) The molten wire is heated further by the current which may be increasing or decreasing at this time. To discuss energetic wire explosions (simulating a nuclear explosion), let us consider only the increasing current case (Fig. 1a). Since the entire exploding wire process occurs in microseconds or less the physical shape of the wire is maintained by inertial and magnetic pressures. The wire continues to be heated by the current and reaches the normal boiling point near the current maximum. However, pressure very significantly affects the boiling point and equilibrium boiling is not expected. Superheating occurs as the temperature of the wire rises past the atmospheric boiling point while the wire material is still in the liquid state.

At some time t_B , with the wire temperature above the normal boiling point, the voltage across the wire rapidly increases to a peak value and the wire (wholly or partially in a vapor state) actually explodes. The controlling mechanism near the time of burst is poorly understood, however several mechanisms have been proposed including (1) an expansion process, (2) a shock process, and (3) an explosive phase change. During a wire explosion a considerable amount of noise and an intense flash of light are observed. One or more strong shock fronts are generated during this same time interval.

Conn had proposed the following six steps for the mechanism of a wire explosion.¹²

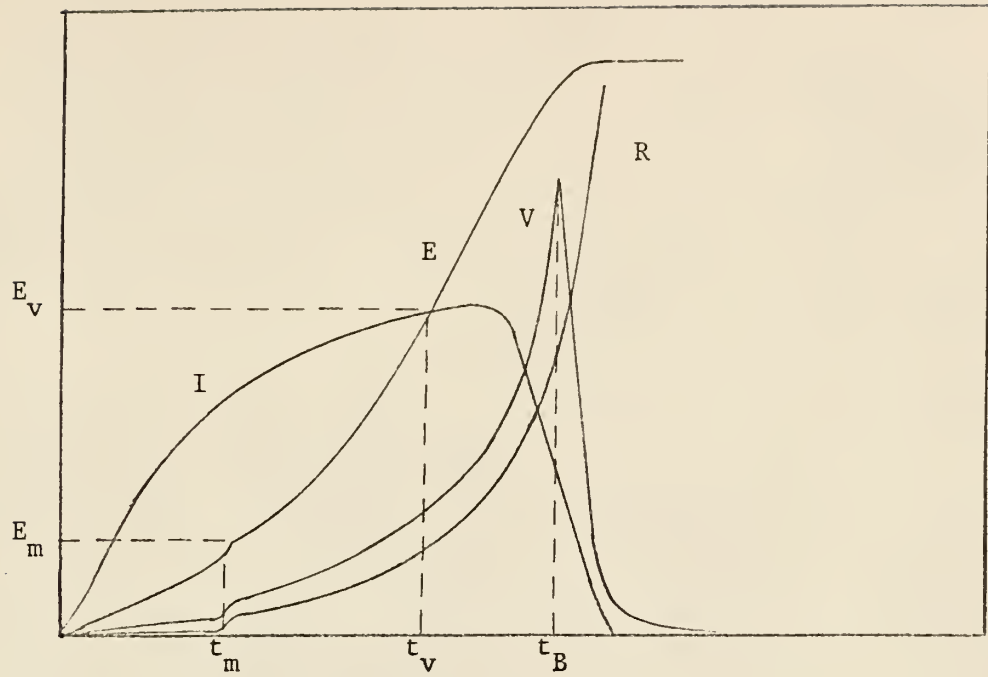


Figure 1a. Fast Wire Explosion

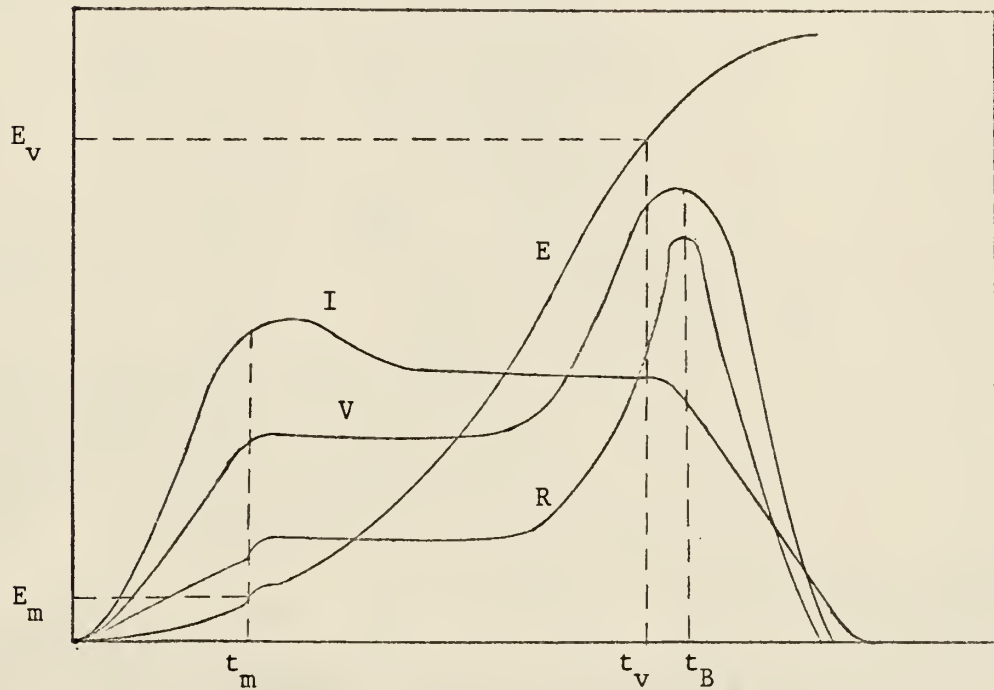


Figure 1b. Slow Wire Explosion

Figure 1. Curves for typical fast and slow wire explosions.

1. Heating of the wire by the heavy current passing through it.
2. Formation of a liquid column of metal replacing the wire.
3. Development of instability in the wire which forms unduloids (figures of rotation) and causes the appearance of striation in the metal vapor.
4. Upon disruption of the arcs formed between the remaining unduloids, the so called 'dark interval' is obtained during which no current flows through the wire, the voltage remaining constant.
5. A sudden flash of light is next observed, the spectrum of which is continuous and independent of the material used. Thereafter emission and absorption lines are observed depending on the materials used.
6. One or several shock fronts are observed during the same time interval.

It is known, however, that certain types of wire explosions exhibit definite deviation from the above behavior. Steps 3 and 4 of Conn's mechanism are strongly dependent on the rate of energy delivery to the wire. Thus it has been suggested by Chace and Levine that rather than describing a general wire explosion as Conn has done it is preferable to classify the explosion based on the rate of energy delivery to the wire. On this basis Chace and Levine have suggested the following four classes of wire explosions: (1) melting, (2) slow explosive, (3) fast explosive, and (4) explosive ablation.¹³ Webb has also classified exploding wires by the rate of energy delivery.¹⁴

The energy deposited in the wire for the melting classification is less than that necessary to vaporize the wire completely. The wire simply behaves as a common fuse by melting and falling apart.

In a slow explosion instabilities have time to develop before sufficient energy to vaporize the wire has been deposited. The explosion occurs slowly enough that these physical distortions affect the mechanism appreciably.

For a fast explosion the energy to vaporize the wire is deposited before significant changes occur in the physical shape of the wire. Unduloids do not form before the wire explodes and thus the explosion mechanism is not affected by physical distortions. If the explosion is fast enough, inertial effects hold the wire in the same physical shape until after enough energy has been deposited to vaporize the wire.

For an explosive ablative type explosion the energy to vaporize the wire is deposited in a very short time interval. In this case the skin effect described by Bennett¹⁵ and the magnetic pressure described by Katzenstein¹⁶ control the explosion mechanism. Appendix G presents a discussion of skin effect and magnetic pressure.

In a slow wire explosion segments of the wire between the unduloids vaporize to produce a rapid rise in resistance.^{14, 17} For a fast explosion an expansion wave proceeds into the center of the wire which also causes a large increase in resistance.¹⁸ The increase in resistance in either case can result in a 'dark interval' during the explosion process. The dense wire vapor is then nonconducting until it has expanded enough for the voltage remaining across the wire to cause breakdown by arcing through the vapor and/or air. If the voltage remaining across the gap when the resistance approaches its peak is large enough the arc breakdown will occur immediately or even before the wire has completely vaporized and no 'dark interval' will be observed. If the voltage remaining across the wire after the first pulse is very low the wire will not become conducting again or in the vernacular of exploding wire technology, there will be no restrike after the onset of current dwell.

2.2 Parameters Affecting a Wire Explosion

Parameters associated with the energy source, the exploding wire, the circuit switch, the transmission lines, and the ambient medium are all important in the mechanism of a wire explosion and in determining the energy deposited in the wire. A capacitor bank is usually used as the energy source but a coaxial cable has been used by a Sandia group.¹⁹ The advantages of the coaxial cable as an energy source are: (1) the current approximates a step function, (2) the discharge circuit equations are algebraic rather than nonlinear differential equations, and (3) the coaxial symmetry provides stabilizing effects on the wire and also provides good frequency response.¹⁹ Since a capacitor bank was readily available and a suitable coaxial cable was not, the capacitor bank was used in this experimental investigation.

The parameters of interest in a capacitor bank energy storage system are the charging voltage and the capacitance. Since the energy stored in a capacitor bank is equal to $1/2 CV^2$, both the charging voltage and the capacitance should be large to obtain the desired energy storage. The internal resistance and inductance of the capacitors should be small in order to produce a fast frequency response as well as to reduce energy loss to a minimum.

Since transmission lines also affect exploding wires, specification of transmission characteristics is necessary to interpret results and to make possible accurate duplication of experiments.²⁰ Therefore, the transmission characteristics should be controlled and specified in each exploding wire experiment. Now if the transmission lines are long the time for energy to propagate from the capacitor bank to the wire can be of the same magnitude as the time for wire explosions and interpretation

of results and accurate reproducibility of wire explosions are not easily obtained. If transmission lines are short (the preferred case), the circuit inductance, resistance, and capacitance can also be treated as lumped parameters. The lumped inductance and circuit capacitance produce a natural 'ringing frequency' response of the system.

Special consideration must be given to the design of the switching circuitry. Large energies (approaching a megajoule) and short delivery times (less than a microsecond) are required. Switches which have been used in exploding wire circuits have been both complex and simple.^{8,21,22} The switch must be able to withstand both the high voltages applied to it and high current pulses flowing through the switch. In addition the rise and jitter times of the switch must be less than a microsecond.

The effect of wire parameters on the wire explosion have been discussed by several people.²³⁻²⁶ It is generally believed that a high intensity short duration energy pulse is better for depositing maximum energy in the wire than a long duration low intensity pulse. However, Zinke et al. suggest that in certain types of wires a relatively slow mechanism may result in high energy densities and high temperatures. In any case the wire parameters must be matched to the circuit parameters to obtain maximum energy deposit.

The wire material and the dimensions of the wire are important in the mechanism and characteristics of a wire explosion. Practical considerations of wire material include ease of attachment, mechanical strength, toxicity, and compatibility with other circuit materials. Intrinsic considerations of the material include resistivity, temperature

coefficient of resistivity, density, specific heat, melting point, boiling point, heat of fusion, heat of vaporization, and ionization energy.

The resistivity of an exploding wire of a given material has been shown to be independent of the current density (up to at least 10^8 A/cm^2) or energy deposition rate up to the energy necessary to melt the wire.²⁷ The measured resistance of an exploding wire agrees with the resistance calculated from tabulated data for temperatures below the vaporization temperature.²⁸ However, the resistance is not a unique function of energy deposited above the vaporization energy of the wire. An increase in the rate of electrical energy deposition results in progressively decreasing slopes of the resistance versus energy curves. The dependence of resistance on the rate of energy deposited is called the 'resistance anomaly'.²⁹ Bennett has shown that an expansion wave, which converts the material behind it into a nonconducting state, can be used to explain the resistance anomaly and the dark interval.¹⁸ The expansion wave proceeds from the wire surface to the wire center; the increase in resistance caused by the expansion wave is characteristic of the resistance anomaly and the dark interval.

Above the melting temperature the resistance increases with the introduction of energy for nearly all metals. At the beginning of melting there is a rapid rise in resistance which is noticeable on the voltage-current traces. In aluminum, copper, and silver wires the resistance increases during the liquid phase with increasing energy deposited. The liquid phase of platinum, tungsten, and iron have small temperature coefficients of resistivity. Thus the liquid phases of exploding wires of platinum, tungsten, and iron are characterized by voltage and current

curves which give a resistance almost independent of temperature.²⁸

Webb et al. in their classification have proposed that metals used for wires fall into two classifications.¹⁴ Low boiling points - low heat of vaporization materials are in class I. High boiling point - high heat of vaporization materials are in class II. Leopold²³ found, in the materials he studied, an approximately constant amount of energy was deposited in the optimum length of wire for each material. If this is true in general, class I materials would be raised to higher temperatures since the excess energy above that required to vaporize the wire would be used to heat the plasma. Also the time required to deposit sufficient energy to vaporize the wire is less for class I materials than for class II materials. With this shorter energy deposit time heat losses by conduction, convection, and radiation would be less for class I materials.

Energy required to ionize the wire material does not increase the temperature of the wire material. Thus, to obtain high temperatures, a wire material which has low numbers of electrons to ionize and low ionization energies is desirable.

Leopold has shown that the dimensions of the wire are important in determining the amount of energy deposited in the wire, the peak power, and the time of burst.²³ Bennett also considered optimum size wires in matching wire resistance to the circuit parameters to obtain maximum energy deposition.²⁵ The time to burst (time interval from initiation of discharge to the voltage peak) decreases with an increase in charging voltage of the capacitor bank, and increases with increasing wire diameter if other parameters are constant. Too thin wires are

poorly matched to the discharge circuit because they explode in short times and use little of the stored energy. If the diameter of the wire is too large, the energy absorbed by the wire will not be sufficient to vaporize the wire. The best time reproducibility is obtained if the wire explodes on the initial portion of the first current pulse. For maximum power and energy deposition the wire should explode near the first current peak (See Fig. 1a).

The power and the energy deposited in the wire also depend on the wire length. There is an optimum length for the maximum energy deposition and peak power. However, the peak power per unit length and the energy density increase with decreasing wire length if end effects are not important.²³

The ambient medium in which a wire explodes has an effect on the behavior of an exploding wire. A striking example is the sensitive dependence of the pause phenomena on the identity or existence of the surrounding gas. The burst spike is flattened and broadened when the wire is confined by tubes which exceed the wire diameter by a factor of up to 3 to 5.³⁰

Energy is rapidly transferred to material surrounding the wire for large temperature differences between the wire plasma and the surrounding medium. If the discharge circuit is designed so that the return current from the wire to the capacitor bank is distributed symmetrically about the wire, the magnetic pinch should confine the wire material for a longer period of time.¹⁶ (Appendix G discusses the effect of magnetic pinch.) Longer confinement times allow the wire to be driven to higher temperatures. Thus, if the magnetic pinch confines the wire material, energy would be transferred more rapidly

to the material surrounding the wire than if the wire material is not confined. Results of Sakurai and Takao indicate that applied axial magnetic fields may confine exploding wires.³¹

Energy is deposited in material surrounding exploding wires during wire explosions. Spectral lines of the confining material have been observed in the emission spectra obtained during the time interval of wire bursts.³⁰ Lower rates of blackbody cooling than expected were observed unless a fairly large amount of deposited energy had been transferred to a more massive body than the wire (such as the surrounding material).³⁰ Thus blackbody cooling at lower rates than expected indicates that energy is deposited in the material surrounding the wire.

3.0 Theory

A quantitative analysis of an exploding wire must consider the electrical circuit, the wire, and the ambient medium. For a capacitor discharge into a wire the electrical circuit can be described by Kirchoff's laws. The law of energy conservation can be used to describe the thermal heating of the wire and the energy losses due to conduction, convection, radiation, hydrodynamic, and other forms of energy.

Assuming the capacitance, the resistance, and the inductance of the circuit can be treated as lumped parameters, the circuit equation can be written as

$$L (di/dt) + R i + V_c = 0 \quad (1)$$

The inductance of the wire (L_w) is much less than the inductance of the remaining discharge circuit (L_c). Therefore, the inductance ($L = L_c + L_w$) is approximately equal to L_c . After a brief heating interval the resistance of the circuit is dominated by the wire resistance. Therefore, R can be considered to be the wire resistance.

The law of energy conservation can be written as

$$(dU/dt) = P - \sigma \epsilon A T^4 - (dW/dt) - Q \quad (2)$$

where:

U is the internal energy in the wire,

P is the rate at which energy is deposited in the wire,

$\sigma \epsilon A T^4$ is the radiative energy losses,

dW/dt is the hydrodynamic energy losses, and

Q is the conductive and convective heat losses.

Thus, the amount of internal energy in the wire depends on the power (i.e., the rate at which energy is deposited in the wire) and the energy losses. At some time after the energy for vaporization has been deposited in the wire the liquid metal expands and forms vapor. It has been estimated that metallic conduction should cease for expansions of 2-5 times.³² With no current flowing there is no power input to the wire. Thus, in a wire explosion it is only the energy added in the short time interval after the wire has exceeded the vaporization temperature and before it begins to expand that is effective in producing extremely high temperatures ($\approx 10^6$ °K). The rate of radiative energy losses at high temperatures is of course very large ($\approx 10^{10}$ watts). Thus, high energy densities and high temperatures in the wire can only be obtained by depositing the energy from the electrical circuit very rapidly (in microseconds or less).

The maximum rate of energy delivery to the wire occurs if the wire is well matched to the circuit parameters. The wire is said to be well matched to the circuit parameters if the short time interval after the wire has exceeded the vaporization temperature and before it begins to expand, occurs near the current peak (See Fig. 1a). Bennett³² has shown that a wire is well matched to the circuit parameters for an optimum mean value of wire resistance which satisfies the relation:

$$1.1 \leq R_{\text{opt}} (C/L)^{1/2} \leq 1.3 . \quad (3)$$

Before the current peak the exploding wire circuit is characterized by a simple RLC circuit and is described by equation (1). During the time period from the start of the discharge until the current peak, the energy which was originally stored in the capacitor bank is trans-

ferred to ohmic heating of the wire and to storage in the circuit inductance. In a well designed exploding wire circuit at the time of the current peak the voltage on the capacitor bank should drop to approximately zero and the energy originally in the capacitor bank should be completely transferred to ohmic heating of the wire and to storage in the magnetic field. Since the voltage on the capacitor bank is approximately zero near the current peak, equation (1) can be approximated by

$$L (di/dt) + R i = 0 . \quad (4)$$

If the wire is well matched to the circuit parameters, the wire material exceeds the vaporization temperature near the current peak at which time the energy stored in the magnetic field is rapidly deposited in the wire. During the time interval when the wire exceeds the vaporization temperature to the time of wire burst, the wire resistance is rapidly increasing. An RL circuit described by equation (4) has a time constant of (L/R) . Therefore since the wire resistance is large just before the wire burst, the energy stored in the magnetic field is rapidly deposited in the wire. Therefore, to obtain high energy densities and high temperatures in an exploding wire it is desirable to have some of the energy stored initially in the capacitor bank used for ohmic heating of the wire, and the majority of the energy from the capacitor bank transferred to the magnetic field of the circuit inductance.

The equations describing the exploding wire circuit could be solved analytically if the resistance, the cross sectional area, and the specific heat of the wire were constant. However, these factors depend on the physical state of the wire, and for wire temperatures above the

vaporization temperature they also depend on the rate of energy delivery to the wire. An equation of state is required for each of the different types of wire explosions if the equations are to be solved to obtain definite results. In addition, solutions of equations require as a corollary a relationship between resistance and the physical state of the wire. Neither an equation of state nor a quantitative relationship for the wire resistance is available. Thus, a combined analytic and experimental approach must be used over limited temperature ranges and limited time intervals to solve the equations.

The wire resistance is calculated using the relation

$$R_w = \frac{V_w - L_w (di/dt)}{i} \quad (5)$$

where:

R_w is the wire resistance,

V_w is the voltage across the wire,

L_w is the inductance of the wire,

i is the current through the wire, and

(di/dt) is the time rate of change of current.

V_w , i , and (di/dt) are measured experimentally. L_w can be calculated from the physical properties of the wire.³³

The energy deposited in the wire material at any time t after the start of the discharge of the capacitor bank can be computed by integrating the instantaneous power over the time interval from the start of the discharge until time t .

$$E_w = \int_0^t R_w i^2 dt' \quad (6)$$

Assuming the inductance of the wire is constant and substituting equation (5) into equation (6) gives

$$E_w = \left(\int_0^t V_w i \, dt' \right) - 1/2 L_w i^2(t) . \quad (7)$$

Thus, the energy placed in the wire can be computed by integrating the product of the voltage and current, and subtracting the energy stored in the inductance of the wire gap at time t .

The internal energy of the wire is related to the temperature of the wire by the relation.

$$\int_{U(T_o)}^{U(T)} dU' = \sum_{j=1}^n \left[\lim_{\delta \rightarrow 0} \int_{T_{j-1}+\delta}^{T_j-\delta} (dU'/dT) \, dT + \Delta U_j u(T-T_j) \right] + \left[\lim_{\delta \rightarrow 0} \int_{T_n+\delta}^T (dU'/dT) \, dT \right] \quad (8)$$

where:

T_o is the initial temperature of the wire,

T_j ; $j=1,2,\dots, n$ are transition temperatures,

$U(T)$ is the internal energy and is a function of temperature,

ΔU_j is the internal energy change at the j^{th} transition, and

$u(T-T_j)$ is the unit step function.

An upper limit of the temperature reached by an exploding wire can be determined by equating the energy deposited in the wire with the change in internal energy of the wire. The energy deposited in the wire can be computed using equation (7). Substitution of this calculated energy into equation (8) permits a determination of the upper temperature limit. (This upper limit is calculated assuming no energy losses in equation (2).)

If radiation losses are considered in equation (2), another

estimate of the maximum possible wire temperature is obtained. For a fast wire explosion the energy is "dumped" in the wire in less time than the instability time constant. Since the maximum temperature is reached before the wire has expanded, the hydrodynamic losses (dW/dt) are negligible. However, at extremely high temperatures the radiation energy losses are much greater than the conductive and convective energy losses (See Appendix F). Thus when large amounts of energy are deposited in fast wire explosions, high temperatures are produced. For such explosions, equation (2) can be approximated by

$$(dU/dt) = P - \epsilon \sigma A T^4 . \quad (9)$$

The maximum internal energy and the maximum temperature are reached when the rate of change of internal energy is zero ($dU/dt = 0$). Thus, from equation (9) the maximum power is

$$P_{\max} = \epsilon \sigma A T_{\max}^4 . \quad (10)$$

Thus, to obtain high temperatures in an exploding wire it is necessary to have high peak powers and small radiating areas. An estimate of the maximum power, P_{\max} , delivered to a constant resistive load from an RLC circuit is ³⁴

$$P_{\max} = (V_o^2/2)(C/L)^{1/2} . \quad (11)$$

Substituting equation (11) into equation (10) and solving for T_{\max} gives

$$T_{\max} = [(C/L)^{1/2} (V_o^2/2 \epsilon \sigma A)]^{1/4} . \quad (12)$$

Therefore, to obtain high temperatures in an exploding wire, it is necessary to have high initial charging voltage on the capacitor,

appreciable capacitance, and low inductance.

To study the high temperature chemistry of the material surrounding an exploding wire, it is necessary to transfer the energy from the wire to the surrounding material. Little energy is lost from the wire material by any method other than radiation until after the wire bursts, and little energy is deposited in the wire after about one microsecond following the wire explosion. If energy is deposited instantaneously along a line, a thermal spike may be used to represent the system. Thus, the energy deposited in a system consisting of a thin central wire and a low thermal conductivity surrounding medium, e.g., earth, can be represented by a thermal spike. If Q' is the energy released per unit length of wire, the temperature distribution in the surrounding medium is as follows³⁵

$$T(r,t) = T_o + (Q'/4\pi C_p \rho)(1/\alpha t) \exp(-r^2/4\alpha t) \quad (13)$$

where:

$T(r,t)$ is the time dependent temperature distribution,

T_o is the temperature before energy is deposited,

C_p is the heat capacity of the surrounding material,

ρ is the density of the surrounding material, and

α is the thermal diffusivity of the surrounding material.

Thus, the time dependent temperature distribution is just a function of Q' and the physical properties of the surrounding material.

Typically, materials such as those in the earth's crust have small thermal conductivities. Therefore, essentially all of the energy would be deposited in a wire surrounded by earth before any energy would be conducted into the surrounding material. Hence, the thermal

spike can be used to predict the time dependent temperature distribution in a sample of earth's crust surrounding an exploding wire.

The temperature or the energy density necessary to study high temperature chemistry or the formation of a cavity in a sample material is usually known or can be estimated. Knowing the temperature necessary to achieve the desired effect, the necessary parameters of the system can be estimated as follows.

1) Calculate the energy which must be deposited in the wire to raise the desired amount of sample material to the desired temperature. To complete this calculation handbook or estimated values of thermal diffusivity, density, and heat capacity for the sample material are used in equation (13). Typical results are shown in Fig. 2.

2) Calculate, using equation (8), the wire temperature at which the wire material will contain the energy calculated in step (1). Handbook values of the physical properties are used for the calculation when they are available. For the extremely high temperatures typical of wire explosions, the specific heat and latent heats must usually be estimated since they are considerably beyond handbook values. The results shown in Figure 3 were calculated assuming an ideal plasma gas and that the i^{th} electron was ionized from each atom when the kinetic energy ($3kT/2$) of the gas particles was equal to the ionization energy I_i , $i = 1, 2, \dots, Z$. Ionization energies tabulated by Moore³⁶ were used for the calculations. (Rouse has calculated more accurate results by using the Saha equation.³⁷)

3) Determine the rate of energy input to the wire (power) which will balance the radiation losses from the wire at the necessary wire temperature. The power corresponding to a given temperature can be cal-

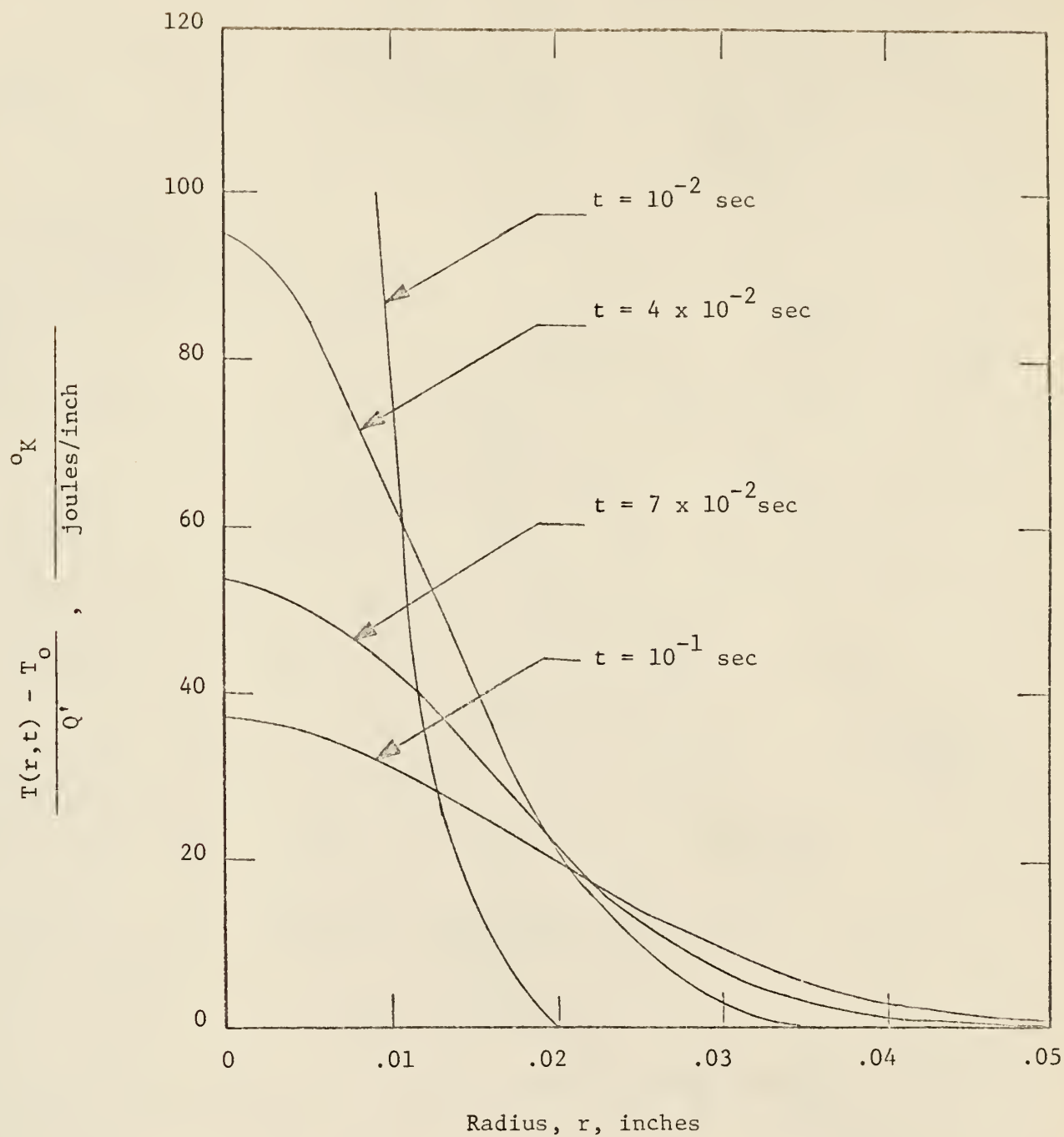


Figure 2. Temperature distributions in a cylindrical thermal spike at various times. Parameters typical of the earth crust were used. $C_p = .2 \text{ cal/g} \cdot ^\circ\text{K}$; $k = .005 \text{ cal/sec} \cdot \text{cm} \cdot ^\circ\text{K}$; $\rho = 2.24 \text{ g/cm}^3$.

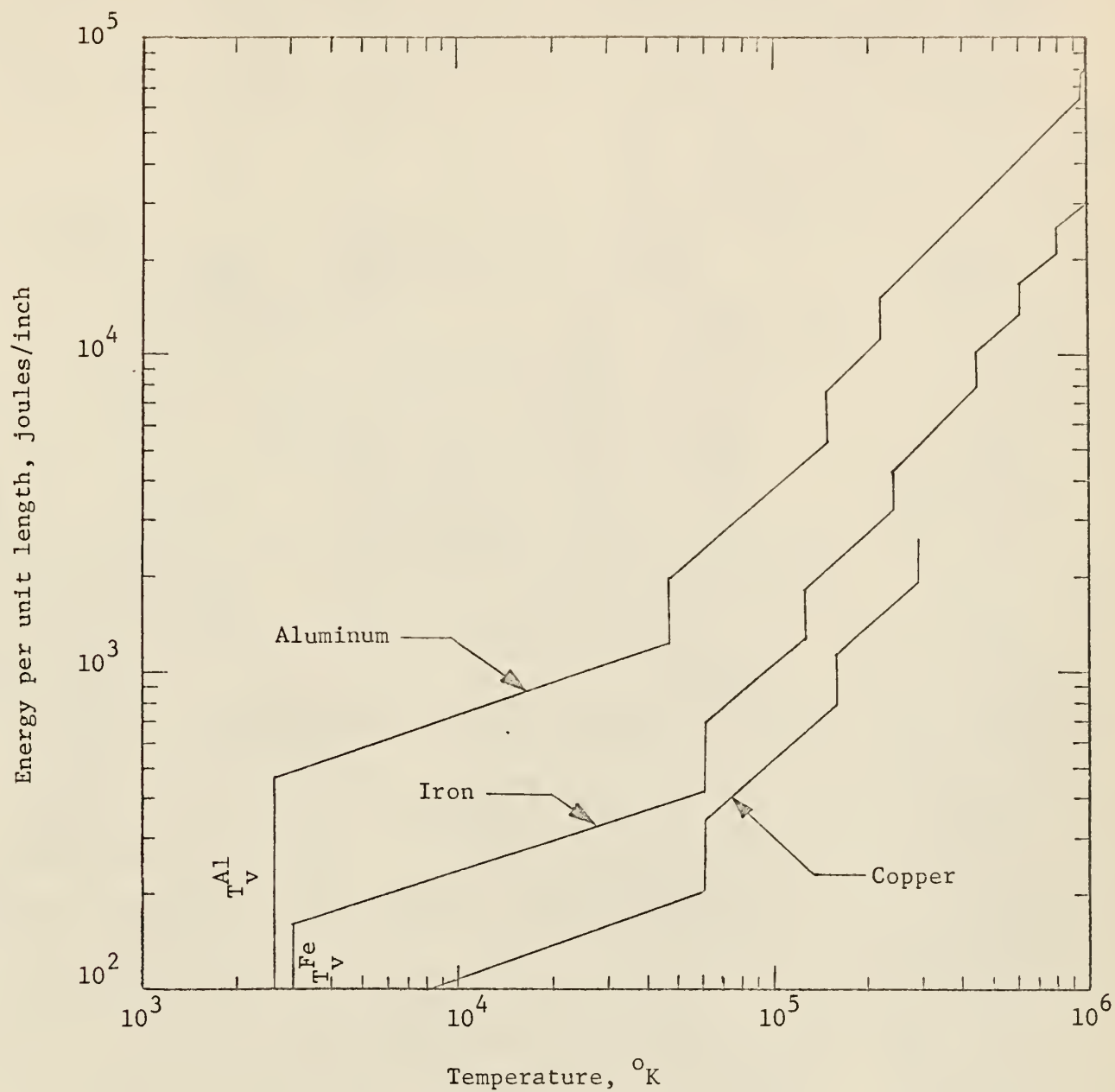


Figure 3. Energy per unit length as a function of wire temperature the first few ionization levels for 10 mil copper, 14 mil iron and 32 mil aluminum wire.

culated using equation (10); typical results are shown in Fig. 4. (The product of the wire diameter and the emissivity of the wire material is used as a parameter.)

4) Determine the electrical circuit parameters necessary to obtain the power calculated in step (3). The maximum theoretical power available from an RLC network to a constant resistive load can be estimated using equation (11). Figure 5 shows the estimated maximum theoretical power available from an RLC network as a function of charging voltage with (C/L) as a parameter. This maximum power is available to an exploding wire if the wire is well matched to the circuit parameters. In determining the electrical circuit parameters, it is necessary that the initial energy stored by the capacitor bank ($E_{co} = 1/2 CV_o^2$) be greater than the energy calculated in step (1).

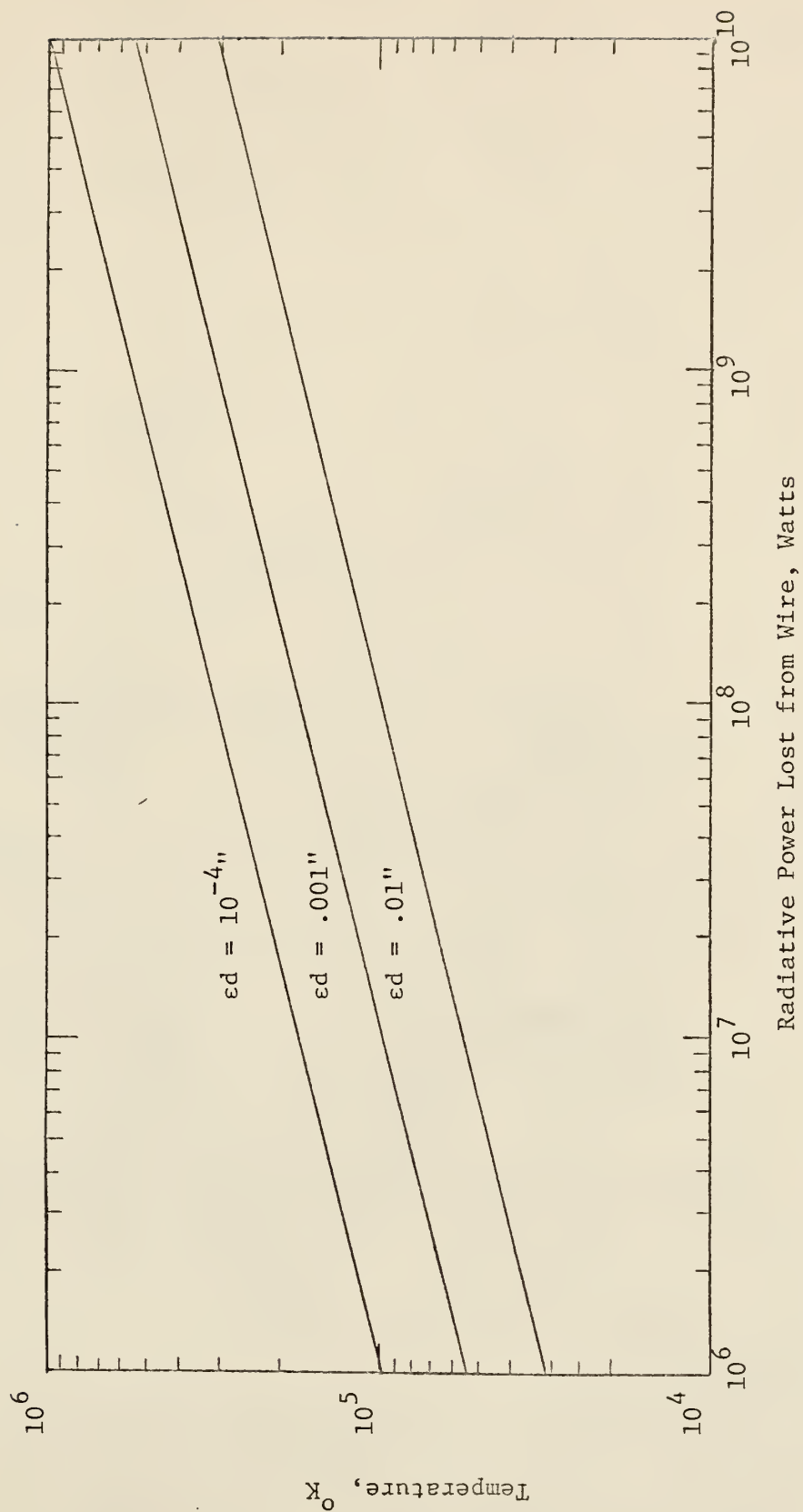
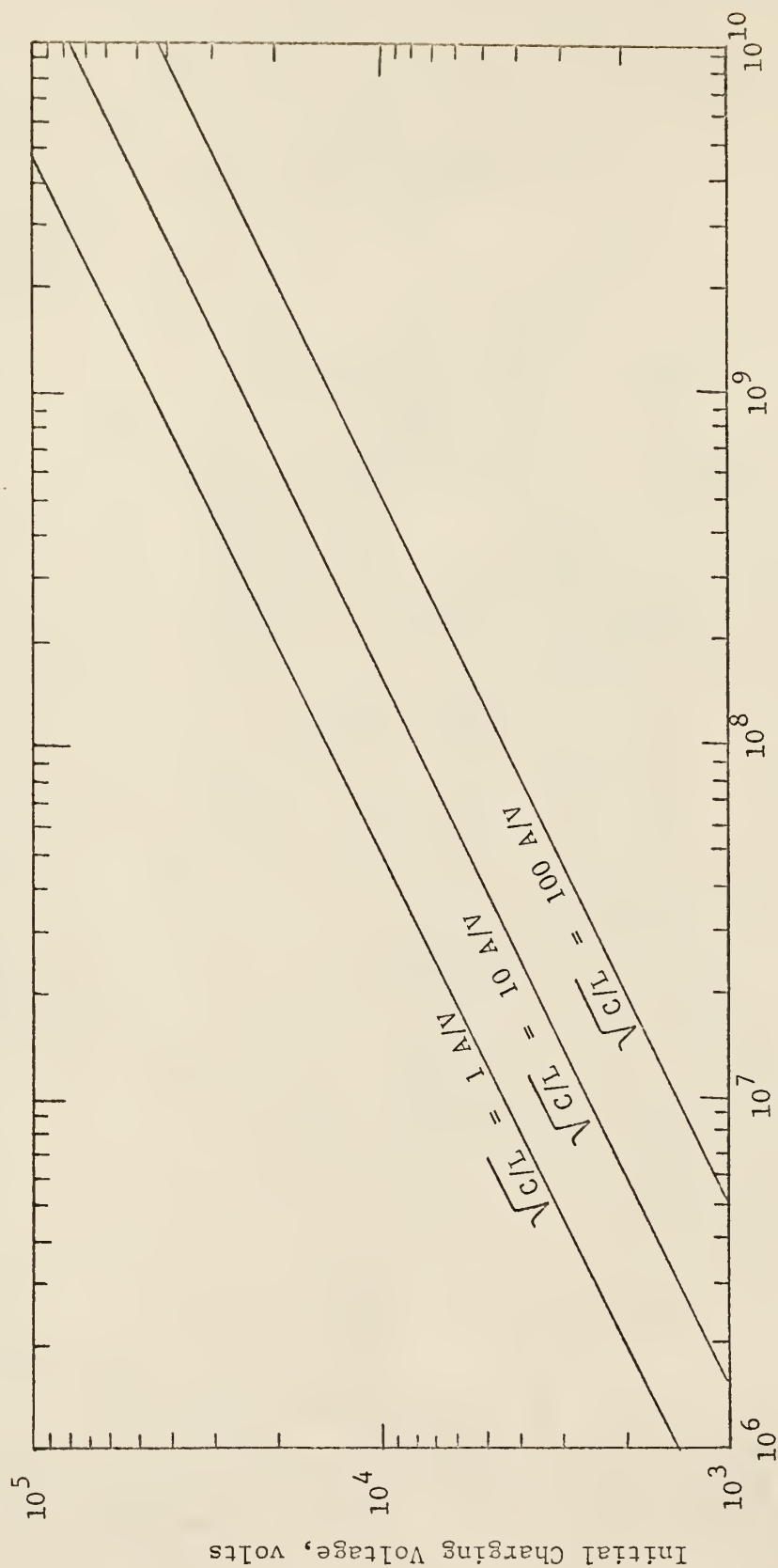


Figure 4. Rate of radiative energy losses from wire as a function of temperature. Product of the emissivity and wire diameter used as a parameter.



Maximum Theoretical Power from Capacitor, watts

Figure 5. Maximum theoretical power that can be delivered to a constant resistive load from an RLC circuit as a function of potential to which the capacitor is charged. C/L used as a parameter.

4.0 Experimental

4.1 Apparatus

A schematic diagram of the discharge circuit, the voltage measuring circuit, and the current measuring circuit is shown in Fig. 6. The discharge circuit consisted of the specimen wire, the air-gap switch, the capacitor bank, the transmission lines, and the high voltage power supply. The capacitor bank consisted of 8 capacitors (General Electric - Pyranol) of nominal 1 microfarad capacitance and a maximum charging voltage of 25 kilovolts.

The air-gap switch was similar to the one described by Harvey and Yevick.²² (Nichrome wire was used as the trigger electrode, which differs from the molybdenum wire used by Harvey and Yevick.) Harvey and Yevick give the following characteristics of their spark gap switch: operational voltage range - 20-35 kV, peak operational current - 100 kA at 500 kHz, maximum peak current - greater than 200 kA, closing and jitter times - less than 0.1 μ sec, and switch inductance - 50 nH with parallel plate return path. During an experiment after the high voltage power supply (North American Philips Co., Inc. - X-ray Supply Unit) had been used to charge the capacitors, the power supply was disconnected from the basic discharge circuit. The power supply was then used to supply a voltage pulse to the trigger electrode of the air-gap switch. This voltage pulse, applied through small blocking capacitors, rendered the air-gap conducting and initiated the discharge of the capacitor bank through the wire. (The capacitor bank and x-ray supply unit were borrowed from the KSU Physics Department.)

Massive brass and aluminum leads were used as transmission lines

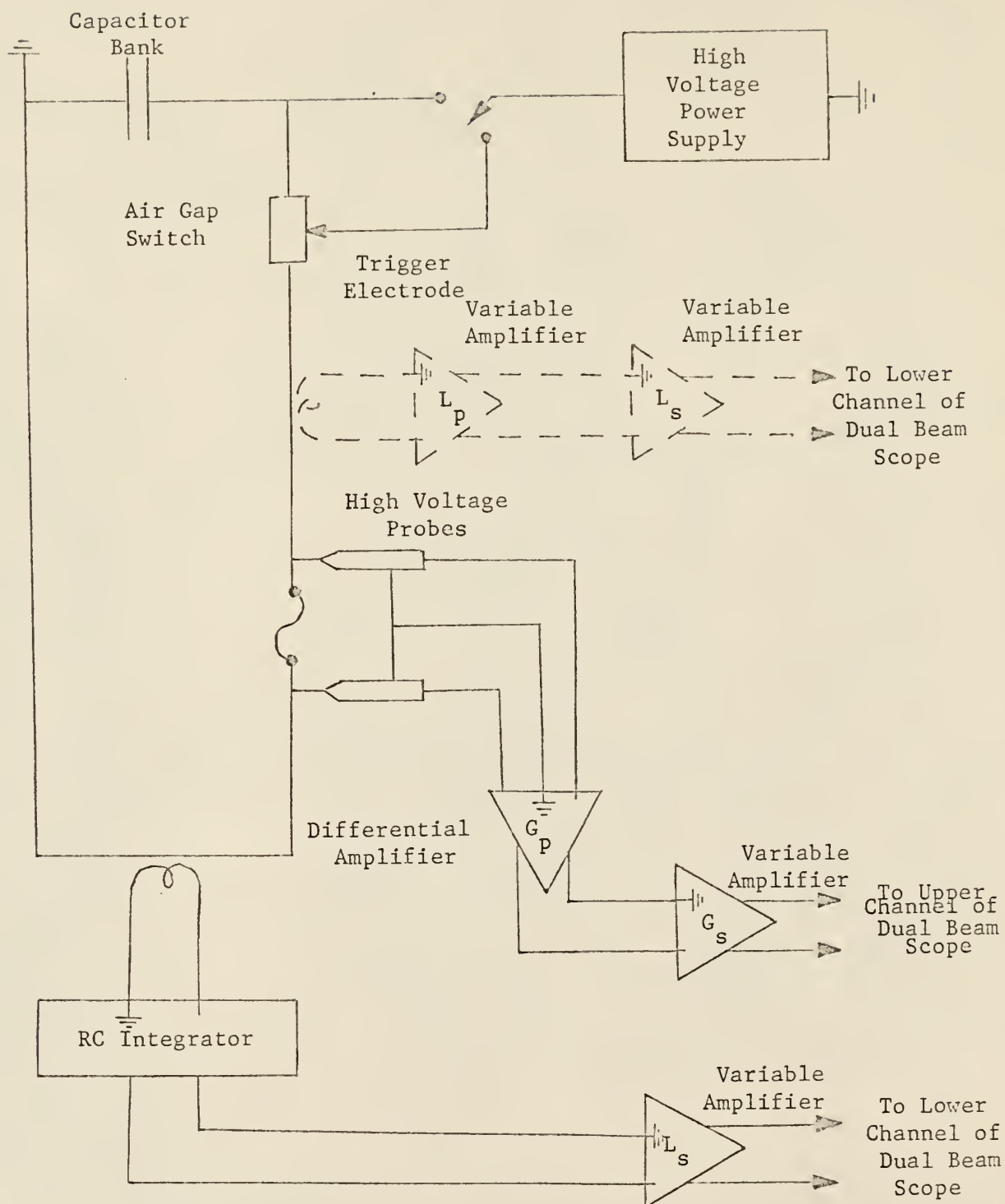


Figure 6. Schematic diagram of measuring circuits.

to keep the extraneous circuit resistance and inductance low. Specimen wires were placed in small holes, drilled in the ends of 5/16" diameter leads; the wires were fastened securely to the leads with set screws.

The circuits used to measure the voltage across the wire and the current through the wire are shown schematically in Fig. 6. The characteristics of the scope and plug in amplifiers obtained from the Tektronix manuals showed that the frequency response of the scope and plug in amplifiers was adequate in the range from DC to 18 MHz and the risetime was 20 nsec. High voltage probes used in this study (Tektronix P6013) had a maximum peak pulse limit of 12 kV below 100 kHz and a risetime of 14 nsec. It should be noted that the voltage measuring circuits ground had no physical connection with the discharge circuit. Operating under this condition, ground loops in the voltage measuring circuit were prevented. The high voltage probes were attached to the brass leads close to the wire. The signals from the high voltage probes were then led to the input terminals of a differential amplifier G_p (Tektronix type G) powered by channel one of a P-127 Tektronix power supply. The output of channel one of the power supply was then applied to amplifier G_s (Tektronix type G) which was used as a variable gain amplifier. Amplifier G_s was in the upper channel of a dual-beam oscilloscope (Tektronix type 551).

The current was measured using a small coil placed near a current lead of the discharge circuit. The voltage induced in this coil was proportional to the time derivative of the current through the lead. The voltage signal from the coil was integrated by a simple RC integrating network with a time constant ($RC = 5$ microseconds) large with respect to the most rapid oscillation. The integrated signal, which was pro-

portional to the current in the discharge circuit, was amplified by amplifier L_s (Tektronix type L) placed in the lower channel of a dual beam scope.

The time derivative of the current was measured using a separate pickup coil. The voltage on the coil was attenuated by amplifier L_p in the second channel of the P-127 power supply. The output of channel two was then applied to amplifier L_s which was in the lower channel of the dual beam scope.

Oscilloscope curves of either voltage and current or voltage and current derivative were measured simultaneously. Note that amplifier L_s was used in both the current measuring circuit and the current derivative measuring circuit. The curves were recorded on 3000 speed/type 47 Polaroid film. A Hewlett-Packard oscilloscope camera (Model 196A) was used to take the photographs. The instantaneous values of voltage, current, and current derivative waveforms were determined from the photographs. A Leitz Coordinate Comparator, available in the Applied Mechanics Department, was used to measure distances on the photographs. The current and current derivative were related to the same time base by aligning prominent voltage peaks or discontinuities of the separate voltage records.

4.2 Calibration Procedure

The parameters of interest in an exploding wire experiment have been discussed in Section 2.0; the power and the energy deposited in the wire were the parameters of specific interest in this study. The power and the energy were calculated with the equations in Section 3.0 using measured values of voltage, current and current derivative. Be-

fore taking the necessary exploding wire data, the measuring circuits were calibrated and the effect of the air-gap switch determined. The experimental sequence was as follows:

- 1) The voltage measuring circuit and the static voltmeter were calibrated.
- 2) The circuit capacitance was measured.
- 3) The circuit inductance and resistance were measured.
- 4) The current measuring circuit was calibrated.
- 5) The effect of the air-gap switch was determined.
- 6) The current derivative measuring circuit was calibrated.

The vertical deflection of the oscilloscope photographic records for the voltage measuring circuit was calibrated using two high voltage power supplies in series (Fluke, Model 412B and Fluke, Model 400BDA). The maximum available calibration voltage was 7 kilovolts. The Fluke power supplies had been previously calibrated using a digital voltmeter (Electronic Associates, Inc. TDVM 5001). The deviation of the vertical deflection of the voltage measuring circuit was within the reading accuracy of the oscilloscope traces for each combination of amplifier settings (G_p and G_s) used in succeeding measurements. The oscilloscope was then used to calibrate the electrostatic voltmeter (Sensitive Research Instrument Corporation, Model ESH) used to measure the charging voltage on the capacitor bank. The fractional standard deviation of the electrostatic voltmeter was .011 volts per volt.

The capacitor bank with either eight or four capacitors in parallel was used to explode wires. The capacitance of each combination was determined by measurements of voltage-time oscillograms obtained by discharging the capacitor bank through calibrated resistors. The calibrated

resistors were placed in the location which was used for the specimen wires. The detailed procedure used in measuring and calculating the capacitance is given in Appendix A. The following values were calculated for the capacitance at an initial charging voltage of 8 kilovolts.

<u>Number of</u> <u>Capacitors</u>	<u>Total Capacitance</u> <u>(microfarads)</u>
4	3.587 \pm .042
8	7.712 \pm .051

The extraneous resistance (resistance of the circuit with no wire resistance) and the circuit inductance were determined by placing a heavy shorting bar (5/16" diameter brass rod) in the position of the specimen wire. Photographic records of the current through the circuit and the voltage on the capacitor bank were obtained. These records were measured using the Leitz Coordinate Comparator. From these measurements the inductance and the extraneous circuit resistance were calculated using the equations of an underdamped RLC circuit (See Appendix A). The same records were used to calibrate the vertical deflection on the oscilloscope records for the current measuring circuit as described in Appendix A. The pickup coil which measured current through the discharge circuit was placed near a lead of the discharge circuit. After calibration, this pickup coil of the current measuring circuit was fixed in position.

The vertical deflection of the current derivative measuring circuit on the oscilloscope traces was also calibrated with the shorting bar in place. Underdamped RLC circuit equations similar to the current waveform calibration were used for the calibration of the current

derivative waveform (See Appendix A).

The effect of the air-gap switch was determined by measuring the circuit resistance. Initial charging voltages of 5, 8, 11, and 15 kilovolts on the capacitors were used. The distance of the air-gap switch was also varied, the extraneous circuit resistance increasing with an increase in the air-gap distance for constant initial voltage. The circuit resistance decreased for the same air-gap setting with an increase in initial charging voltage. Variation in circuit resistance due to atmospheric conditions was of the same order of magnitude as the variation due to the switch setting. Since the circuit resistance was small (~ 0.035 ohms) compared to the wire resistance (except for a short time interval after the initiation of the discharge) neither the air-gap setting nor atmospheric conditions significantly affected the circuit resistance during the explosion of the wire.

Moses and Korneff³⁸ have suggested that induced voltage in the high voltage probes may contribute significantly to the voltage measurements. This was checked by shorting the tips of the high voltage probes together with a shorting bar. The probes were then placed near their actual position when measuring the voltage across a wire, and a wire was exploded. (The probes had no physical connection with the discharge circuit while checking for induced voltages.) It was determined that the induced voltage was not significant. However, the position of the oscilloscope with respect to the discharge circuit was important. If the scope was close to the discharge circuit, significant induced voltages were noted. Thus, for exploding wire measurements the scope was positioned so that stray signals were not monitored.

4.3 Exploding Wire Measurements

Voltage, current, and current derivative were measured for bare wires exploded at atmospheric conditions. The calibrated circuits shown in Fig. 6 were used for the measurements. The wire material, wire size, circuit capacitance, and circuit charging voltage were varied. Table I shows the wire and circuit parameters used in this study. The experimental sequence used to obtain exploding wire data was as follows:

- 1) A wire of interest was inserted in the holes in the ends of the brass leads and fastened securely with set screws. The brass leads with high voltage probes attached were then adjusted so the wire was straight between the leads.
- 2) Leads to amplifier L_s were attached for either the current measuring circuit or the current derivative measuring circuit. The vertical scale of the voltage measuring circuit and the vertical scale of either current or current derivative circuit were set to desired values. The time scale on the oscilloscope was set to a desired value. The scope was set for single sweep operation. (Scale settings were determined by a trial procedure until the magnitudes of a particular wire explosion were determined.)
- 3) The safety ground on the capacitor bank was disconnected and the capacitor bank was charged to the desired voltage using the high voltage power supply. (If the capacitor bank discharged through the switch before reaching the desired voltage, the electrodes of the air-gap switch were set farther apart.)
- 4) The camera shutter was opened for a time exposure.
- 5) Circuit discharge was initiated by a voltage pulse to the trigger

electrode of the air-gap switch. (If the capacitor bank did not discharge through the switch when a voltage pulse was applied, the capacitor bank was grounded and the switch air-gap distance was decreased.) The scope was triggered by the signal from the voltage measuring circuit.

- 6) The safety ground was allowed to spring back and ground the capacitor bank. The safety ground prevented a charge from remaining or accumulating on the capacitor bank.
- 7) The oscilloscope was retriggered to obtain a zeroline reference for each photograph.
- 8) The camera shutter was closed.
- 9) Portions of the wire still connected to brass leads were removed.
- 10) The camera film was developed if desired. (More than one set of traces were obtained on one picture by adjusting the multiple picture knob on the camera.)

The consistency of results was determined by exploding eleven standard wires on two successive days. The wire and circuit parameters were not varied for the standard wire explosions. Iron wire 14 mils in diameter and one inch long was used as the standard. Circuit conditions used for the standard wire were 8 microfarads and 11 kilovolts. The following values were calculated for the standard wire explosions (The error limits reported are estimated standard deviations for single observations.):

Table I. Data taken for exploding wires

Wire Parameters			Circuit Parameters*	
Wire Material	Wire Size		Capacitance (μ F)	Voltage (kV)
	Diameter (in.)	Length (in.)		
(Wires exploded at ambient atmospheric conditions)				
Aluminum	.032	1	8	11
Aluminum	.032	1	8	15
Copper	.010	1	4	11
Copper	.010	1	4	15
Copper	.010	1	8	8
Copper	.010	1,3	8	11
Copper	.010	1,3	8	15
Copper	.020	1/2,1,2	8	11
Copper	.020	1/2,1,2,3	8	15
Iron	.014	1	4	11
Iron	.014	1	4	15
Iron	.014	1	8	8
Iron	.014	1,3	8	11
Iron	.014	1	8	15
Nickel-Chromium	.028	1	8	11
Nickel-Chromium	.028	1	8	15
(Wires exploded in sample cell geometry)				
Copper	.010	1	8	11
Copper	.020	1	8	11
Iron	.014	1	8	11

*Circuit inductance for all cases was 1.33 microhenrys.

Time to burst	$3.04 \pm .22$ microseconds,
Peak Voltage	$12.91 \pm .55$ kilovolts,
Peak Resistance	$1.90 \pm .21$ ohms,
Peak Power	$91. \pm 11.$ megawatts, and
Energy Deposited	$119. \pm 15.$ joules.

Data for other experiments conducted at ambient atmospheric conditions as listed in Table I were then measured. For each set of conditions listed in Table I a minimum of two sets of voltage-current curves and one set of voltage-current derivative curves were determined (3 wire explosions). The records taken with the oscilloscope camera were measured using the coordinate comparator. To determine if the discharge and measuring circuits were operating consistently a standard wire was exploded periodically.

After analyzing the bare wire results data were obtained for wires exploded in the sample cell geometry. The experimental sequence used for wires exploded in the sample cell geometry was the same as for the bare wires except the sample cell was included in the discharge circuit. Figure 7 shows a drawing of the cross-section of the sample cell. (As noted earlier this cell can be used to hold material in close proximity around the wire during the explosion and as discussed in Section 2.0 the ambient medium has an effect on exploding wire characteristics.) The sample cell was designed to use the magnetic pinch principle. Since the return current from the wire to the capacitor bank was symmetrical about the wire, magnetic pressure tended to confine the wire material after vaporization (See Appendix G). Longer confinement times should result in more energy deposition in the wires;

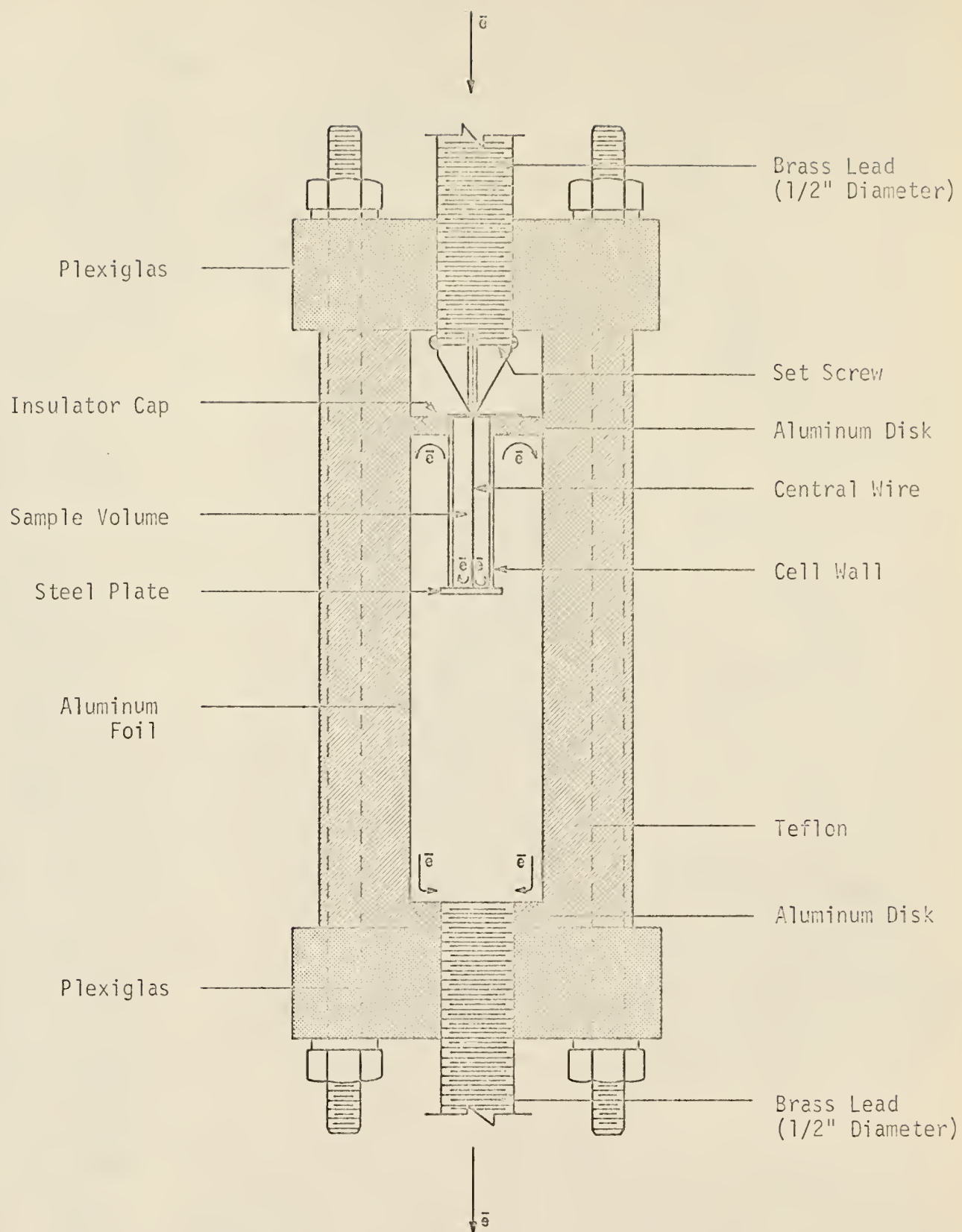


Figure 7. Schematic of Sample Cell Geometry

the attainment of high energy depositions and consequently high temperatures was an objective of this research.

Since voltages in the kilovolt range were used for wire explosions in the sample cell, voltage breakdown or arcing tended to occur between points of the current path in the sample cell. This voltage breakdown allowed the current to short circuit. Therefore, the pointed brass lead and the outside of the cell were covered with electrical tape to prevent arcing; in addition an insulator cap was used to prevent arcing from the brass lead to the cell wall. Three mylar disks, each .010 inch thick, made up the insulator cap.

Several materials (mylar, mica, polyethylene, plexiglas, teflon, and compressed CaCO_3) were tested for use as an insulator cap. However, the energy density and pressure of the wire explosions either melted or shattered all tested materials except mylar. The melting or shattering of the insulator cap resulted in arcing from the brass lead to the cell wall and thus if the insulator cap melted or shattered before the time of burst, the amount of energy deposited in the wire was significantly reduced. Since maximizing the energy trapped in the material surrounding the wire was of interest, the melting or shattering of the insulator cap after the time of burst was also undesirable.

One inch long stainless steel tubes were used for the sample cell walls. The inside diameter of the tubes used were 1/16", 1/8", and 3/8". To provide insulation between the wire and the cell wall, a silicon based caulk was placed in the sample volume and allowed to dry at atmospheric conditions. If sufficiently high temperatures had been produced by the wire, the silicon caulk would also have simulated an environment of sand around an underground nuclear explosion. The resid-

ual acetone, after drying the caulk at atmospheric conditions, would have simulated hydrocarbon vapor formed after a nuclear explosion. The caulk, however, was insufficient insulation to prevent arcing from the central wire to the cell wall for the two smaller diameter tubes. Thus, only the 3/8" diameter tube was used for the sample cell measurements.

Analysis of the wire explosions at atmospheric conditions showed that the two sizes of copper wire and the iron wire were better matched to the circuit parameters than the other wires noted in Table I. Therefore, these wires were exploded in the sample cell geometry. The wire and circuit parameters used for the sample cell explosions are also listed in Table I.

5.0 Results and Discussion

5.1 General Considerations of Exploding Wire Results

The parameters which significantly affect the results of an exploding wire experiment are discussed in Section 2.0. Table I lists the values of parameters used in exploding wire experiments conducted during the course of this study. (Wire material, wire diameter, wire length, ambient environment, circuit capacitance, and circuit charging voltage were the parameters varied.) Equations developed in Section 3.0 were used to calculate the quantities of interest for the analysis of the exploding wire data; the details of the calculations are given in Appendix E. Figures 8 through 33 show voltage, current, resistance, power, and energy as functions of time for the parameters listed in Table I. Error bars were determined but were not indicated on the already complex graphs. (Errors are discussed in Section 5.2.)

The characteristics of the voltage, current, resistance, power, and energy curves for an exploding wire have been examined by other investigators. The curves of Figs. 8 through 33 were examined to determine if the wire experiments conducted in this study and the results of other investigators (discussed in Section 2.0) were consistent. Quantitative agreement could not be checked since the discharge circuits of other investigators did not have the same capacitance, inductance, and charging voltage of the circuits used in the present study. Thus, only qualitative agreement with the results in the literature was possible for the voltage, current, resistance, power, and energy curves of Figs. 8 through 33.

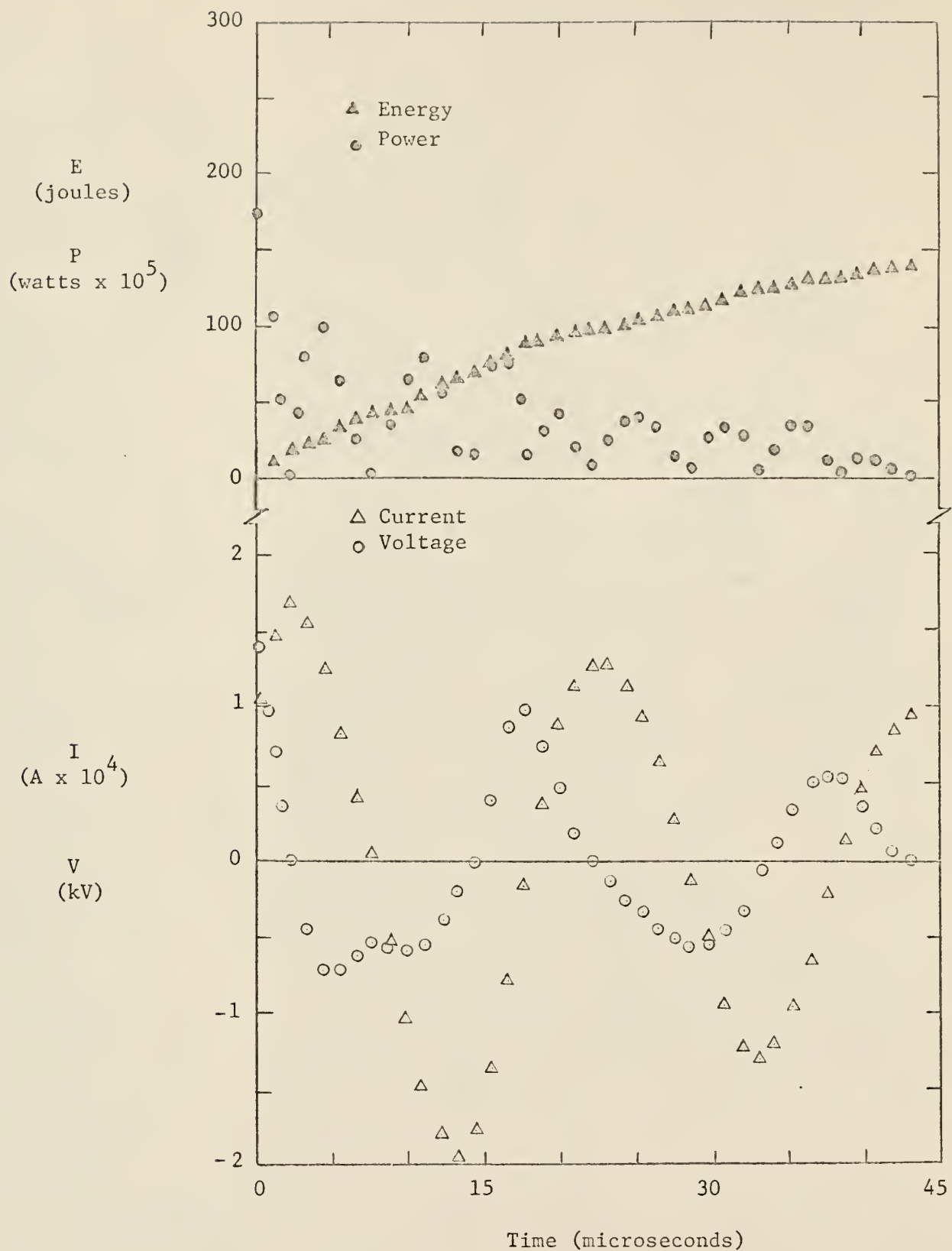


Figure 8. Curves for 32 mil x 1 inch aluminum wire exploded at 8 μF and 11 kV.

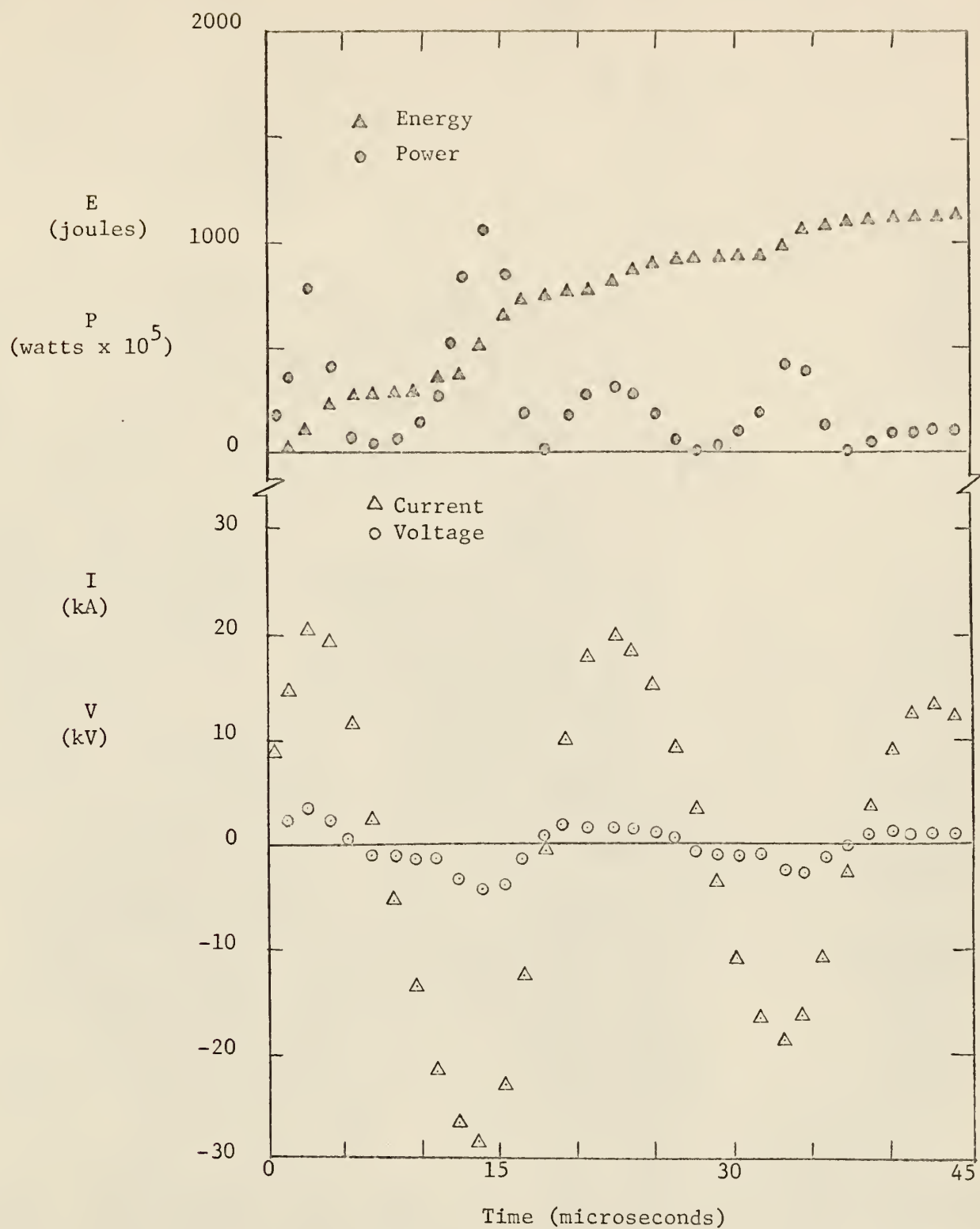


Figure 9. Curves for 32 mil x 1 inch aluminum wire exploded at 8 μ F and 15 kV.

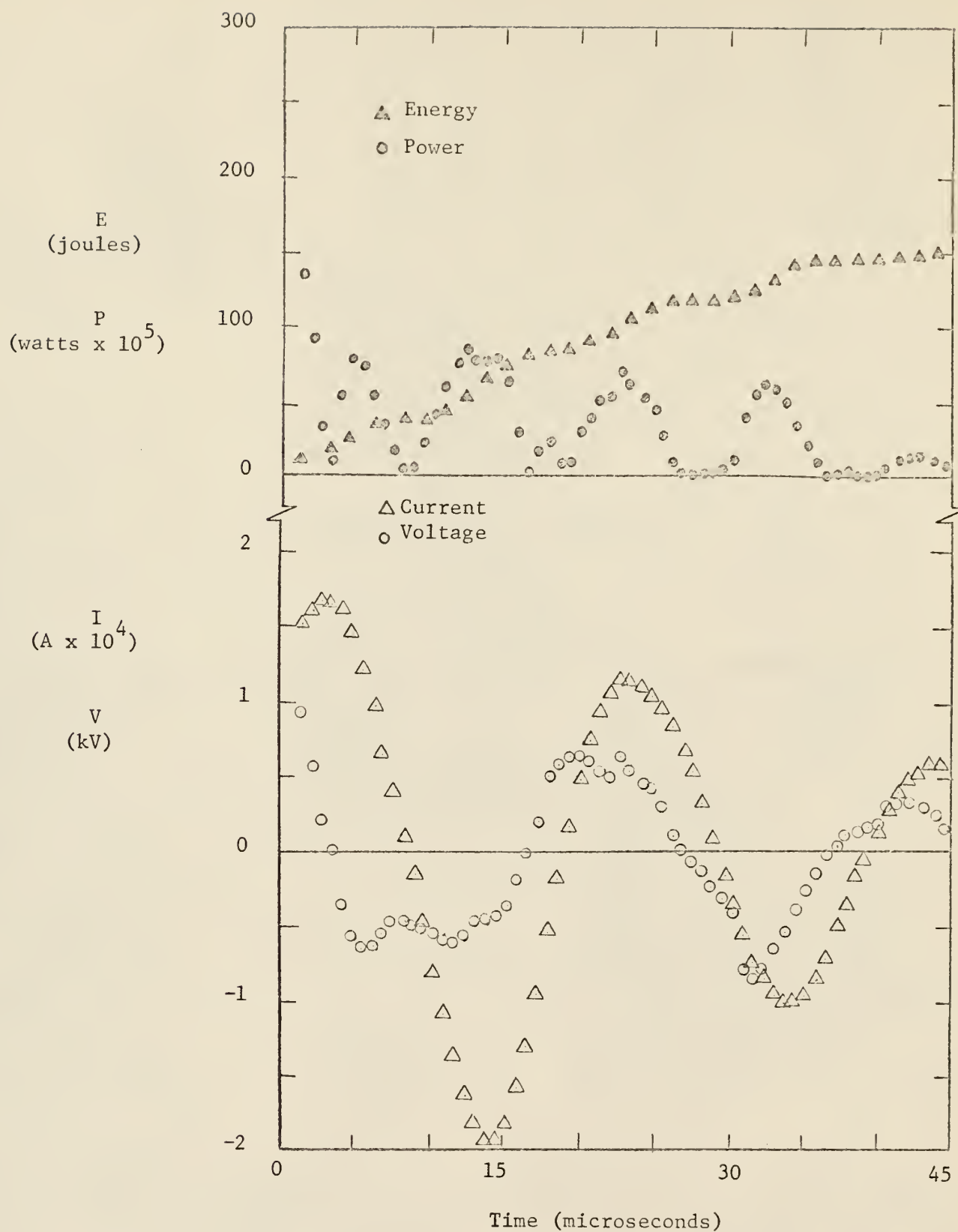


Figure 10. Curves for 20 mil \times 1/2 inch copper wire exploded at 8 μ F and 11 kV.

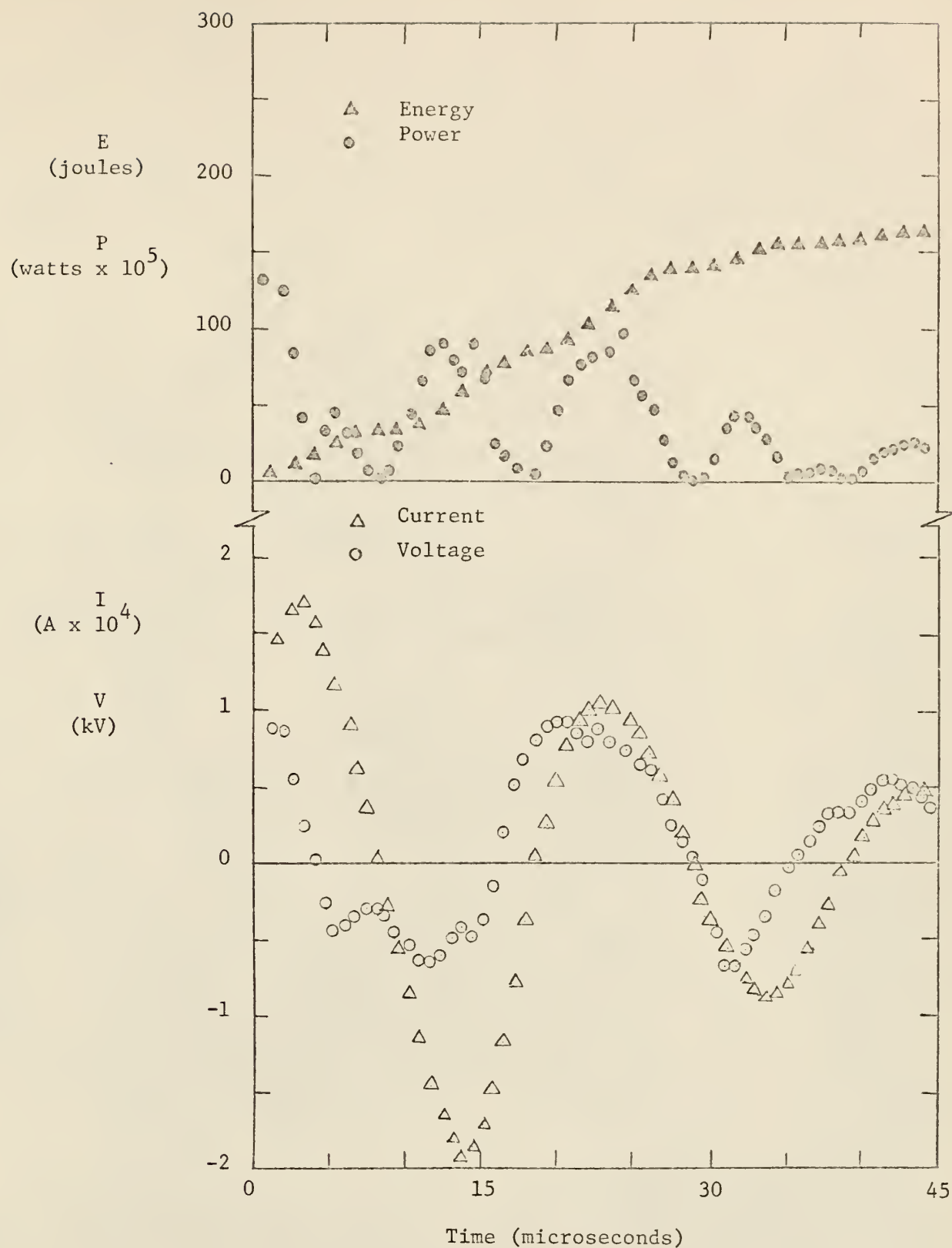


Figure 11. Curves for 20 mil \times 1 inch copper wire exploded at 8 μ F and 11 kV.

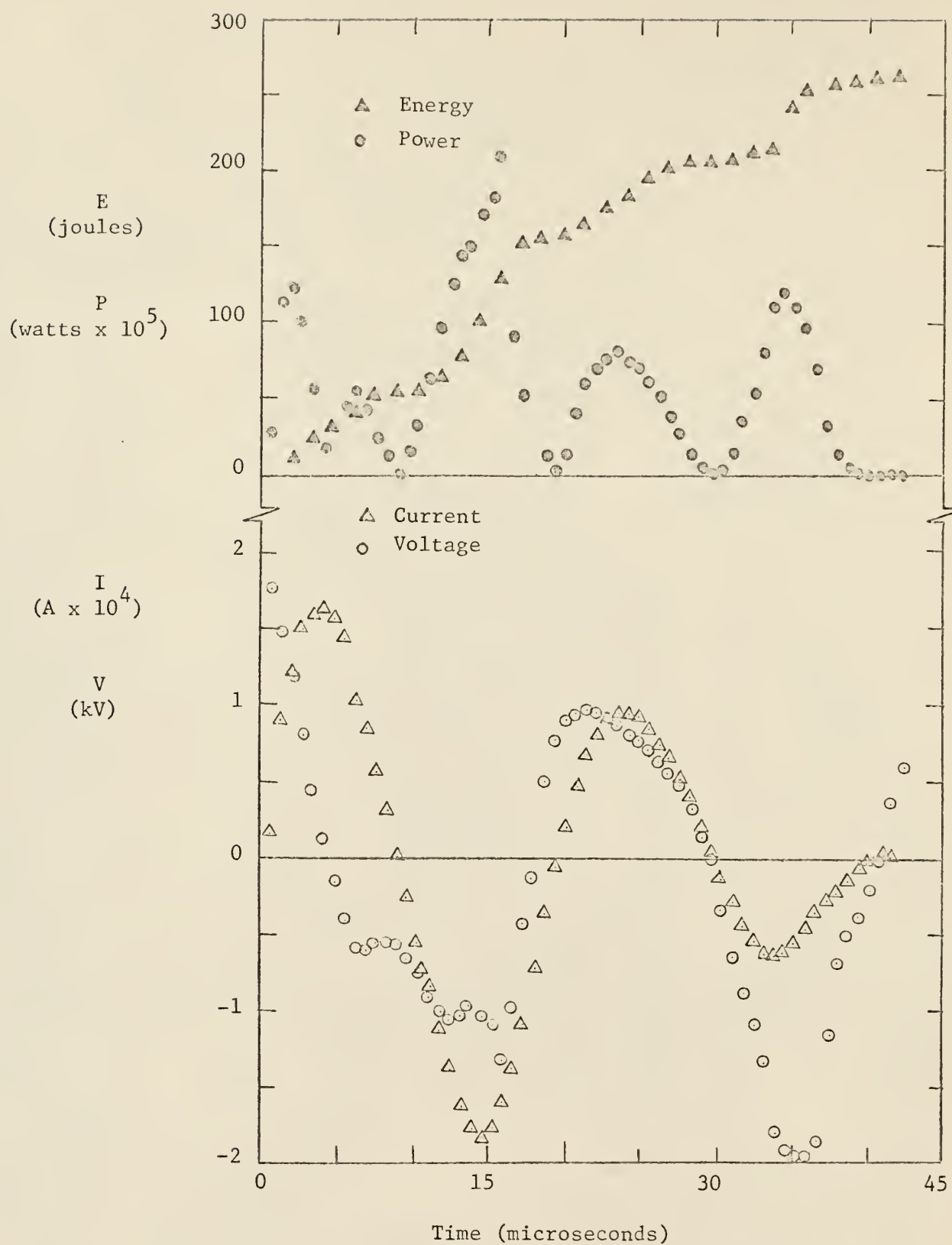


Figure 12. Curves for 20 mil \times 2 inch copper wire exploded at 8 μ F and 11 kV.

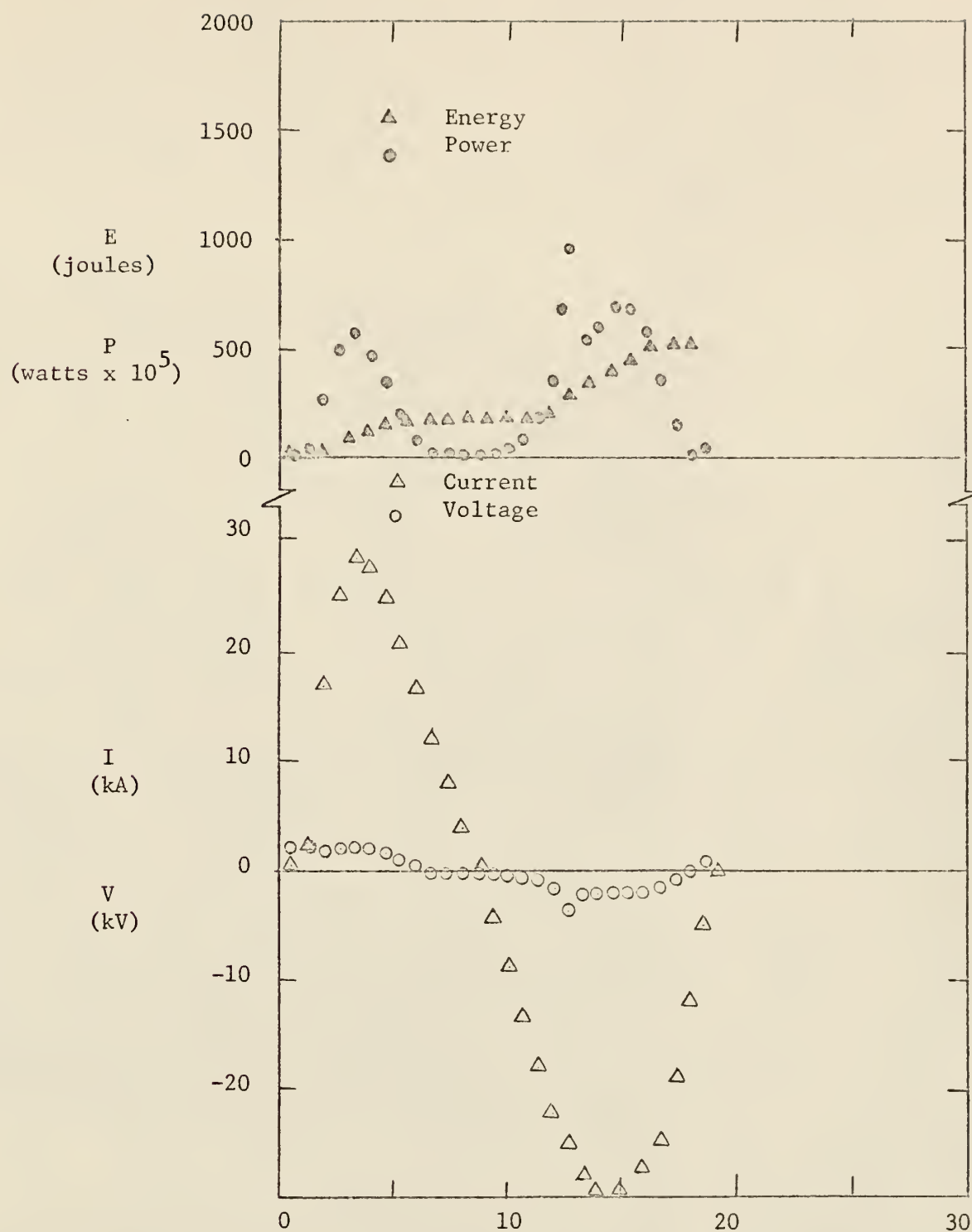


Figure 13. Curves for 20 mil x 1/2 inch copper wire exploded at 8 μF and 15 kV.

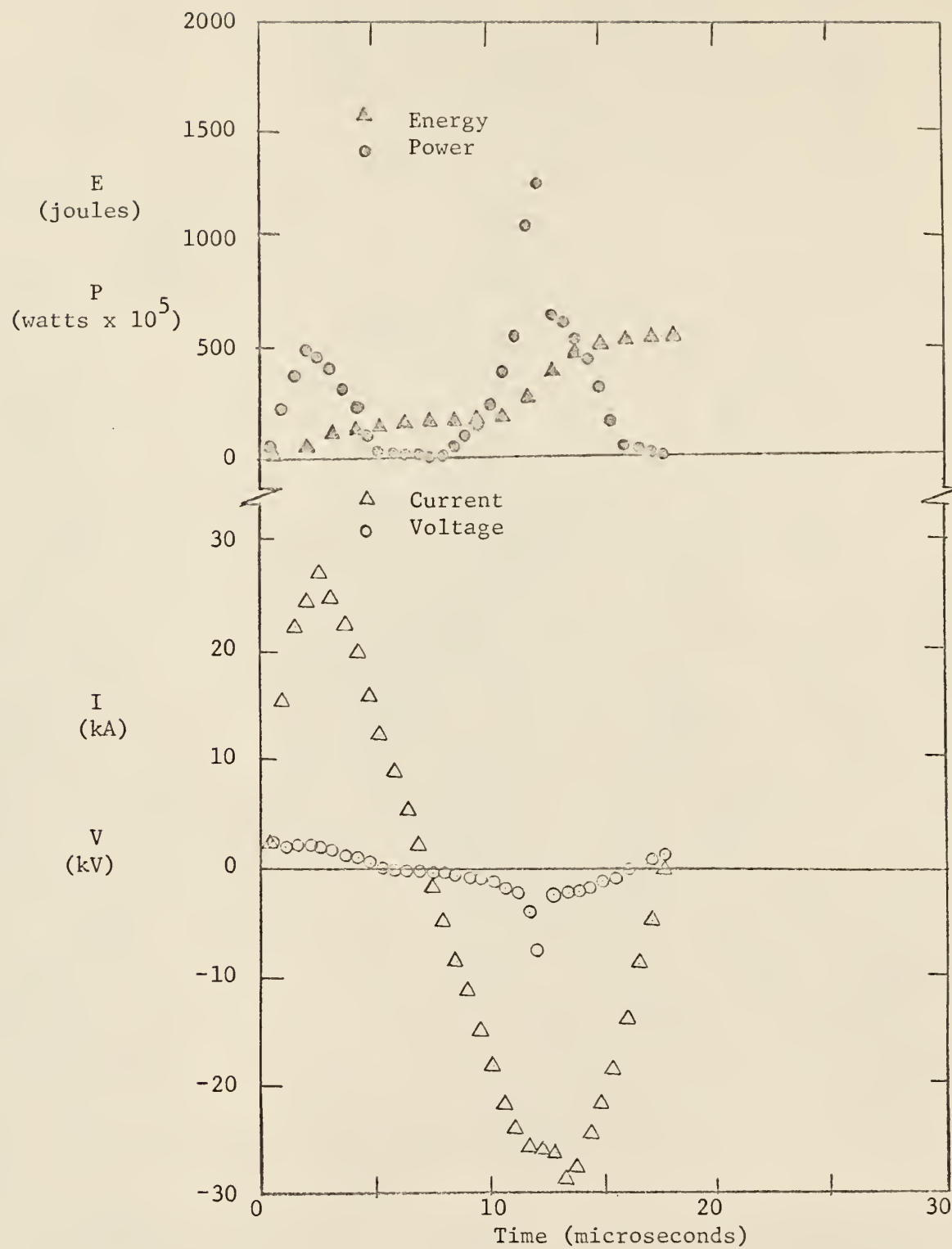


Figure 14. Curves for 20 mil x 1 inch copper wire exploded at 8 μ F and 15 kV.

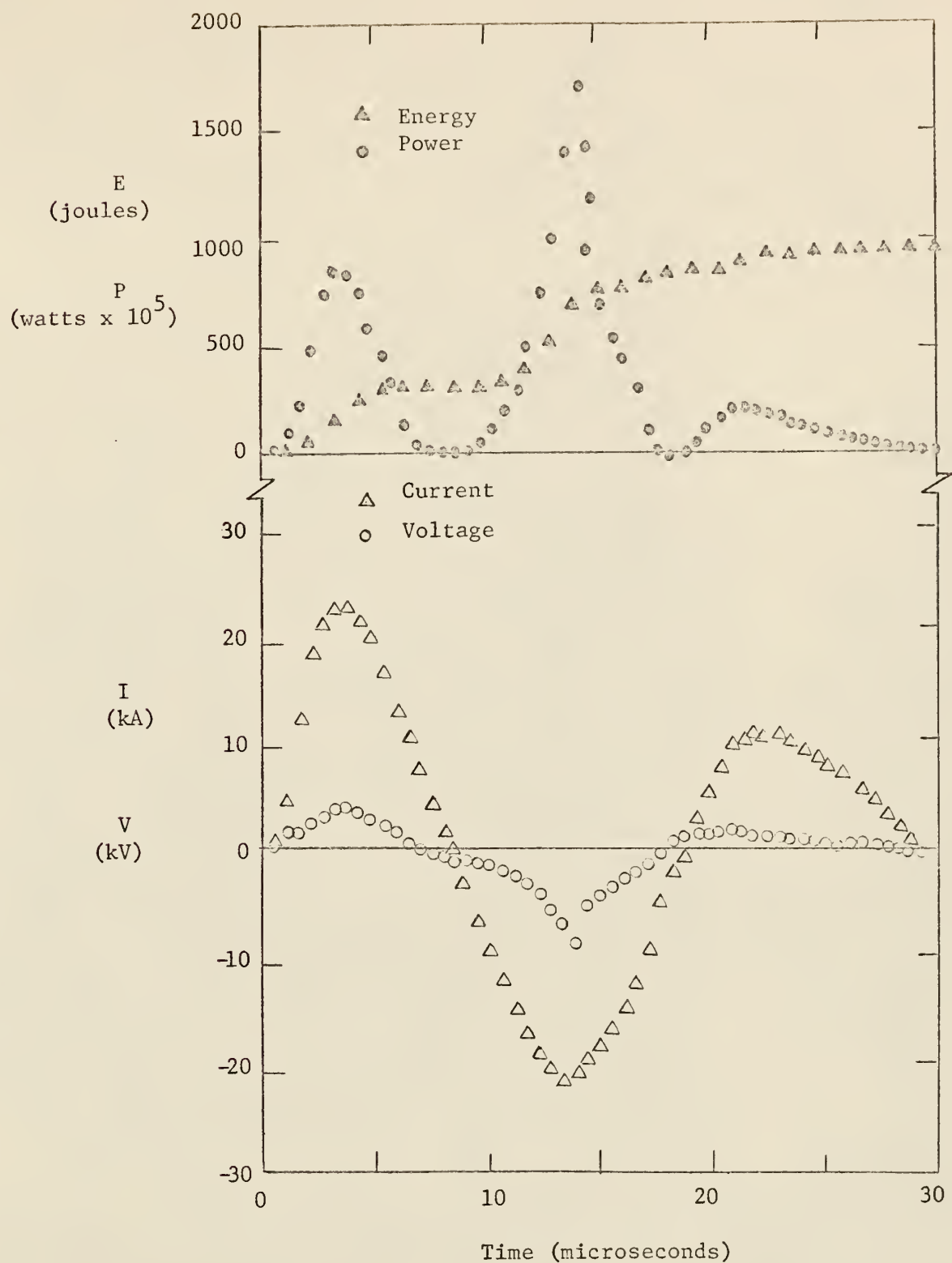


Figure 15. Curves for 20 mil x 2 inch copper wire exploded at 8 μ F and 15 kV.

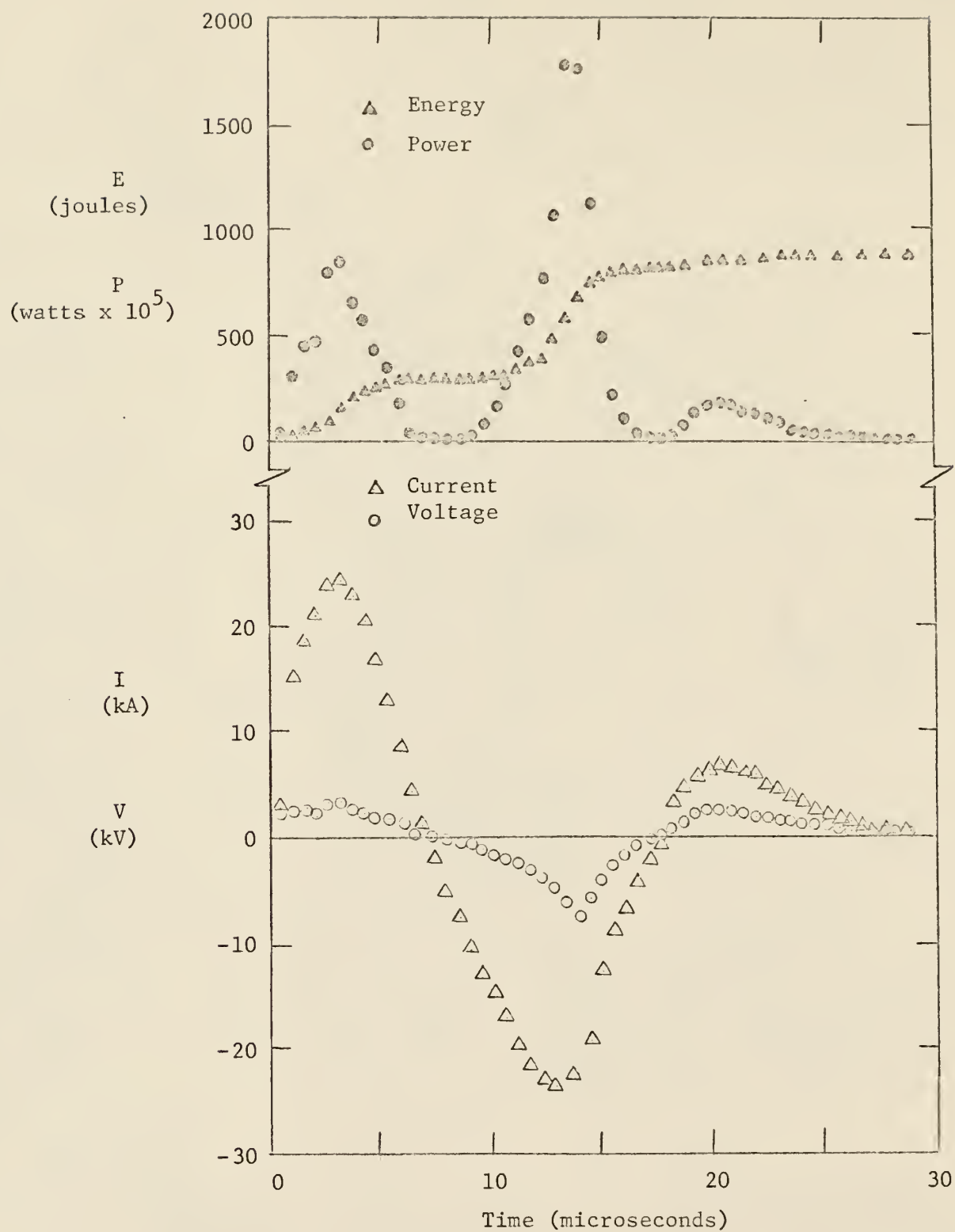


Figure 16. Curves for 20 mil \times 3 inch copper wire exploded at 8 μ F and 15 kV.

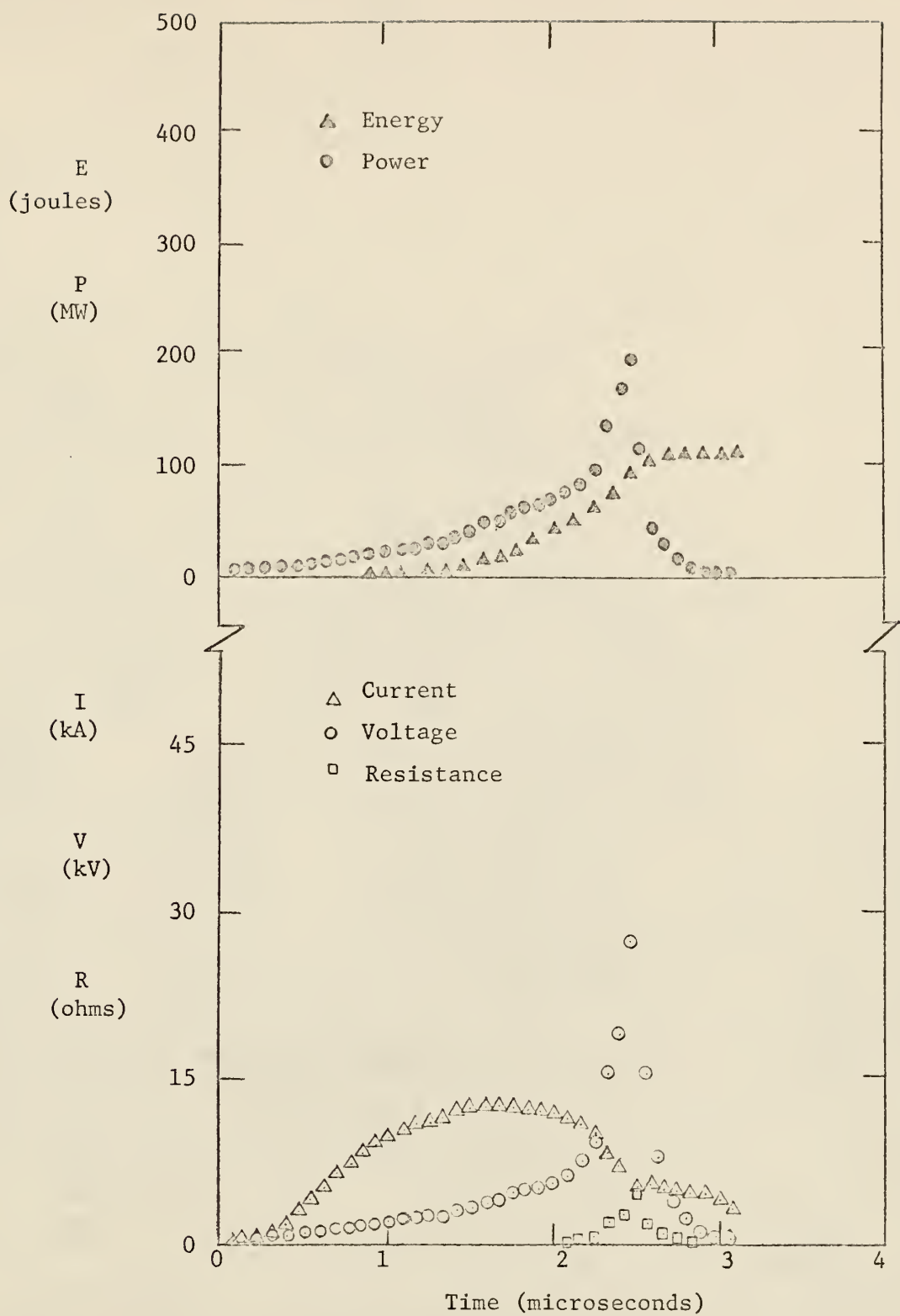


Figure 17. Curves for 10 mil x 1 inch copper wire exploded at 4 μ F and 11 kV.

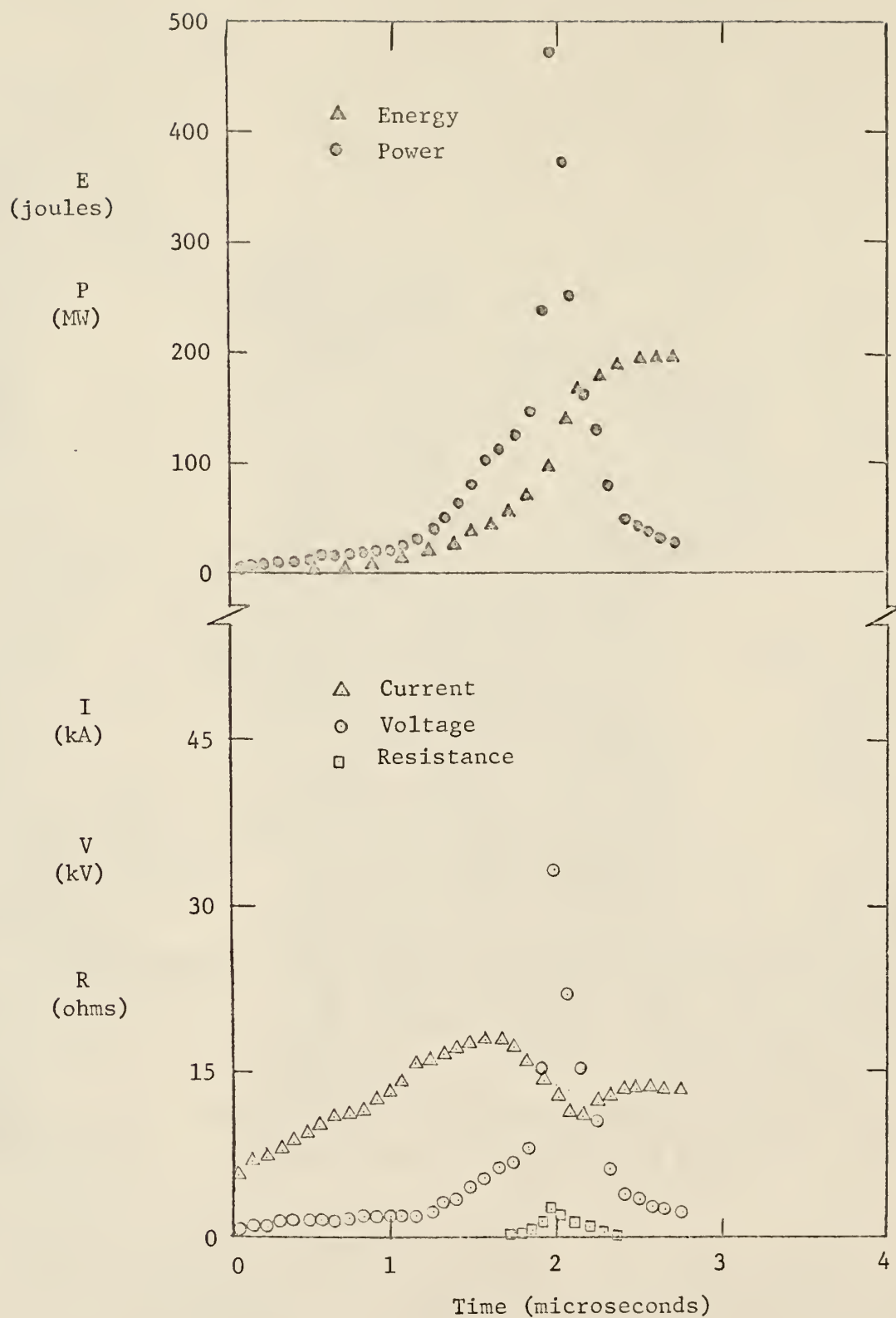


Figure 18. Curves for 10 mil x 1 inch copper wire exploded at 4 μ F and 15 kV. .

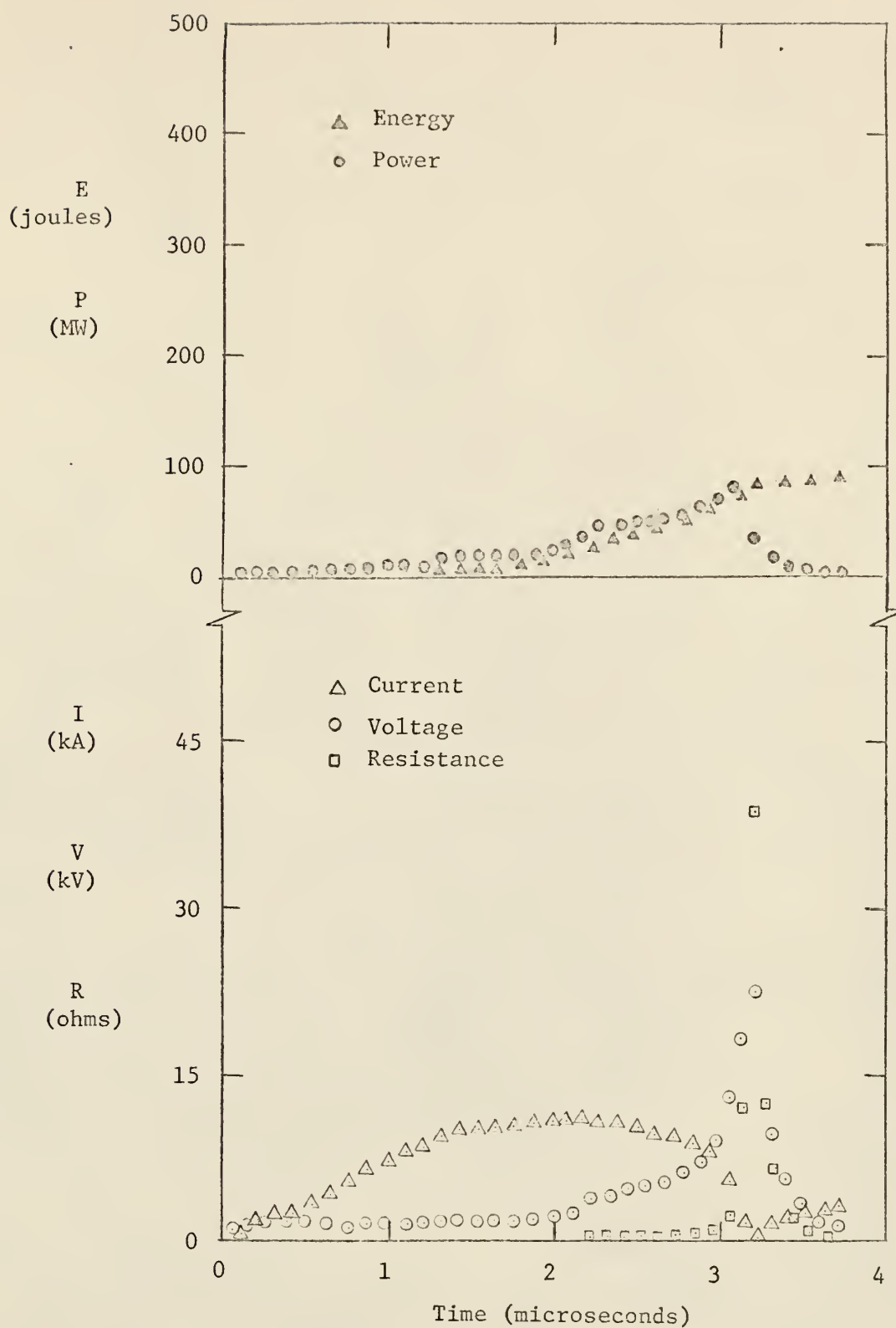


Figure 19. Curves for 10 mil x 1 inch copper wire exploded at 8 μ F and 8 kV.

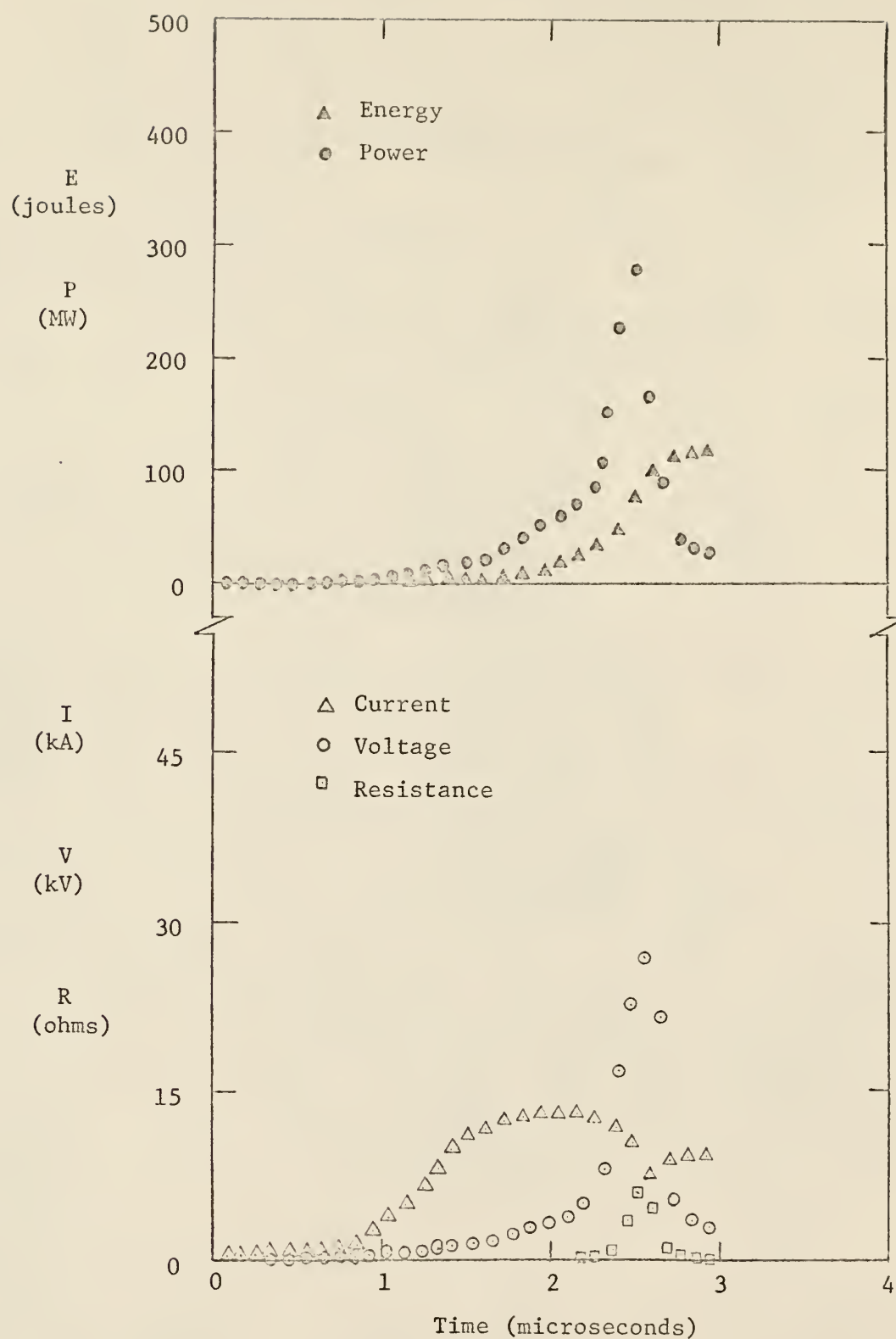


Figure 20. Curves for 10 mil x 1 inch copper wire exploded at 8 μ F and 11 kV.

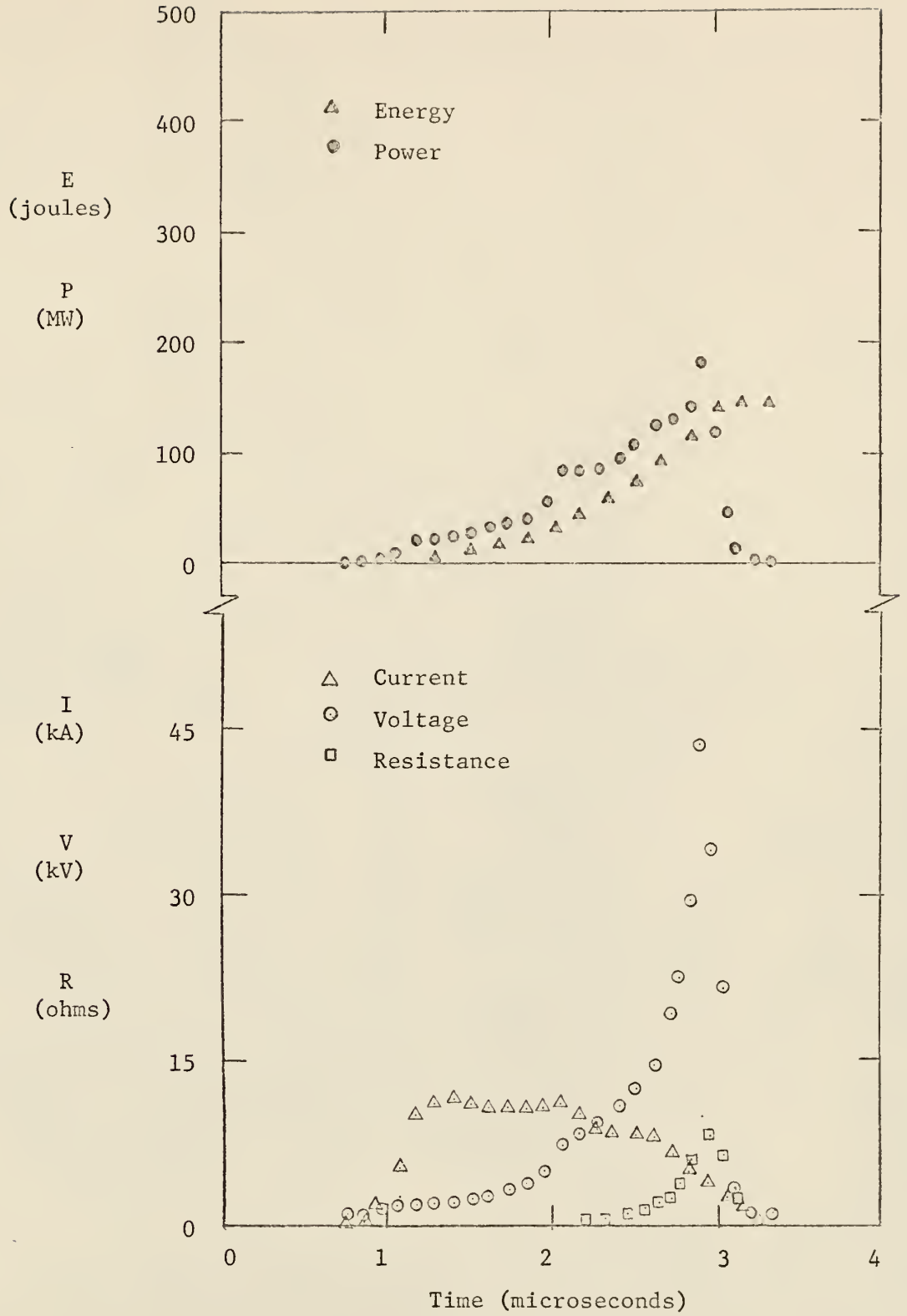


Figure 21. Curves for 10 mil x 3 inch copper wire exploded at 8 μ F and 11 kV.

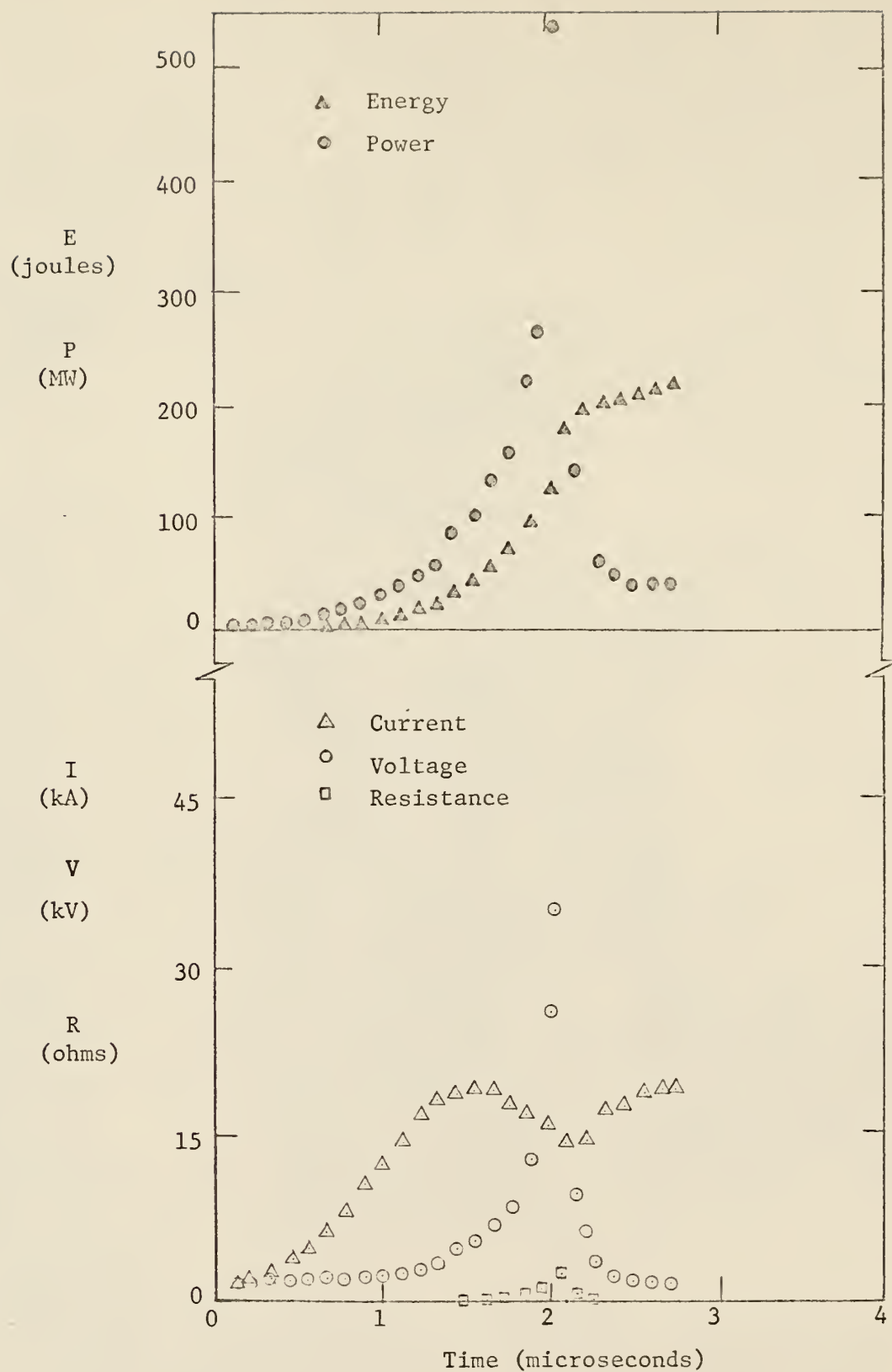


Figure 22. Curves for 10 mil x 1 inch copper wire exploded at 8 μ F and 15 kV.

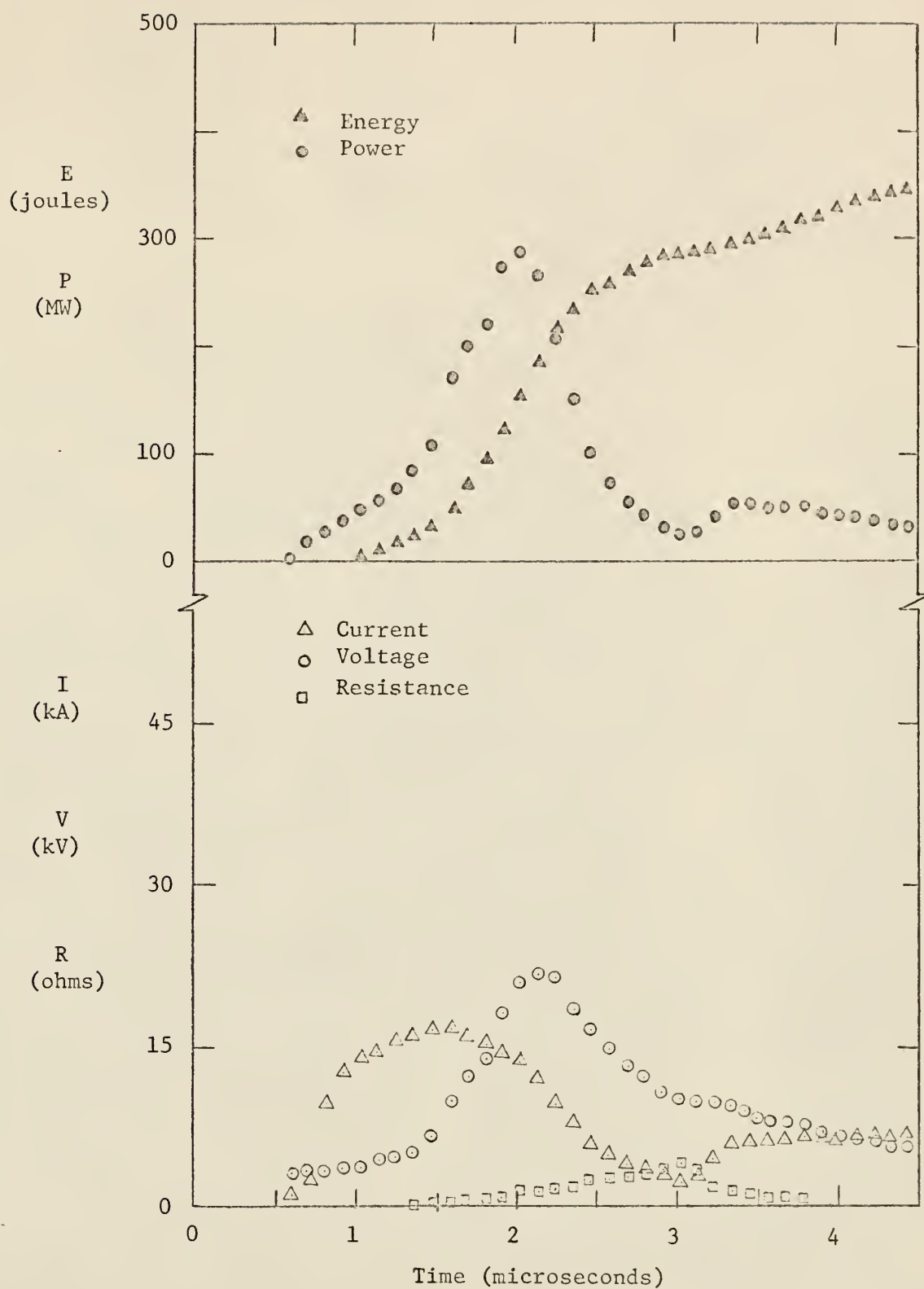


Figure 23. Curves for 10 mil x 3 inch copper wire exploded at 8 μ F and 15 kV.

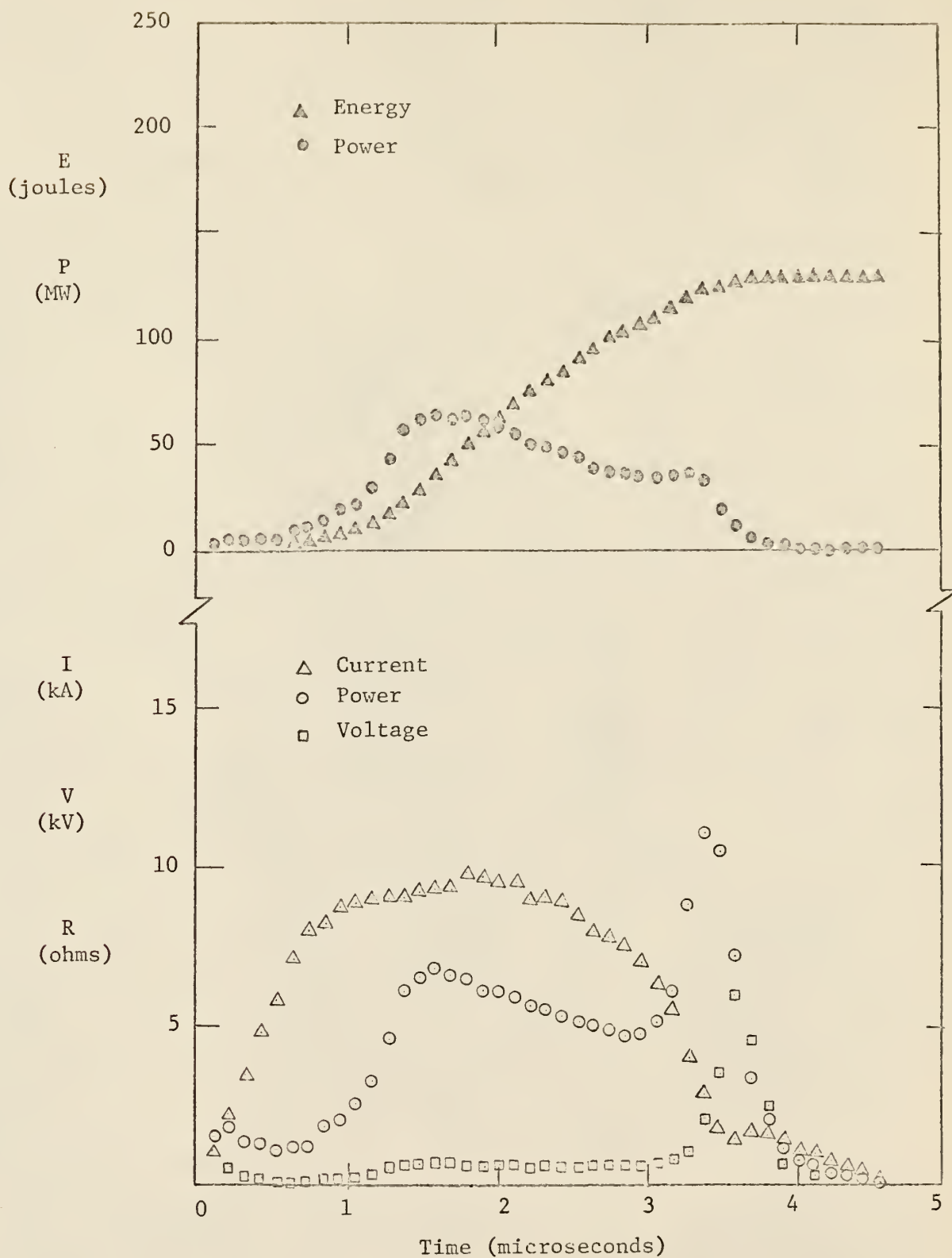


Figure 24. Curves for 14 mil x 1 inch iron wire exploded at 4 μ F and 11 kV.

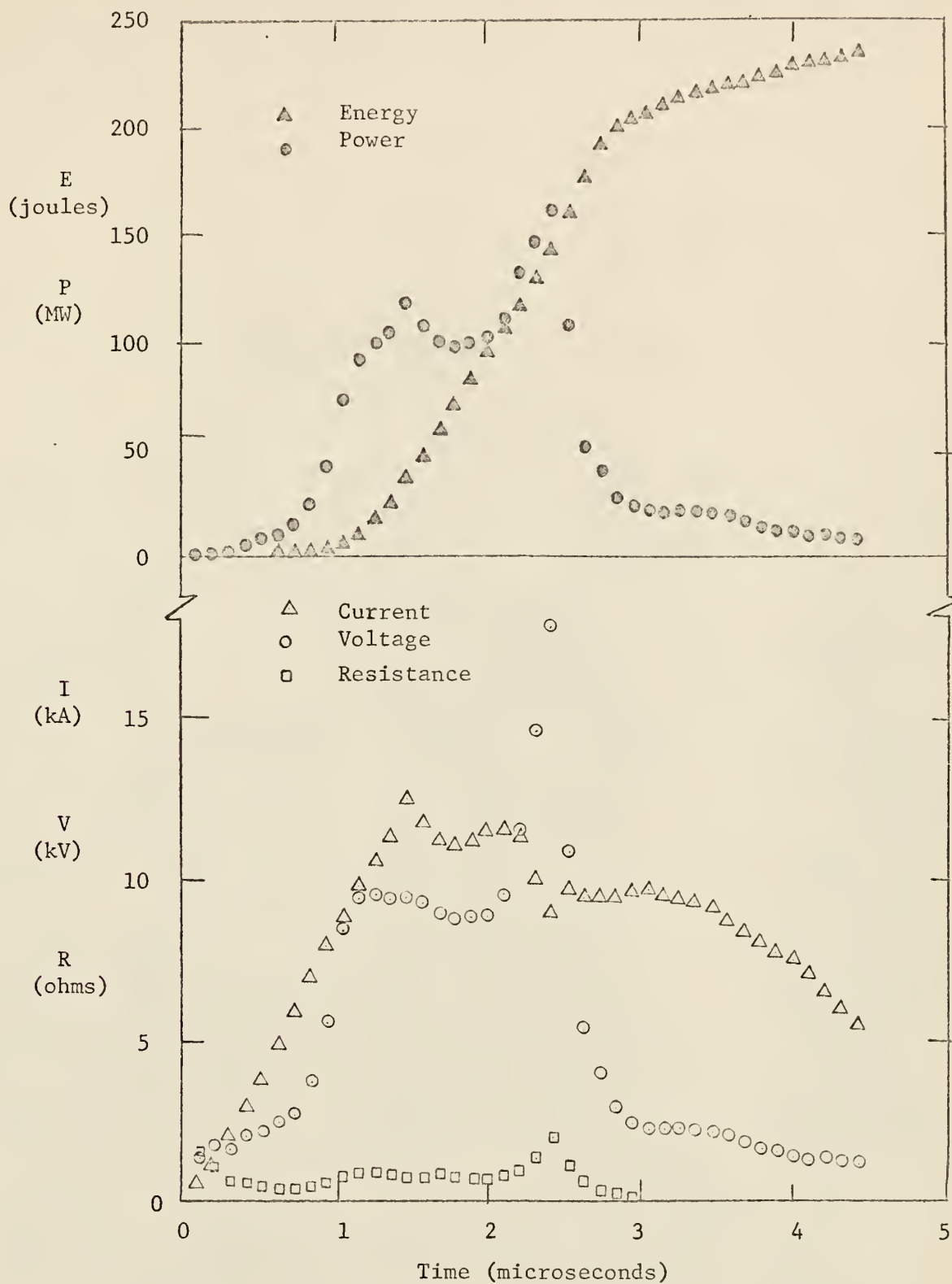


Figure 25. Curves for 14 mil x 1 inch iron wire exploded at 4 μ F and 15 kV.

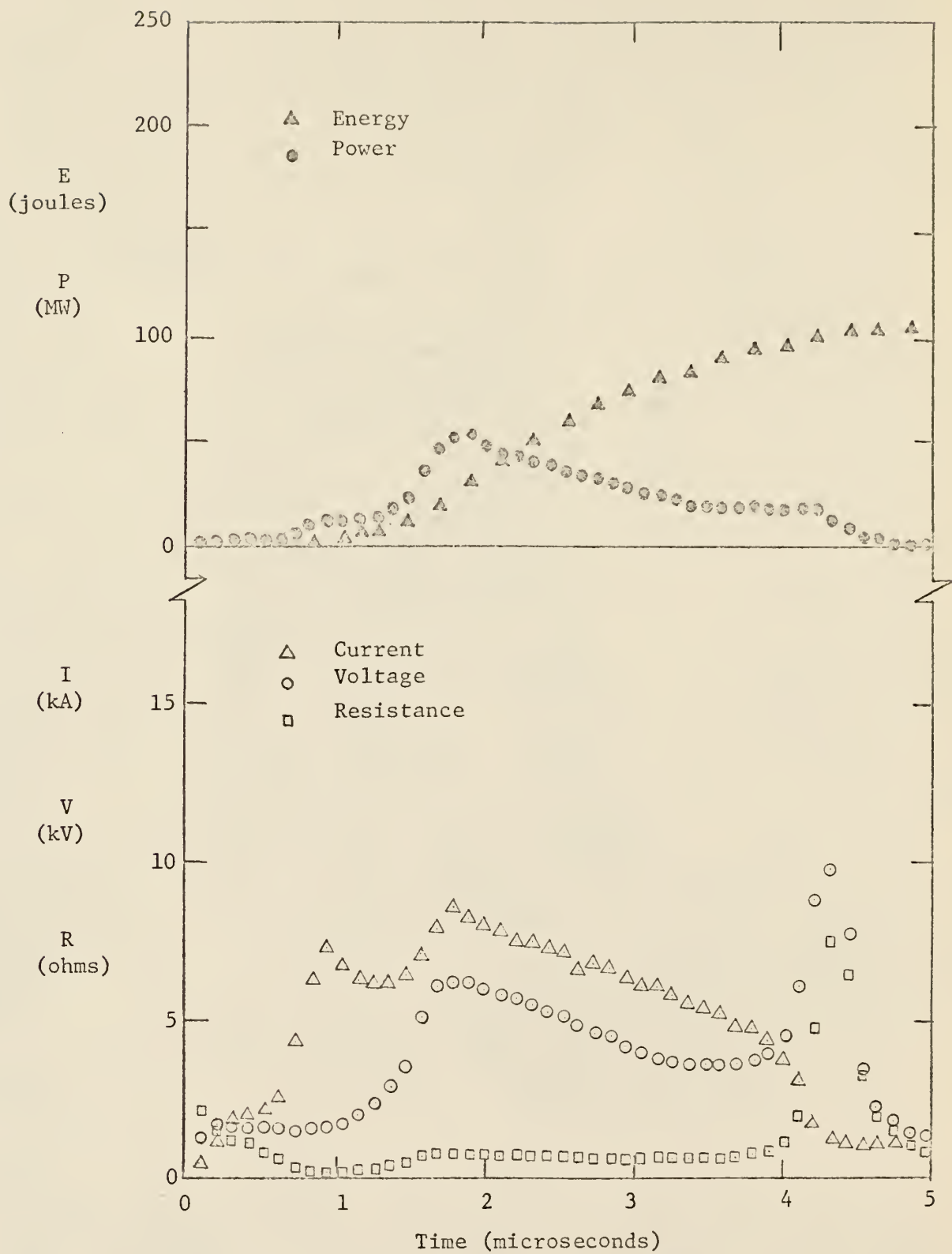


Figure 26. Curves for 14 mil x 1 inch iron wire exploded at 8 μ F and 8 kV.

material for longer periods of time after the vaporization energy is deposited. Toward this end a sample cell employing the magnetic pinch principle (See Appendix G) was constructed and tested to determine its effect on the energy density of wire explosions.

5.8 Results of Wire Explosions in Sample Cell

Because higher temperatures were desired than obtained from bare wire explosions, a sample cell was designed to confine the wire material after vaporization in the hope this would lead to more effective and uniform heating of the wire material with consequently higher energy deposition. In the bare wire studies highest energy densities had been obtained for the wires well matched to the circuit parameters; these wires included the 14 mil iron wire, the 10 mil copper wire, and the 20 mil copper wire. Since deposited energy density increased with a decrease in wire length and end effects were not significant for one inch wires but were for half-inch wires, one inch lengths of the above wires were selected for study in the sample cell. In the final sample cell design, 3/8 inch diameter stainless steel tubes were used for the cell walls. The exploding wire was located at the center of the tube and insulated from the walls with a silicon based caulk. Data, taken with the 10 mil copper wire exploded at 8 microfarads and 11 kilovolts in the sample cell, indicated that arcing between the wire and cell walls had occurred; therefore data for the 10 mil copper wire were not reported.

Figure 32 shows the results of a 14 mil iron wire exploded at 8 microfarads and 11 kilovolts in the sample cell. Comparison of Fig. 32 with Fig. 27 shows the effect of the sample cell geometry on a wire explosion. The current curves differ during the initial portion of the

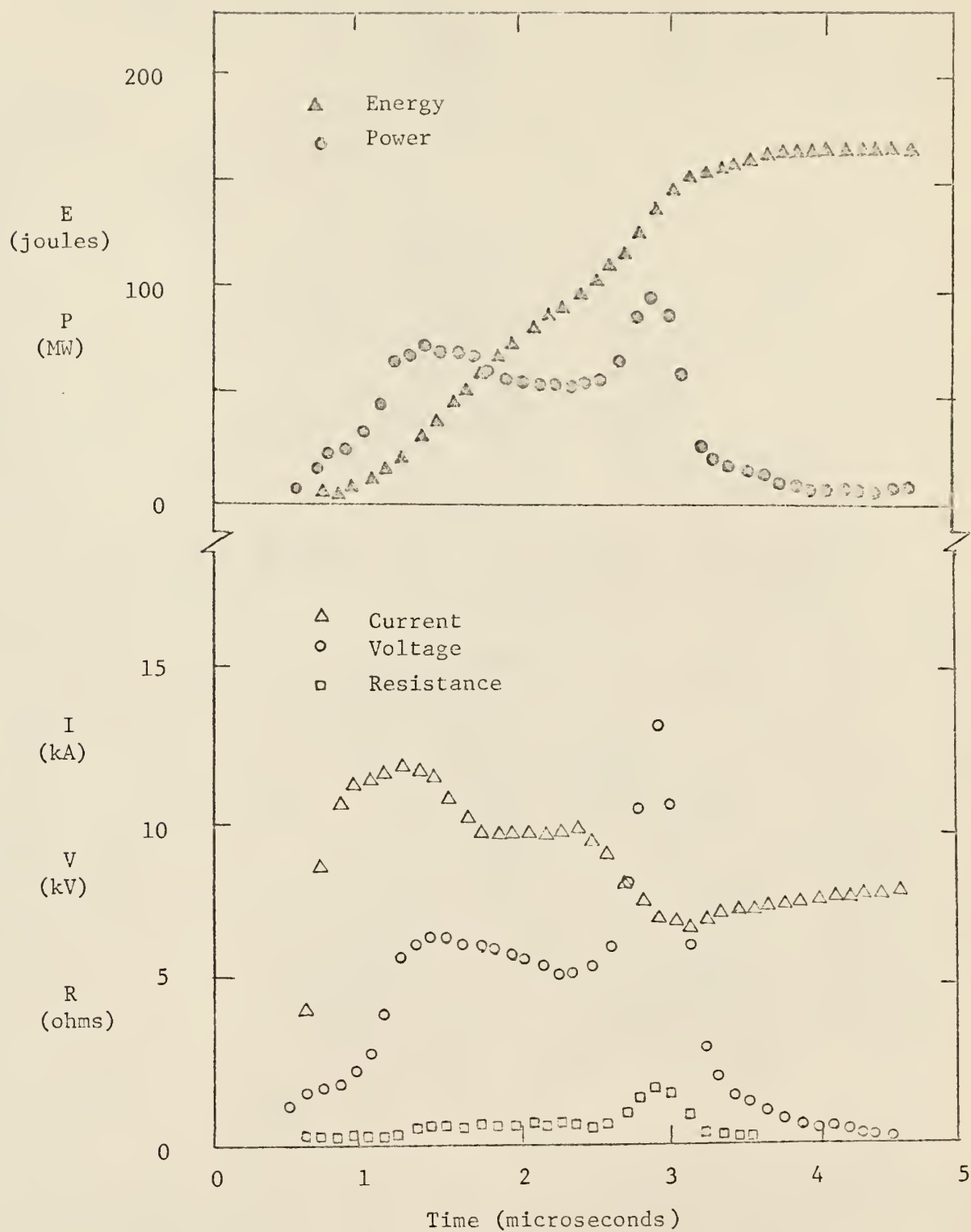


Figure 27. Curves for 14 mil x 1 inch iron wire exploded at 8 μ F and 11 kV.

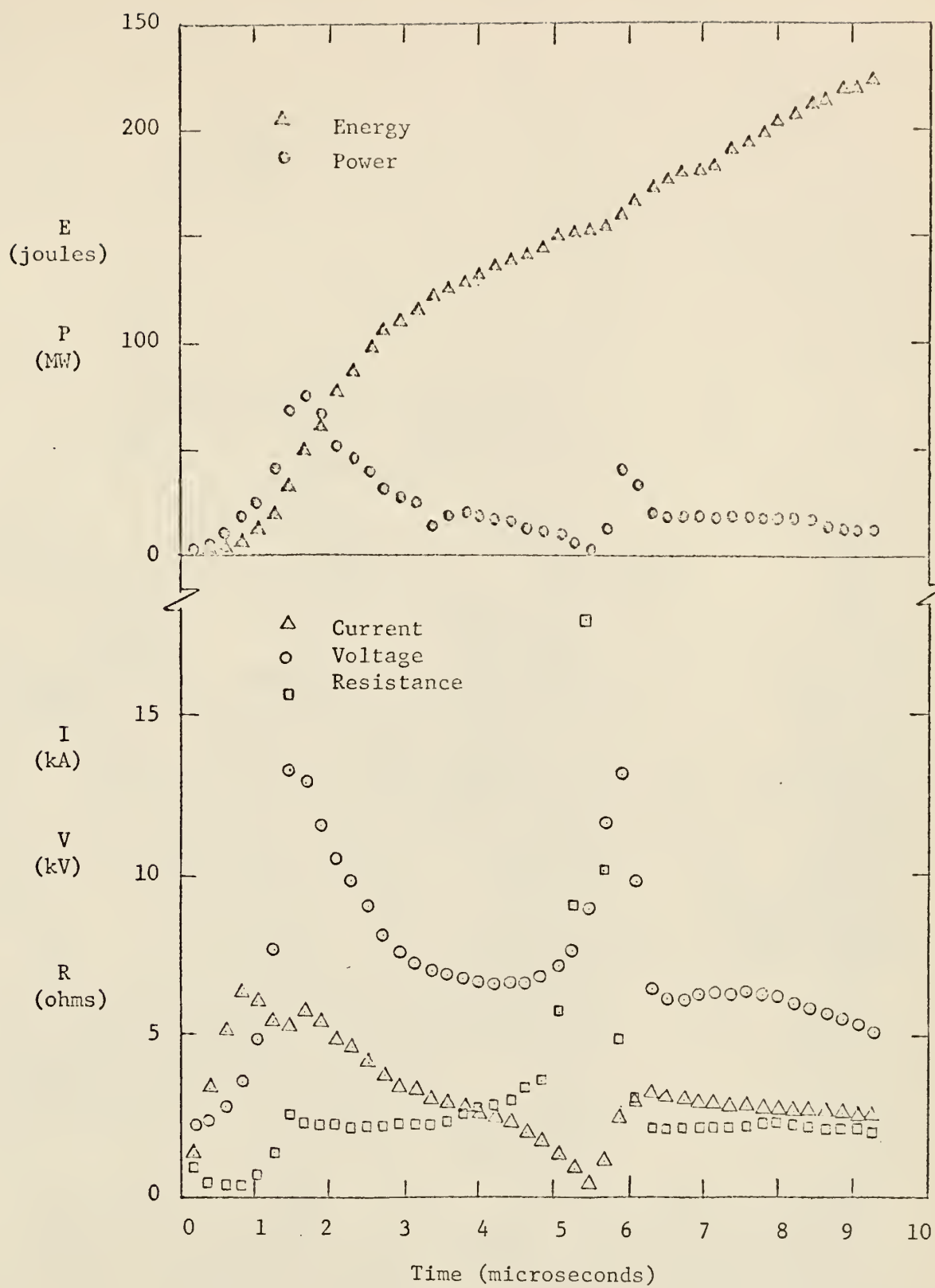


Figure 28. Curves for 14 mil x 3 inch iron wire exploded at 8 μ F and 11 kV.

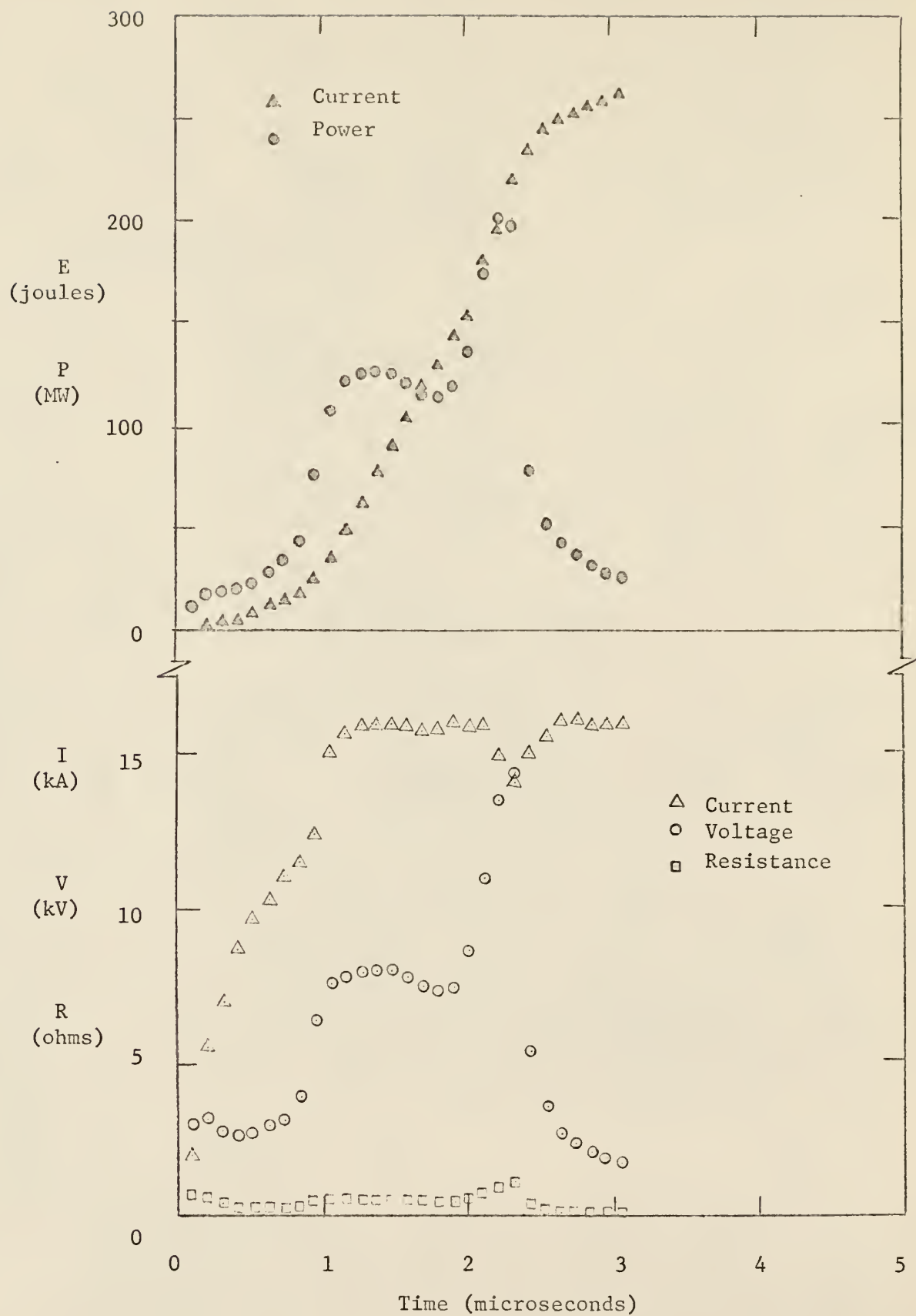


Figure 29. Curves for 14 mil x 1 inch iron wire exploded at 8 μ F and 15 kV.

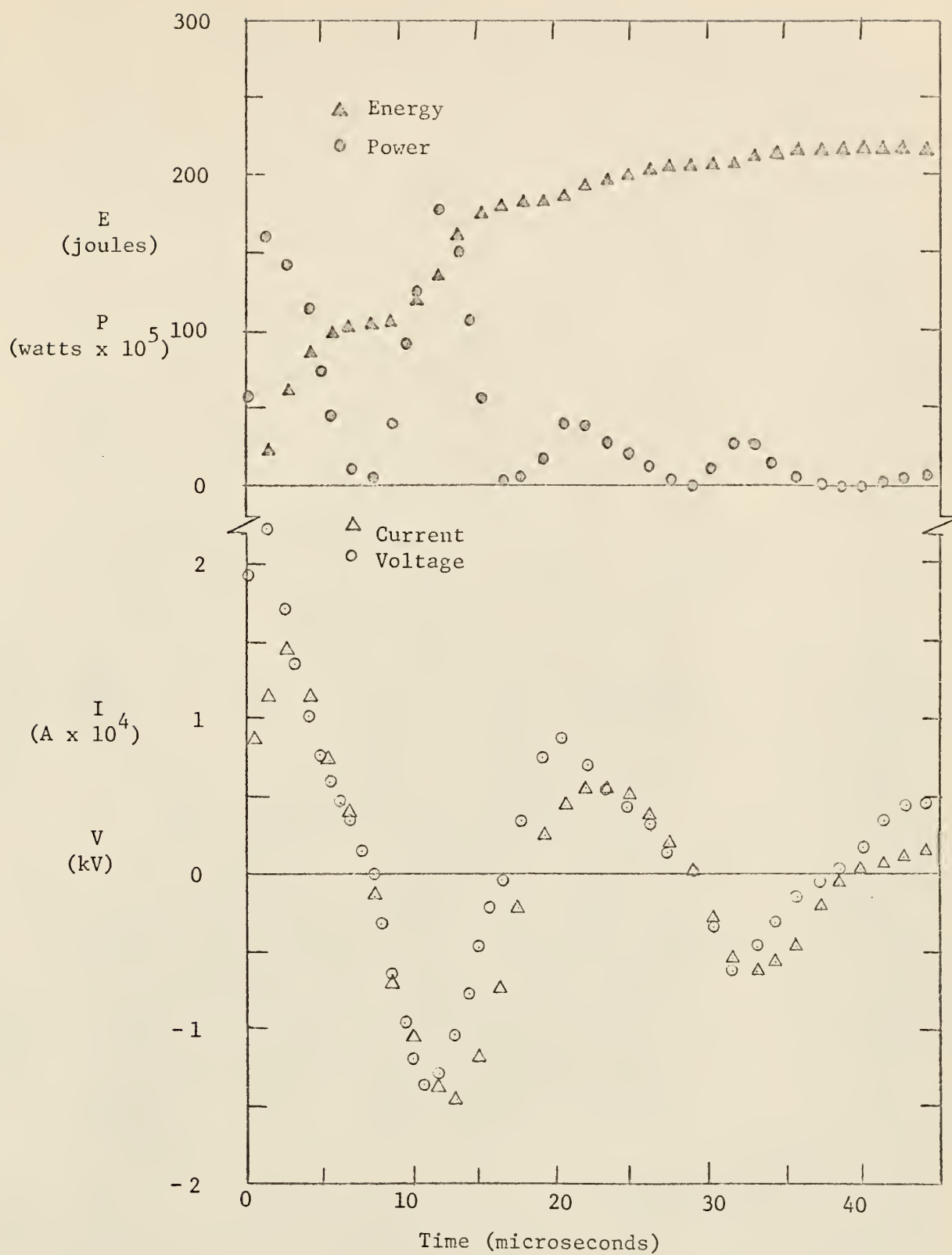


Figure 30. Curves for 28 mil x 1 inch nickel-chromium wire exploded at 8 μF and 11 kV.

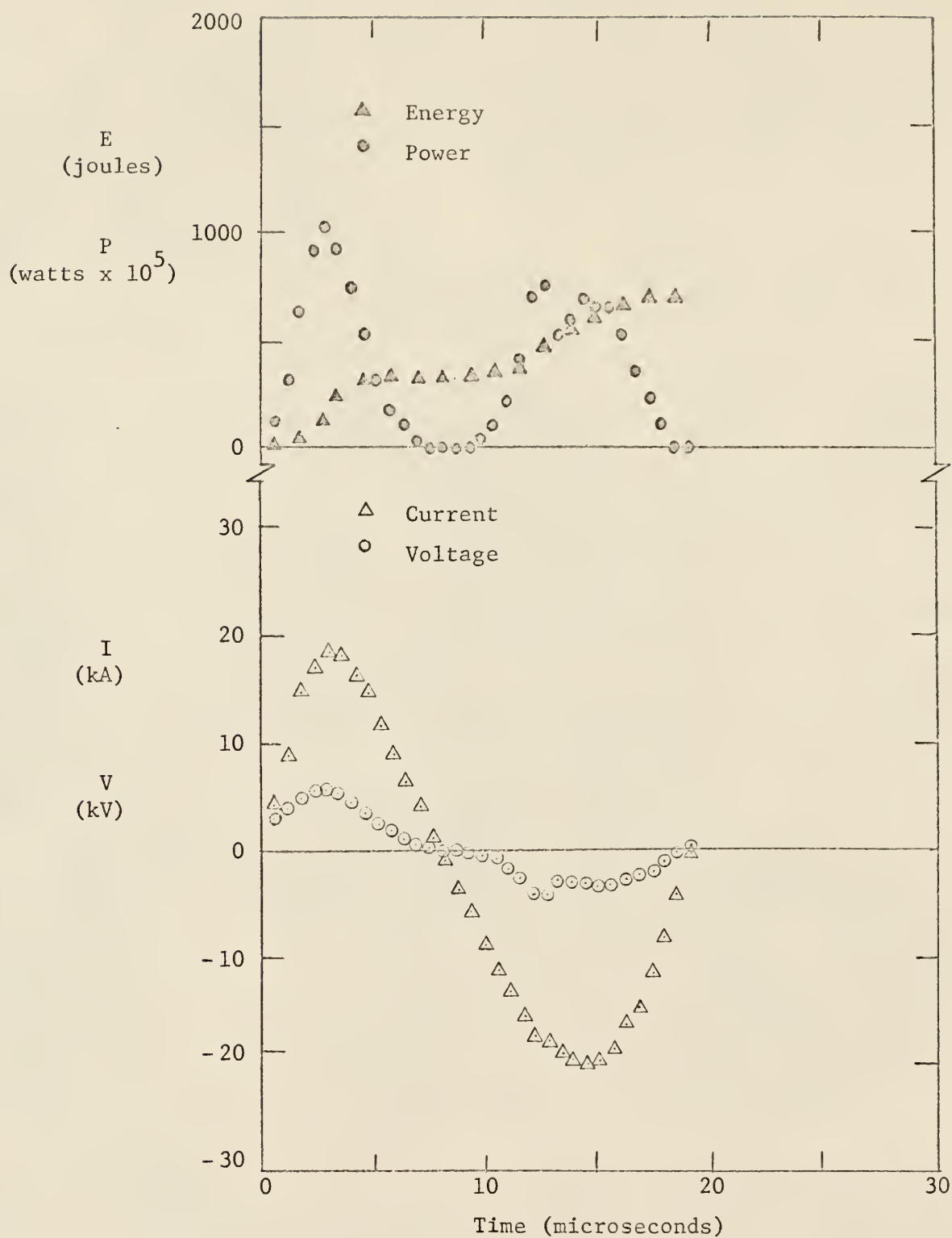


Figure 31. Curves for 28 mil x 1 inch nickel-chromium wire exploded at 8 μ F and 15 kV.

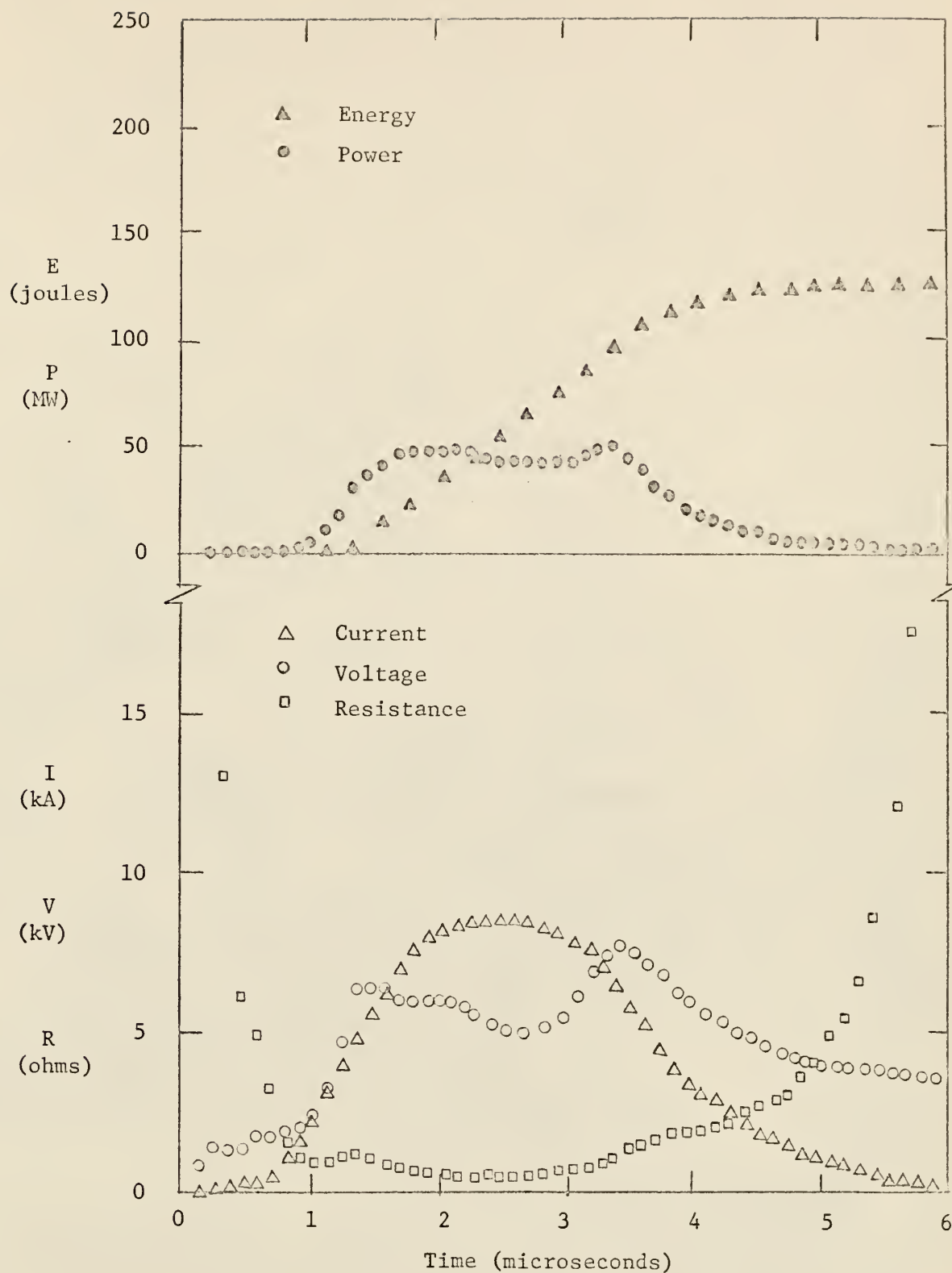


Figure 32. Curves for 14 mil x 1 inch iron wire exploded in sample cell geometry at 8 μ F and 11 kV.

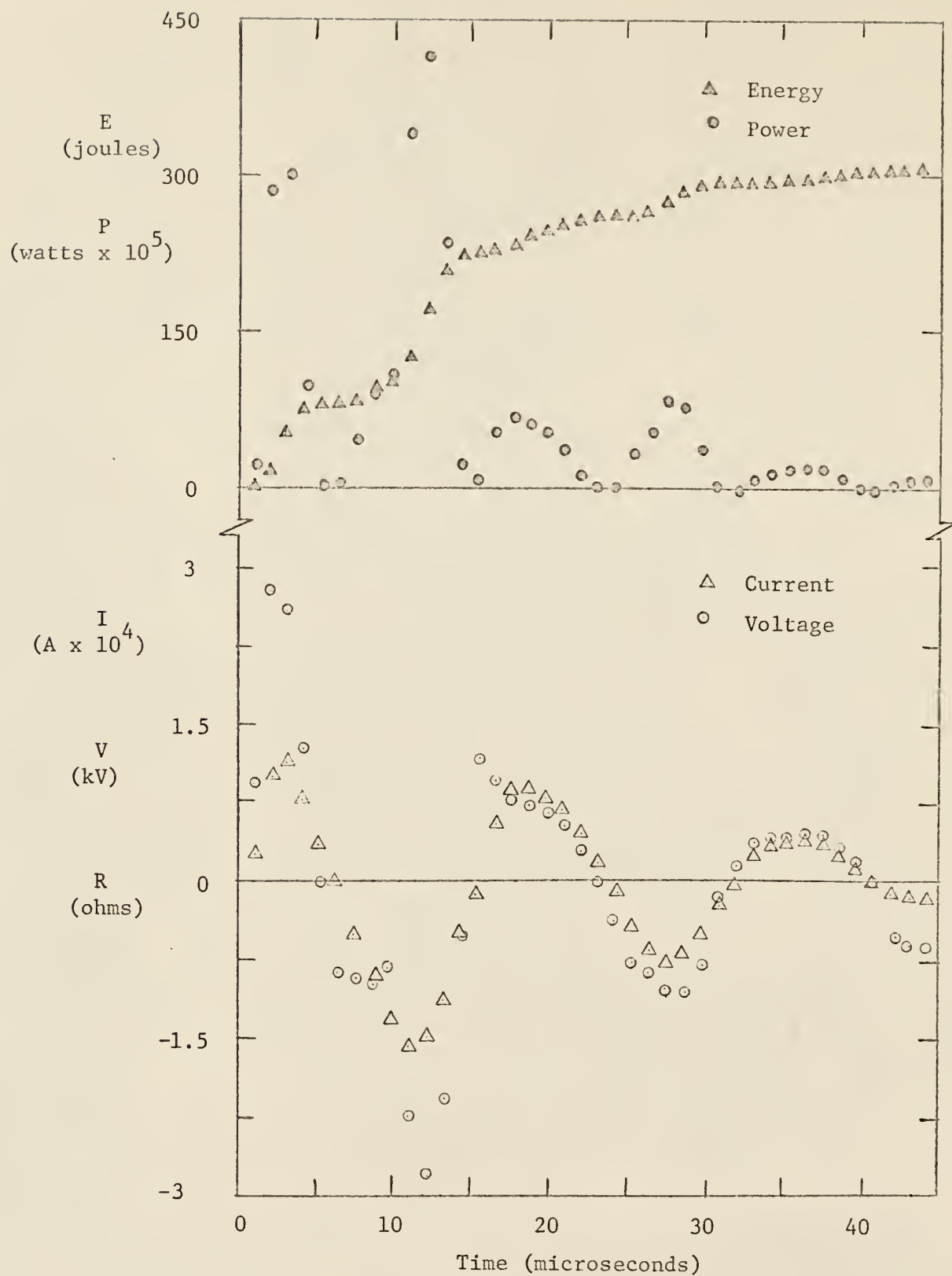


Figure 33. Curves for 20 mil x 1 inch copper wire exploded in sample cell geometry at 8 μF and 11 kV.

The resistance curves were examined to see if they were consistent with the known physical properties of the wire and the relative energetics of the wire explosions. Wire resistance increases with an increase in energy content if the temperature coefficient of resistivity is positive. Melting of a wire is characterized by small rapid changes in the resistance curve while vaporization is indicated by a large rapid increase in the wire resistance to a peak value.

The resistance anomaly is characteristic of wire explosions when the deposited energy is greater than the energy necessary to vaporize the wire (i.e., The wire resistance depends on the rate of energy deposited.) The resistance reaches larger magnitudes for slower (less energetic) explosions. Near a resistance peak a dark pause is observed if the voltage across the wire gap does not cause arc breakdown of the surrounding material. The voltage and current also have characteristic responses for a dark interval; the current is approximately zero and the voltage remains relatively constant.

The voltage and current curves of Figs. 8 through 33 were examined for the characteristic differences between low heat of vaporization material (class I) and high heat of vaporization material (class II). The voltage and current curves for copper (class I material) were significantly different than the voltage and current curves of iron (class II material). Typically, class II materials melt near the peak current (Fig. 1b). The current rapidly decreases during melting and then remains nearly constant until vaporization. Thus, class II materials exhibit a relatively low current level when the energy to vaporize is reached. For class I materials the current peaks near the end of vaporization (Fig. 1a) and rapidly decreases near the voltage peak. Thus,

class I materials exhibit a high current level when the energy to vaporize is attained.

Class II materials require a larger energy deposit to vaporize a wire. Thus, the time to burst is longer for class II material while the voltage and power peaks are broader. Peaks of voltage and power curves correspond to explosive vaporization. Since class II materials require longer time periods to deposit the vaporization energy, the explosion mechanism tends to be affected by unduloids. Typically the entire length of a class II material wire does not vaporize.

The voltage, current, power, and energy curves were examined to determine the effect of wire dimensions on wire explosions. The voltage and current curves determined if wires were well matched to the circuit parameters. As discussed in Section 2.0, a wire is well matched to the circuit parameters if the wire explodes near the first current peak. The time of burst, (time at the voltage peak) which depends on wire parameters and circuit parameters, was examined and compared to results in the literature. The energy curves and the power curves of Figs. 8-33 were compared to determine if burst energy and peak power per unit length increased for decreasing wire length as reported by Leopold.²³ (Specific values of the energy and power curves obtained from the calculated results are given in Table II.) Since Leopold found that energy deposited up to one microsecond after the wire burst is effective in transferring energy to material surrounding the wire, the energy plateau after the wire burst was also considered in the analysis.

Transition energies of specific interest in the analysis of ex-

Table II. Calculated experimental results of exploding wires
(See pages 71-78 for discussion of error.)

WIRE	PARAMETERS		CIRCUIT*		Time to		ENERGY		ENERGY DENSITY	
	Material	Size (in.)	C (μ F)	V ₀ (kV)	Burst (μ sec)	Peak Power (MW)	Burst (joules)	Plateau (joules)	Burst (eV/atom)	Plateau (eV/atom)
Wires exploded at ambient atmospheric conditions										
Al	.032 x 1		8	11	-	9	-	70	-	0.55
Al	.032 x 1		8	15	13.8	113	509	730	4.01	5.75
Cu	.020 x 1/2		8	11	-	9	-	81	-	2.32
Cu	.020 x 1		8	11	-	9	-	85	-	1.22
Cu	.020 x 2		8	11	-	21	-	157	-	1.12
Cu	.020 x 1/2		8	15	11.2	96	237	514	6.81	14.8
Cu	.020 x 1		8	15	11.8	187	305	543	4.38	7.80
Cu	.020 x 2		8	15	13.8	173	606	837	4.35	6.01
Cu	.020 x 3		8	15	13.8	179	586	810	2.81	3.88
Cu	.010 x 1		4	11	2.48	196	92	112	5.29	7.01
Cu	.010 x 1		4	15	1.96	472	107	202	6.15	11.6
Cu	.010 x 1		8	8	3.22	84	85	89	4.88	5.11
Cu	.010 x 1		8	11	2.52	280	92	122	5.28	7.01
Cu	.010 x 3		8	11	2.89	183	123	143	2.36	2.74
Cu	.010 x 1		8	15	2.04	543	151	221	8.68	12.7
Cu	.010 x 3		8	15	2.25	282	200	351	3.83	6.72
Fe	.014 x 1		4	11	3.53	65	124	129	3.62	3.77
Fe	.014 x 1		4	15	2.53	158	176	236	5.14	6.90
Fe	.014 x 1		8	8	4.46	54	101	105	2.95	3.07
Fe	.014 x 1		8	11	2.93	94	133	162	3.89	4.73
Fe	.014 x 3		8	11	6.06	74	159	225	1.55	2.19
Fe	.014 x 1		8	15	2.37	208	207	263	6.05	7.68
Ni-Cr	.028 x 1		8	11	-	19	-	182	-	1.24
Ni-Cr	.028 x 1		8	15	14.3	103	571	701	3.88	4.77
Wires exploded in sample cell geometry										
Cu	.020 x 1		8	11	12.1	42	172	226	2.47	3.25
Fe	.014 x 1		8	11	3.42	49	100	126	2.92	3.68

*Circuit inductance for all cases was 1.33 microhenrys.

ploding wires were the energies necessary (1) to melt the wire, (2) to vaporize the wire, and (3) to ionize electrons from the wire. Handbook values of specific heats, latent heats, and ionization energies were used to calculate the energy densities in Table III.^{36,39}

Assuming thermal equilibrium and energy densities greater than the vaporization energy, the particle energy and percent ionization can be calculated with the Saha equation. Rouse³⁷ calculated ionization equilibrium for a number of elements (including aluminum and iron) by the use of the Saha equation. Rouse considered the ionization of any number of electrons from the atoms as a function of temperature (up to 10^7 °K) and density of the gas. Since energy densities obtained in this experimental investigation were less than or only slightly greater than the ionization energy of the first electron, the Saha equation was not used. Instead, approximate results were calculated (e.g., Fig. 3) assuming that ionization took place if kinetic energies of the plasma particles was the same magnitude as the ionization energy.

5.2 Estimate of Error in Exploding Wire Results

The errors present in the measured discharge circuit parameters (charging voltage, extraneous circuit resistance, and circuit inductance), the calibration of the measuring circuits (voltage, current, and current derivative), and the measurements made with the coordinate comparator are discussed in Appendix A. Errors present in the calibration of the measuring circuits and those present in the measurements of the oscilloscope records by the coordinate comparator determined the errors in the final measured and calculated quantities. (The

Table III. Material properties and energy densities to melt, vaporize, and ionize wire material used for exploding wire experiments^{36,39}

Material	ρ (g/cm ³)	C_v ($\frac{\text{cal}}{\text{deg}\cdot\text{mole}}$)	T_m (°K)	T_v (°K)	E_m	Energy Density*		$(E_v + I_1)$
						E_v (eV/atom)	I_1	
Aluminum	2.70	7.0	932	2600	.304	3.76	5.98	9.74
Copper	8.92	7.5	1356	2868	.479	4.13	7.72	11.85
Chromium	7.20	6.0	2173	2495	.638	3.89	6.76	10.65
Iron	7.86	8.4	1808	3008	.717	4.83	7.87	12.70
Nickel	8.90	7.6	1728	3010	.656	5.01	7.63	12.64

*Increase in energy density above room temperature (300° K) to melt, vaporize, and ionize wire material.

propagation of variance formula was used in the error analysis of calculated quantities.)

Since the accuracy with which the various photographic records could be read determined the error associated with the voltage measurements, the error of the photographic measurements was taken to be the only source of error in the voltage curves. In general, the standard deviation in the voltage measurements was less than 3% except when the voltage was near the zeroline. The inductive voltage drop across a wire was corrected using the relation, $L_w (di/dt)$, where the initial value of the wire inductance was used for L_w . Since the inductance of a cylinder decreases with an increase in radius and a wire expands during an explosion, smaller values of L_w should have been used. (L_w was, in general, a function of time.) The inductive corrections were generally less than 2% except near the beginning of the discharge, where the current varied rapidly (di/dt large) and the voltage measured was relatively low. Note also that the voltage was always near the peak value when the wires were significantly expanded (i.e., near or above the vaporization point). Thus, the inductive corrections were much less than 2% when the wires were significantly expanded. As discussed in Section 4.2, the possibility of induced voltages in the high voltage probes was checked and found to be small. Thus, the standard deviation in the measured resistive voltage drop across a wire (total voltage minus the induced voltage) was less than 5% except near the initial portion of a discharge or where the voltage was low.

Errors in the calibration of the current measuring circuit and in reading of the oscilloscope current records determined the errors

characteristic of current curves in Figs. 8 through 33. The fractional standard deviation of the calibration of the current measuring circuit was .033 amperes per ampere. The standard deviation of distance measured using the coordinate comparator was .00497 inches. The standard deviation in the current measurements due to both current calibration and coordinate comparator measuring errors was less than 5% except when the current approached zero. Contact bounce in the closing of the air-gap switch, which was operated at lower voltage than the operational voltage range given by Harvey and Yevick,²² was observed on the initial portion of the current curves (one microsecond or less). Because of contact bounce, the current was not uniquely determined for the initial portion of a discharge. Thus, the standard deviation in current measurements during the initial portion of the discharge may have exceeded five percent.

The energy curves, calculated by the integration of the power curves, were of course determined in part by the initial current values. (Other calculated curves were not affected at later times by the inability to obtain accurate initial current measurements.) However, since the power curves also depend on the voltage curves and since voltage was low during the initial time interval (first microsecond of a discharge) in which current was not uniquely determined, the power was at a low level during the initial portion of each discharge. Thus, the portion of the power curves with the greatest fractional standard deviation had small amplitude and large errors were not introduced in the overall energy calculations.

To calculate the energy curves the power curves were integrated numerically by Simpson's rule. In carrying out the integration process

for the energy curves, a sufficient number of experimental points were measured to keep the estimated integration error less than one percent. Accuracy of the integration of the power curves was estimated by the relation⁴⁰

$$E_s \doteq -(\Delta t/90) [y_{-1} + y_{n+1} - 4(y_0 + y_n) + 7(y_1 + y_{n-1}) - 8(y_2 + y_4 + \dots + y_{n-2}) + 8(y_3 + y_5 + \dots + y_{n-3})] ,$$

where:

Δt is the time interval between measured points,

n is the number of intervals used in the numerical integration,

and

y_i is the instantaneous power after the i^{th} time interval.

By applying the propagation of variance formula to Simpson's rule, it was also noted that the fractional standard deviation of calculated energy was less than the fractional standard deviation of the power at any time, if a sufficient number of intervals were used in the numerical integration. Thus, in the energy calculations a sufficient number of intervals were used to keep the integration error less than one per cent and to also insure that the fractional standard deviation of the calculated energy was less than .10 joules per joule at the time of burst. Therefore, the estimate of standard deviation for the curves of the calculated quantities (resistance, power, energy) was generally less than 10%. Exceptions occurred if the current curves or the voltage curves were near the zeroline, and during a short time interval when contact bounce of the switch was important.

In determining the estimates of the maximum standard deviations

reported above, standard deviations were estimated for all the points of reported curves using the propagation of variance formula and the known estimated standard deviations of the measuring circuits; these maximum estimated standard deviations were as follows: voltage - 5%, current - 5%, and calculated values - 10%. To determine if significant differences existed between wire explosions with identical circuit and wire parameters, eleven standard iron wires were exploded as discussed in Section 4.3. (The estimated standard deviation of quantities near the time of burst should have been significantly less than the maximum standard deviation estimated by the propagation of variance formula, since neither the current nor the voltage curves were near the zeroline and contact bounce was also unimportant at the time of wire burst.)

Experimental standard deviations noted for the standard iron wires were as follows: time to burst - 7%, peak voltage - 4%, peak resistance - 11%, peak power - 12%, and energy to burst - 13%. Since the estimated standard deviations for values obtained near the time of burst of the standard wires were not significantly less than the maximum standard deviation estimated by the propagation of variance formula, it was concluded that actual differences existed in the wire explosions. The existence of such differences in the standard wire explosions was also indicated by the estimated standard deviation of the time of burst, since the sweep rate of the oscilloscope was more consistent than the estimated standard deviation. It is concluded that reproducibility of wire explosions was not within the calibration accuracy of the measuring circuits because of inhomogeneities in the wires and slight variation in the degree of contact between the wires and the brass leads of the discharge circuit.

Since only one size of wire with one set of circuit conditions was used in determining the reproducibility of wire explosions, error for other conditions can only be discussed qualitatively. The iron wire results (voltage, current, resistance, power, and energy) for all cases reported (Figs. 24 - 29) should be characterized by approximately the same fractional standard deviation as determined for the standard wire explosions. However, time reproducibility was expected to be better for wires exploded near the beginning of the capacitor discharge.²³ (e.g., The results of Fig. 29 should have better time reproducibility for the time of burst than the results of Fig. 28.)

In general, the 10 mil copper wire explosions had better time reproducibility than the iron wire explosions since the copper wire explosions occurred earlier in the discharge than the iron wire explosions. However, since the voltage for the 10 mil copper wire explosions increased rapidly to high values, the response of the high voltage probes could have limited the voltage measurement accuracy. Thus, the vertical error of curves for the 10 mil copper wire may have been larger near the voltage peaks than the error noted for the standard iron wire.

The wires which exhibited oscillatory behavior exploded after long time intervals (10-50 microseconds). Thus, inhomogeneities in the wires had long time intervals to affect the wire explosions. Inhomogeneities in the wires affected the formation of unduloids and the hydrodynamic motions which were present in slow wire explosions. Thus, slight initial inhomogeneity in a wire could have caused significant differences in measured and calculated quantities for an exploding wire. (e.g., The wires which exploded on the second current pulse did not show good time reproducibility for the time to burst.) Therefore, larger errors than

observed for the standard wire explosions were expected and observed for wires which exhibited oscillatory behavior in current and voltage waveforms.

5.3 Aluminum Wire Results

Figures 8 and 9 show the results for 32 mil diameter (28 gauge) one inch long aluminum wires. The capacitance used in both cases was 8 microfarads, and the charging voltages were respectively 11 and 15 kilovolts. Aluminum wires did not explode for capacitor discharges at 11 kilovolts but remained clamped in the circuit after capacitor bank discharge, although they were weakened at the point of attachment to the massive brass leads. The wires' physical appearance indicated surface melting and possibly some surface oxidation had occurred. The voltage and current traces had the characteristics of an RLC underdamped circuit for the entire discharge.

When the capacitor bank was initially charged to 15 kilovolts and then discharged through an aluminum wire, the voltage peaked during the second current pulse. Sufficient energy to vaporize the wires was deposited before the time of burst. However, Table II shows that deposited energy densities were not sufficient to cause appreciable ionization, since the energy density at which electrons are ionized from aluminum atoms is 9.74 eV/atom (See Table III). Since the voltage peaks were not relatively high and the voltage increases were not rapid, the aluminum wire explosions were classified as slow explosions. Data were not taken at 4 microfarads capacitance for aluminum wires since low energy oscillatory responses do not generate the high temperatures and high energy densities necessary to simulate a nuclear ex-

plosion.

5.4 Copper Wire Results

Figures 10, 11, and 12 show the results for 20 mil diameter copper wires exploded at 8 microfarads and 11 kilovolts. The voltage and current curves resemble the oscillatory response of an underdamped RLC circuit discharge. Sufficient energy to vaporize the wire was not deposited until after the fourth current pulse. Thus, physical distortions dominated the explosion mechanism; the wire melted and fell apart like a fuse. Arc breakdown of the surrounding air allowed the discharge to continue the oscillatory response. As in the case of 32 mil aluminum wire, data were not taken at 4 microfarads capacitance for 20 mil copper wire.

Figures 13 through 16 show the results for 20 mil diameter copper wires exploded at 8 microfarads and 15 kilovolts. These curves are particularly interesting since the explosion occurs during the second current pulse. Most of the reported exploding wire results are for cases of explosion during the first current pulse or slow discharges with oscillatory current and voltage curves.

The voltage peak (time of burst) was not completely reproducible when 20 mil copper wires were exploded using the same wire and circuit parameters. Since literature results indicate that best time reproducibility is noted for wires exploding near the beginning of the first current pulse,²³ good time reproducibility was not expected for wires exploding on the second current pulse. Factors which affected the time to burst were the wire-circuit contact and inhomogeneities of the wires. For example, small initial differences in a wire would be

greatly increased by physical distortions over extended discharge intervals (10-15 microseconds to the second current pulse).

Figure 34 shows the peak power as a function of wire length for the 20 mil copper wires exploded at 8 microfarads and 15 kilovolts. The peak power was approximately constant for the wire lengths of 1", 2", and 3" but definitely lower for the 1/2" wire. The peak power per unit length increased with decreasing wire length. Since the measured peak power per unit length of the 1/2" wire was not as large as predicted by extrapolating the results for the other three wire lengths to 1/2 inch, end effects were particularly important for the 1/2" long 20 mil diameter copper wire.

The results shown in Fig. 34 indicate that the peak power per unit length of wire for wires which explode on the second current pulse depends on wire length in the same way as wires which explode on the first current pulse. The increase in peak power per unit wire length with a decrease in wire length observed for the 20 mil copper wire agrees with the results of Leopold.²³ Leopold's results, however, are for wire explosions during the first current pulse and different circuit and wire parameters than used in this work. The peak power curve of Leopold shows a maximum, but only a broad maximum was indicated in results reported here. Figure 34 indicates that the maximum occurs for wires longer than 1/2" but insufficient data were available to determine at exactly what wire length the maximum occurred.

The energy deposited in the various wire lengths are compared to the amount of energy necessary to vaporize the wire in Fig. 35 with the time interval after burst used as a parameter. The amount of energy above the vaporization energy was greatest for the 1/2" wire for all

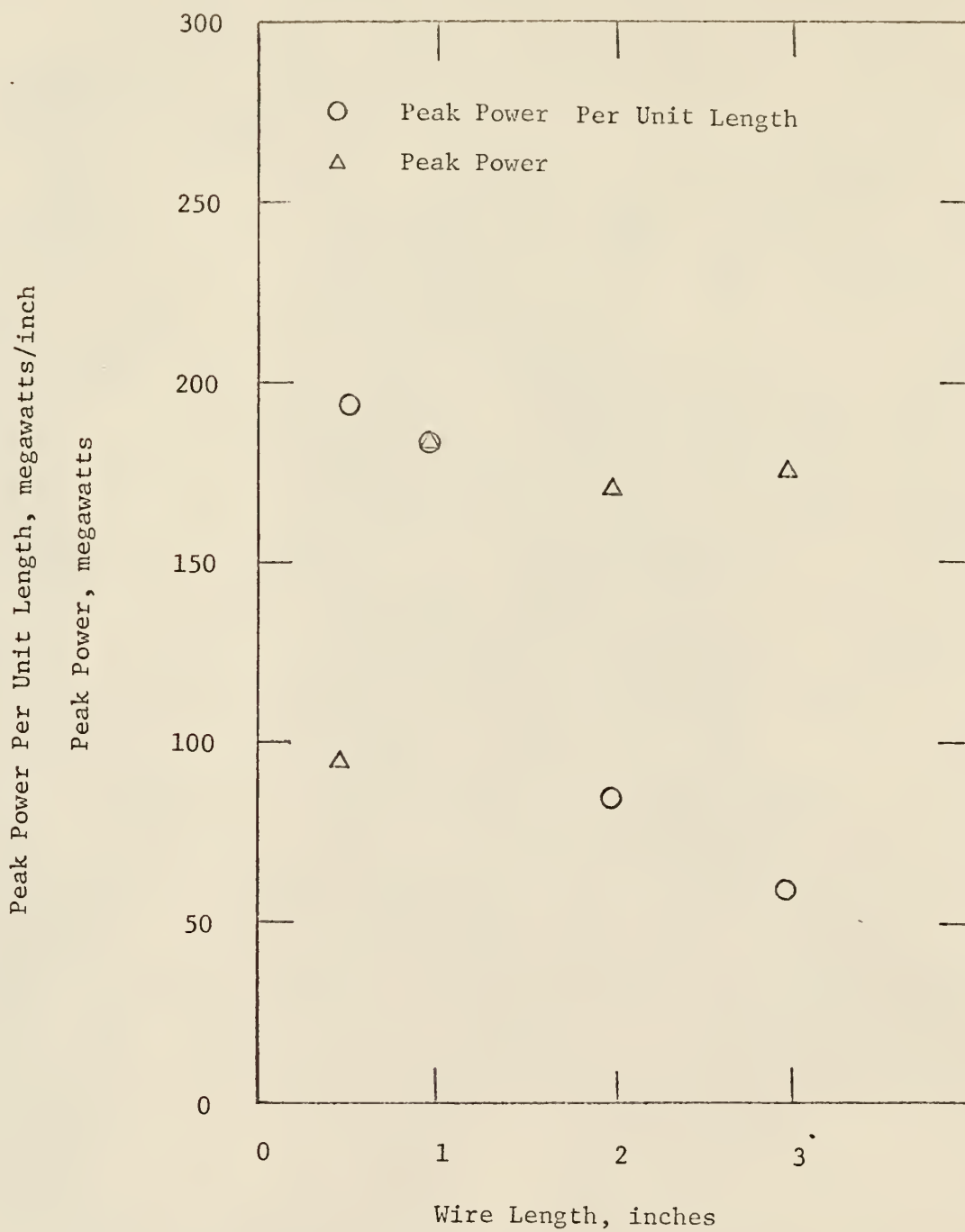


Figure 34. Peak power as a function of wire length.

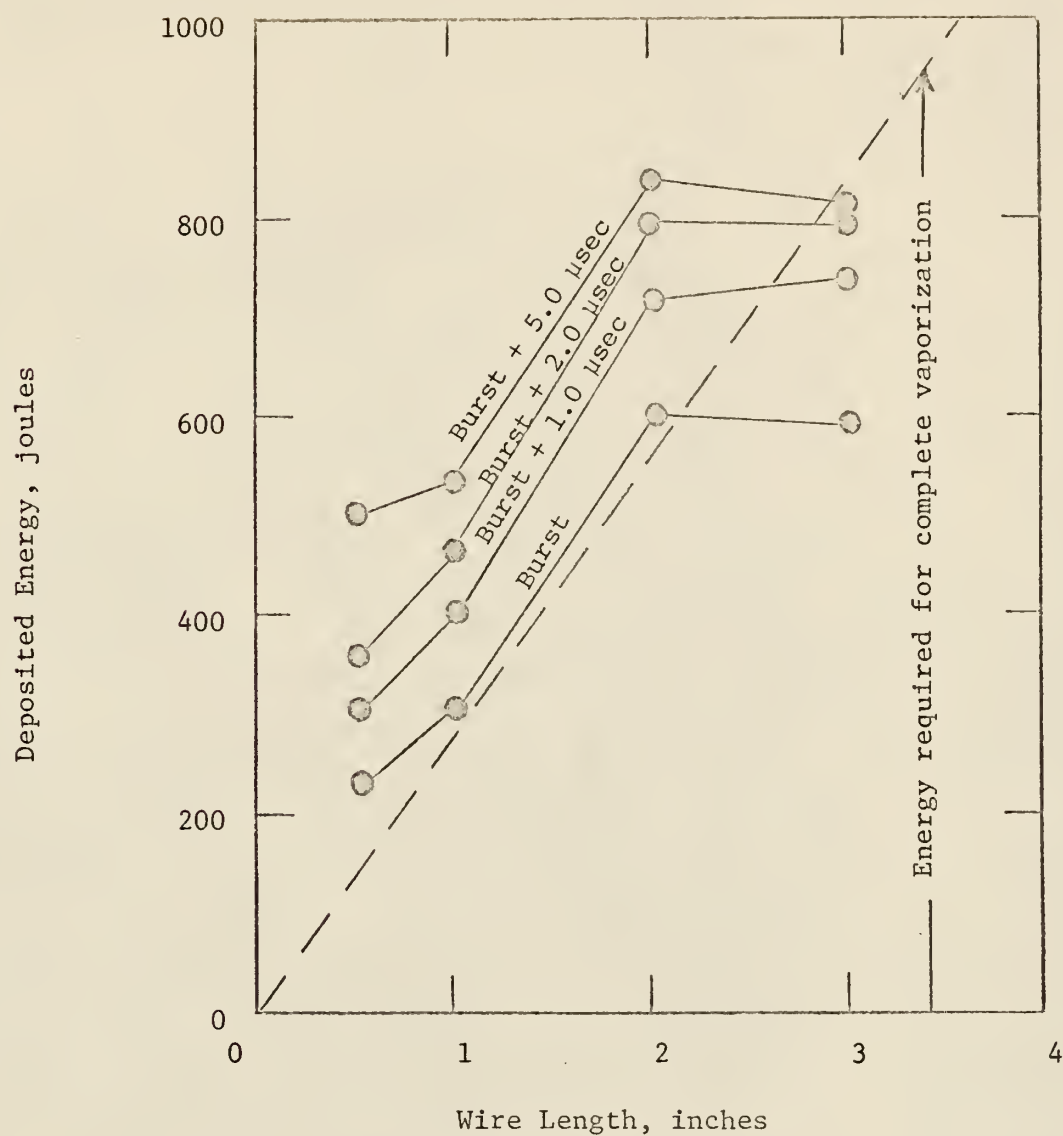


Figure 35. Energy deposition profiles for 20 mil diameter copper wire of various length.

time intervals of interest. The amount of energy above the vaporization energy was about the same for the 1" and 2" wires for the time intervals of interest. The vaporization energy was not deposited in the 3" wire before the end of the second current pulse.

Figure 36 shows the energy density deposited in a 20 mil copper wire as a function of wire length with the time after burst used as a parameter. Here the energy density increased with decreasing wire length. The more time considered after burst the sharper the increase in energy density with decrease in wire length. The results, however, do not determine if the energy deposited immediately after burst raised the temperature of the wire higher than the temperature at burst. Leopold's results showed that the energy deposited in a short time interval (approximately one microsecond) after the time of burst is important in obtaining high energy densities or at least keeping the energy densities at high levels.²³ Thus, explosions of shorter wires have high energy densities for longer periods of time than explosions of longer wires if end effects are not important.

The curves of Figs. 17 through 23, showing the results obtained for 10 mil diameter copper wire, have the same shape as those reported by Bennett.²⁵ The voltage traces exhibit the step change in voltage which corresponds to the melting of the wire. The magnitude of the voltage peaks were about twice the charging voltage of the capacitor bank; the peak power was also significantly greater than the theoretical estimate for an RLC discharge with constant resistance. These voltage and peak power characteristics are also observed in results reported by Bennett.²⁵

As discussed in Section 2.2, the temperature coefficient of wire

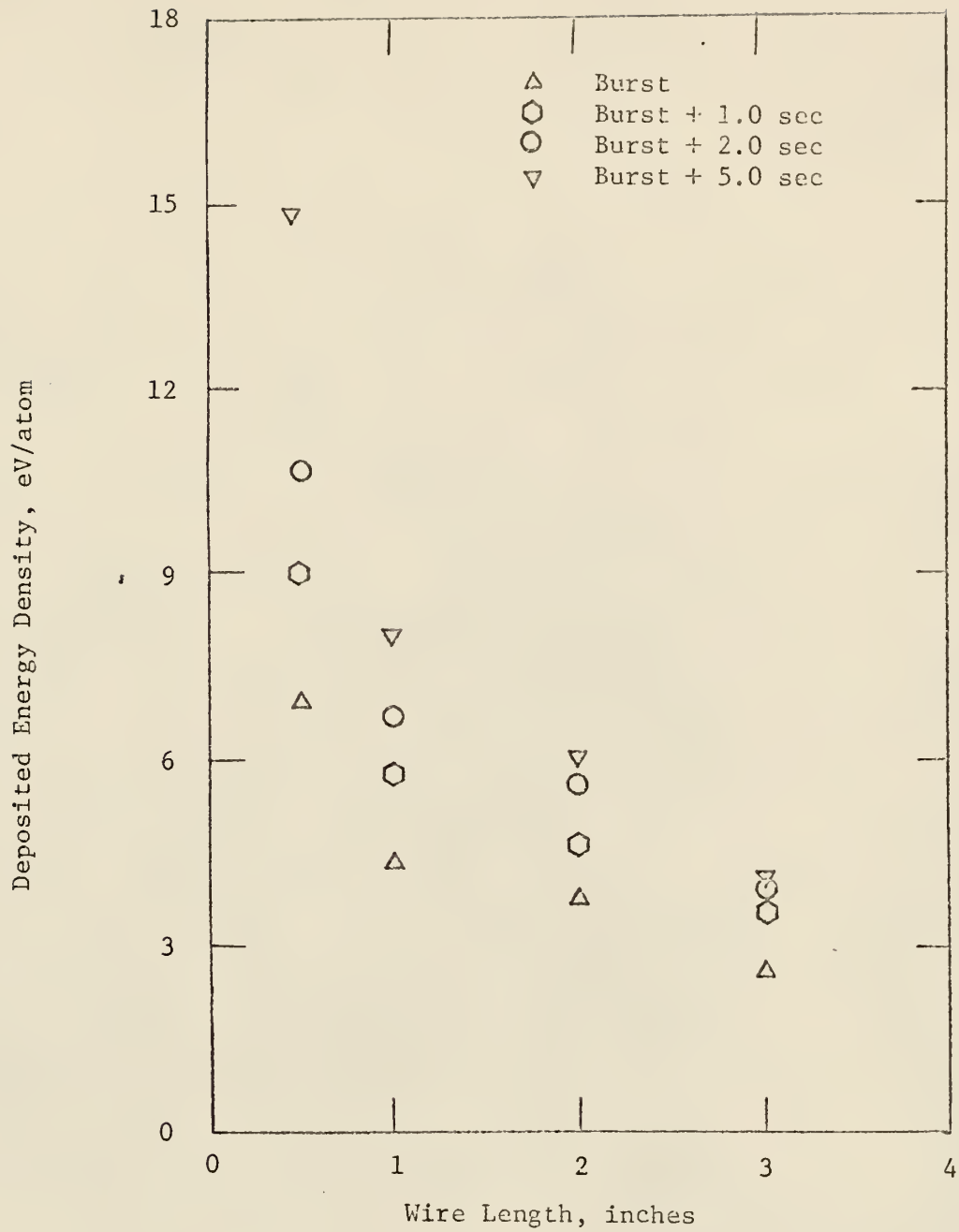


Figure 36. Deposited energy density for 20 mil diameter copper wire of various length. Time after burst used as parameter.

resistance determines the shape of the resistance curve between melting and vaporization. The temperature coefficient of resistivity for the liquid phase of copper is positive and thus, the resistance curves for the 10 mil copper wire explosions increase between the melting and the beginning of vaporization. Comparison of the resistance curves for 10 mil copper wire explosions (Figs. 17 through 23) show that the curves corresponding to the more energetic explosions had lower resistance peaks; thus the resistance anomaly was observed. The dark pause which is related to the resistance anomaly (discussed in Section 2.2) was observed for two of the less energetic wire explosions (i.e., the 3 inch wire which exploded at 8 microfarads and 11 kilovolts and the 1 inch wire which exploded at 8 microfarads and 8 kilovolts).

The time to burst, which was taken to be the time interval from the initiation of discharge to the voltage peak, decreased with a decrease in wire length while an increase in the initial charging voltage decreased the time to burst. The data taken for the 10 mil copper wire did not show a significant dependence of the time to burst on capacitance. The explosion of the 10 mil copper wire during the first current pulse and the explosion of the 20 mil copper wire during the second current pulse were consistent with reported results.^{23,24} The literature results in general show that the time to burst increases with an increase in wire diameter if other parameters are held constant.

Since copper has a low heat of vaporization¹⁴ it would be expected that the time to deposit sufficient energy to vaporize the copper is short compared to the time necessary for instabilities to develop. The current curves of Figs. 17 through 23 have maximum values near the end of vaporization which agrees with the characteristics of a class I

material described by Webb.¹⁴ The 10 mil copper wire results in Table II are also consistent with results reported by Leopold,²³ i.e., (1) peak power and deposited energy increase with an increase in circuit capacitance or circuit charging voltage, and (2) energy density and peak power per unit length increase with decreasing wire length.

The energy density necessary to completely vaporize a one inch copper wire 10 mils in diameter is 4.13 eV/atom (See Table III). In contrast with the iron wire results sufficient energy was deposited to vaporize completely the copper wires before the time to burst, except for the three inch wire exploded at 8 microfarads and 11 kilovolts. However, within the reliability of the handbook data used in the the theoretical calculations and the experimental standard deviation, the vaporization energy for the 3 inch copper wire exploded at 8 microfarads and 15 kilovolts was deposited before the energy plateau was obtained.

Although, in general, sufficient energy was deposited to vaporize completely the copper wires before the time of burst, unduloid characteristics were observed in the explosions. The voltage curves for the 3 inch wires show vaporization peaks even though, as noted above, sufficient energy was not deposited to vaporize entirely the wire material at the time the voltage peaks were noted. Unduloids were more prominent in the explosive mechanism for longer wires, since the burst times were longer. (These unduloids were probably formed in regions of the wire with initially higher resistivity where more energy was deposited and where the positive coefficient of resistivity of copper further increased inhomogeneity to form the unduloids. Thus, the

specific energy deposited along the length of wire was not constant and vaporization peaks in the voltage curves were observed even though the total energy deposited was not sufficient to vaporize completely the wire.

If the energy deposited in the 10 mil copper wires were greater than necessary to vaporize entirely the wire, it would be expected that the remaining energy would be used to heat the wire material above the vaporization temperature. If the energy density were raised higher than 11.85 eV/atom, electrons would be ionized from the copper atoms. At the time of burst the highest energy density obtained in the 10 mil diameter copper wire explosions in this study (i.e., for a one inch wire exploded at 8 microfarads and 15 kilovolts) was 8.68 eV/atom.

Although the energy densities deposited at the time of burst were less than the ionization energy (The energy density necessary for ionization of copper atoms is approximately 11.85 eV/atom.), Leopold's results show that the energy deposited in a short time interval after the time of burst is important in obtaining high energy densities. Thus, deposited energy densities in the first current pulse (last column of Table II) were considered to determine if electron ionization was achieved. Considering the first pulse energies of the two most energetic 10 mil copper wire explosions (12.70 eV/atom and 11.60 eV/atom), it is seen that some electron ionization was probably achieved. However, even for these energetic cases, the energy densities were not great enough to completely ionize the first electron from all copper atoms in the wire. Therefore, the temperature needed for the ionization of the first electron from the copper atoms was an upper limit of the temperatures reached by copper wires exploded during this study.

5.5 Iron Wire Results

The results for iron wires exploded at atmospheric conditions are shown in Figs. 24 through 29; the characteristics of the resistance curves were determined by the physical condition of the wire at various times during the discharge. The small jump in resistance noted between one and two microseconds after the initiation of the discharge was caused by melting of the wire. Since the temperature coefficient of resistance for the liquid phase of iron is small, the resistance curves have a nearly constant value between the end of melting and the beginning of vaporization.²⁸ The resistance reached larger magnitudes for the less energetic explosions, a characteristic of resistance anomaly of exploding wires. From these curves it is noted that when energy available from the capacitor bank was decreased, or when the length of the wire was increased, the restrike occurred later in the explosion. It is also apparent that arc breakdown of the air surrounding the wire occurred earlier in the explosion for the more energetic cases.

The time to burst (time interval from the initiation of the discharge to the voltage peak) decreased with a decrease in wire length; an increase in the initial charging voltage also decreased the time to burst. The data taken for the iron wire did not show a significant dependence of the time to burst on capacitance. The time to burst of the 14 mil iron wire was greater than the 10 mil copper wire with other parameters constant; this was expected since iron has a higher boiling point than copper and also the iron wires were of larger diameter than the copper wires.

A comparison of results noted for one inch and three inch iron

wires exploded at 8 microfarads and 11 kilovolts were consistent with the results of Leopold;²³ the energy density and the peak power per unit length were greater for the shorter wires. Iron, with its large heat of vaporization is classified as a class II material by Webb.¹⁴ The current curves in Figs. 24 through 29 have peaks near the time of melting (i.e., near the resistance jump) and the current curves are at low values or rapidly decreasing at the time of burst. Thus the current curves for the iron wire explosions are characteristic of those for a class II material.

The energy to raise an iron wire from room temperature to the atmospheric boiling point and completely vaporize the iron was calculated from heat capacity and latent heat values (See Table III). The results of the iron wire explosions show that except for the more energetic explosions, sufficient energy to vaporize the wires completely was not deposited before burst. (Compare values in column 9, Table II, with values in column 7, Table III.) Even for the most energetic cases, corresponding to Figs. 25 and 29, the deposited energy before burst was not much greater than the vaporization energy. Sufficient energy to vaporize the wire for the case corresponding to Fig. 27 was deposited during the first current pulse but after the time of burst. In remaining iron wire experiments, sufficient energy to vaporize the wire completely was not deposited.

The time to deposit sufficient energy for vaporization of class II materials is typically long compared to the instability time constant. Thus, the mechanism of the iron wire explosions was controlled by physical distortions of the wire (unduloids), and only segments of the wire were vaporized. Fewer unduloids were formed and larger portions of the

wire were vaporized in the more energetic wire explosions with higher peak powers.

The ionization energy at which the first electron is ionized from an iron atom is 12.70 eV/atom. Table II shows that energy densities obtained experimentally in this investigation were not sufficient to ionize electrons from iron wires. The results in Table II also show that peak power and deposited energy increase with an increase in circuit capacitance or circuit charging voltage. Thus, an increase in charging voltage or circuit capacitance would increase the deposited energy and produce higher temperatures. However, all eight available capacitors were used to obtain data presented in Table II and an increase in voltage was not practical during the present work because the high voltage probes were already being used at their upper operating limit.

5.6 Nickel-Chromium Wire Results

Figure 30 shows the results for a 28.5 mil (21 gauge) one inch long nickel-chromium wire exploded at 8 microfarads and 11 kilovolts. Hot metal was scattered from the original wire position in the discharge circuit indicating that the wire simply melted and was blown apart. The voltage and current were oscillatory.

Figure 31 shows the results obtained when a nickel-chromium wire was exploded at 8 microfarads and 15 kilovolts. Sufficient energy was deposited during the first pulse of this explosion to reach the boiling point of chromium (2495° K) and to vaporize the chromium. However, the power was low when the vaporization energy had been deposited and heat losses kept the temperature below the boiling point of chromium until

the second current pulse. The voltage peak occurring on the second current pulse exhibited a rapid rise but did not have large magnitude. At the time of burst sufficient energy had been deposited to reach the boiling point of iron (3008°K) or nickel (3010°K), but sufficient energy had not been deposited to vaporize the wire material completely. The vaporization of either chromium alone or only segments of the wire completely vaporizing caused the voltage spike. Since long times (≈ 15 microseconds) were available for physical distortions to affect the explosion, the most probable mechanism was complete vaporization of segments of the wire.

As noted, sufficient energy was apparently deposited before the end of the second current pulse to vaporize the nickel-chromium wire completely. However, the wire did not remain together more than about a microsecond after the voltage peak which was early in the second pulse. Thus, the explosion was dominated by arc discharge near the end of the second current pulse and the wire did not actually absorb energy during the last half of the second current pulse.

5.7 Summary of Bare Wire Results

The characteristics of the voltage, current, resistance, power, and energy curves of Figs. 8 through 31 are examined in Sections 5.3 through 5.6. These curves show good qualitative agreement with the literature; quantitative agreement could not be ascertained, however, since the circuit parameters were generally different from those described in the exploding wire literature. Significant variation between separate wire explosions was noted for wire explosions with identical circuit and wire parameters (See Section 5.2). It is expected that the

experimental error in future experiments can be reduced if a more consistent method is devised for attaching the wire to the brass leads and if additional improvements in the triggering circuit are made.

The characteristics of the curves shown in Figs. 8 through 31 are consistent with the physical properties of the wires. Melting of a wire was characterized by a small jump in the resistance curve while the temperature coefficient of resistivity was in agreement with the behavior of the resistance curves in the time interval between phase changes. The voltage curves had vaporization spikes for cases which had deposited energy densities less than the vaporization energy at the time of burst; this is characteristic of a typical unduloid mechanism. The physical characteristics of low heat of vaporization and high heat of vaporization materials were observed in the 10 mil copper wire and the 14 mil iron wire results respectively. The resistance anomaly, which is dependent on the physical condition of the wire, existed for wire explosions which had sufficient energy deposited for vaporization.

The characteristics of the explosions noted in this study may be summarized as follows: (1) oscillatory voltage and current response, (2) explosion of the wire on the second current pulse, and (3) explosion of the wire on the first current pulse. Oscillatory responses are known to be characteristic of exploding wires with slow energy deposit; they produce low temperatures and are thus not of interest in simulating a nuclear explosion. The wire explosions noted during the second current pulse were unique to this study; literature results showed either oscillatory responses or responses with explosion during the first current

pulse only.

The energetics of this study's wire explosions were consistent with exploding wire literature, i.e., energy density increased with an increase in charging voltage and a decrease in wire length. (End effects were important for wires shorter than about one-half inch.) The relation between copper wire diameter and time to burst was consistent with literature results, i.e., the time to burst decreased with a decrease in wire diameter. Copper, a low heat of vaporization material, exhibited more energetic wire explosions than iron, a high heat of vaporization material. The copper wires which exploded near the peak of a current pulse were well matched to the circuit parameters and produced the more energetic wire explosions.

If an appreciable amount of material is used to simulate the chemical environment of an underground nuclear explosion, electrons must be ionized not only from the wire material but also from the material surrounding the wire. To obtain appreciable ionization of material surrounding the wire, the wire material must have much greater energy densities initially than required for the surrounding material. Tables II and III show that the energy deposited in the wires before burst was not sufficient to ionize electrons from the wire material. Although energy deposited in a short time interval (approximately one microsecond) after the time of burst can actually be added to the system,²³ energy densities obtained during these experiments were still not sufficient to ionize material surrounding the wires. Thus, energy densities greater than obtained in the bare wire explosions of this study must be achieved. Increased energy deposit in the wires can be attained by increasing the charging voltage or capacitance; as an alternative,

containment of wire material for a longer period of time would also result in increased energy deposit.

The upper temperature limit attained by wires exploded during this study was estimated by the two methods developed in Section 3.0. The two methods assumed respectively (1) no energy losses from the wire before the time of wire burst, and (2) radiation losses were the only significant energy losses during the discharge. (The assumption of the second method results in radiation losses balancing the power input to the wire at the time of the peak power.) The results calculated by the two methods are reported in Table IV and show that the maximum temperatures estimated by the second method are an order of magnitude larger than the maximum temperatures estimated by the first method. From this observation it appears that a discrepancy has resulted since the second method considered energy losses while the first method did not. However, the cases reported in Table IV have power curves which increase rapidly to their peak values; this means that the power (rate of energy deposit) was more than sufficient to balance the radiant energy losses at the time of the peak power. Therefore it is concluded that enough energy was not actually deposited in the wire before the peak power to account for the maximum temperatures estimated by the second method.

The time of burst of an exploding wire is near the peak power (i.e., at the peak voltage); a wire is therefore not confined after the peak power. If it were possible to keep wire intact a longer time, sufficient energy would be deposited to produce temperatures that better correspond to an equality between radiation losses and peak power. Therefore it is desirable to develop a technique to contain the wire

Table IV. Maximum estimated temperature of exploding wires

Material	WIRE	PARAMETERS			MAXIMUM ESTIMATED TEMPERATURE		
		Size (in.)	C (μ F)	CIRCUIT V_o (kV)	Method #1 ($^{\circ}$ K)	Method #2 ($^{\circ}$ K)	
Al		.032 x 1	8	15	5,250	74,300	
Cu		.020 x 1/2	8	15	10,500	95,500	
Cu		.020 x 1	8	15	3,800	94,800	
Cu		.020 x 2	8	15	3,700	78,100	
Cu		.010 x 1	4	11	6,400	114,000	
Cu		.010 x 1	4	15	8,700	142,000	
Cu		.010 x 1	8	8	5,300	92,400	
Cu		.010 x 1	8	11	5,000	124,000	
Cu		.010 x 1	8	15	15,000	147,000	
Fe		.014 x 1	4	15	3,800	99,400	
Fe		.014 x 1	8	15	6,000	106,000	

current pulse; the current was initially lower for the sample cell geometry than for the bare iron wire explosion. This result would be expected if adding the sample cell arrangement to the circuit increased the circuit resistance. (Increased circuit resistance would lower the current for the initial portion of the discharge.) Note also that the current during the initial portion of the discharge was not accurately determined because of experimental difficulties (See Section 5.2).

The current noted for both the bare wire and the wire in the sample cell were nearly the same magnitude shortly after the wire melted but before the vaporization voltage peak. In this region the observed currents for the two cases were within the variation observed for the currents of the eleven standard one inch iron wire explosions. Since the wire resistance dominated the circuit resistance during the time interval after the wire melted (for both bare wire explosions and sample cell explosions), current and voltage were not expected to be affected by the sample cell during the time interval after the wire melted but before the vaporization voltage peak.

The current rapidly decreased to low values immediately after the time of burst for an iron wire in the cell geometry; thus increased wire resistance was observed in the cell geometry. This increase in wire resistance in the cell geometry was expected based on the work of Reithel and Blackburn with confined wires.²⁹

The explosion of a 14 mil iron wire one inch long at 8 microfarads and 11 kilovolts was not as rapid in the cell arrangement as under ambient atmospheric conditions; the time to burst in the cell geometry was 3.42 microseconds while the time to burst for a bare iron wire was 3.04 microseconds. The increased time for the iron wire to explode in the sample

cell arrangement agrees with the results of Nash et. al., who reported that pulses were broadened and flattened for confined wire explosions.

The energy deposited in the iron wire in the sample cell geometry was not significantly different from the deposited energy in the bare iron wire experiments. The average energy deposited at the time of burst for 11 bare wire explosions was 119 joules with an estimated standard deviation of 15 joules. The energy deposited in the iron wire in the cell geometry was 100 joules, which is lower than the average of the bare wire explosions by about one standard deviation.

The peak power was definitely lower for the sample cell geometry than for the bare wire geometry. The average of the 11 standard one inch wires was 91 megawatts with an estimated standard deviation of 11 megawatts. The peak power for the sample cell geometry, 49 megawatts, was lower because the voltage pulse of the confined wire was not as high as those for the bare wire. The voltage peak in the cell geometry was apparently limited by sparkover from the wire to the cell wall during the time interval of the peak voltage drop across the wire. Although the peak power was lower for the sample cell geometry, the amount of energy deposited was not significantly different. Thus, if sparkover had not limited the voltage peak, higher energy densities would have been deposited for the sample cell geometry than for bare wire explosions. It is therefore evident that more attention must be given to sample cell design with improved short circuit prevention.

One inch long, 20 mil diameter copper wires were also exploded at 8 microfarads and 11 kilovolts in the sample cell. Comparing the sample cell results of Fig. 33 with the bare 20 mil copper wire results of Fig. 11, it is noted that the explosion in the sample cell showed a definite

voltage peak during the second current pulse while the peak was not observed for the bare wire explosions. The sample cell's voltage peak indicated that the sample cell stabilized and confined the wire after melting. This conclusion is based on the fact that the period of the waveforms was shorter for confined wires than for bare wires. (In fact, the bare wire period was nearly the same as the period of the free response with a shorting bar used in place of the wire.) The shorter period of the sample cell wire explosion indicated that the coaxial feature of the sample cell geometry had reduced the inductance of the circuit. The second pulse peak power levels were about 5 times larger using the sample cell geometry as compared with bare wire results for the same voltage and capacitance. The deposited energy was also greater for the sample cell geometry. The calculated energy required to vaporize the 20 mil copper wire completely at the atmospheric boiling point was 282 joules. Since the sample cell voltage peak was near the end of the second current pulse, most of the second current pulse energy (226 joules) was deposited in the wire. Thus, the deposited energy was less than the energy to completely vaporize the wire. Since the voltage peak was broad and flat, the explosion in the cell geometry was not expected to completely vaporize the 20 mil copper wire.

The voltage peak for the 20 mil copper wire was less than 3 kilovolts in the cell geometry. The peak voltage for the iron wire in the cell geometry was 7.7 kilovolts, while the voltage peak for bare iron wire was about 13 kilovolts. Thus voltage drop across the iron wire in the cell geometry was probably limited by sparkover. Consistent with this interpretation was the observation that when attempting to use sample cells with diameters less than $3/8$ " it was not possible to obtain

meaningful results because of voltage sparkover. The 10 mil diameter copper wire exploded at 8 microfarads and 11 kilovolts in air had a voltage peak of approximately 27 kilovolts (See Fig. 20). A voltage trace taken for a 10 mil diameter copper wire exploded at 8 microfarads and 11 kilovolts in the sample cell geometry had the characteristic jump associated with the wire melting, but the voltage suddenly dropped to zero a short time after the wire melted. Sparkover from the wire to the tube wall would account for the sudden voltage drop. Thus, although the sample cell geometry stabilized and confined wires after melting, breakdown of the insulation between the wire and the tube wall caused sparkover to the cell wall, limiting the voltage peak and precluding the attainment of more energetic explosions. Therefore, future work should consider the design of an improved sample cell.

6.0 Conclusions

The basic considerations in the simulation of the chemical environment of a nuclear explosion are the generation of high temperatures, high pressures, strong shock waves, nonequilibrium conditions, and a material environment of the correct composition. Knowing the material environment of a nuclear explosion and the necessary temperature distribution and/or energy densities about 30 seconds after the shot (the approximate time at which the chemistry of the fallout is determined) the required exploding wire circuit parameters to simulate a nuclear environment can be calculated theoretically as discussed in Section 3.0. However, for the theoretically calculated circuit parameters to produce the desired temperatures, wires must be well matched to the circuit parameters.

Since radiation energy losses are large at high temperatures, energy must be deposited rapidly in an exploding wire to simulate a nuclear explosion. Thus, it would seem that peak power would be the important factor in describing the energetics of a wire explosion. However, the experimental results for wire explosions during the second current pulse (See Section 5.4) show that these wire explosions had high energy densities and thus give experimental evidence that extremely fast explosions with extremely high peak powers may not be absolutely necessary to obtain temperatures above 10^5 °K.²⁶ It was also concluded from these experimental results that parameters other than peak power are important in obtaining the greatest energy deposit and highest temperatures.

Since enough energy was not deposited before the peak power to account for the maximum temperatures estimated by the method of balancing

radiation losses with peak power (See Section 5.7), it was concluded that deposited energy must be considered as well as the peak power. It was noted for the wire explosions of this study that only 15-40% of the energy initially stored in the capacitor bank was deposited in the wires before burst. Therefore, when using the design method proposed in Section 3.0 one must insure that about 6 times the energy needed to raise the wire material to the desired temperature is available from the capacitor bank.

If sufficient energy is available the theoretical design method proposed in Section 3.0 is applicable to fast wire explosions; further the experimental results of this study indicate that temperatures within an order of magnitude of design temperature are obtainable from a circuit designed by the theoretical method proposed in Section 3.0. The experimental results show that peak power (theoretically calculated using equation 11) predicted from the circuit parameters can be exceeded with copper wire if the wire size is well matched to the circuit parameters. (This situation results because the wire resistance can vary causing an experimental peak power greater than that theoretically calculated assuming constant wire resistance.) However, determining the temperature of the wire based on the peak power leads to an overestimation of the temperature by about an order of magnitude. Thus experimental temperatures attainable for fast wire explosions may be an order of magnitude lower than that predicted by the design method proposed in Section 3.0.

Although the wire explosions of this study were too slow to produce explosive ablative type wire explosions (See Appendix G), more energetic explosions may produce this type of explosion. The skin effect present

in explosive ablative explosions would result in lower temperatures than could be attainable if the skin effect were not present. Since the proposed design method was shown to underestimate the experimental temperature for fast wire explosions, experimentally attainable temperatures for explosive ablative type wire explosions would be more than an order of magnitude lower than temperatures predicted by the theoretical method proposed in Section 3.0.

With respect to the design of exploding wire circuits and experiments to obtain particular desired temperatures it should be noted that several different combinations of circuit and wire conditions can be used to obtain the desired temperatures and energy densities. However, in designing the experiments the circuit parameters determine the cost of necessary experimental equipment. Thus, the optimum design (minimum cost consistent with experimental objectives) would be obtained by selecting the circuit parameters with theoretical expressions while also considering economic factors and experimentally determining the wire parameters best matched to the selected circuit parameters. Rapid matching of the wire parameters to the circuit parameters is possible since the qualitative effects of wire parameters (discussed in Section 2.2) are known.

Experimental results show that broadening the peak of the power curve (resulting from longer confinement of the wire material after the vaporization energy was deposited) would produce higher energy densities even though the peak may be slightly lowered. The sample cell was designed to accomplish this confinement. Although only limited experimental results were obtained in the sample cell geometry some useful results were noted (See Section 5.8). Energy deposited in a 20 mil copper wire in the

cell geometry was greater than that deposited in a bare copper wire; however, energy deposited in a confined iron wire was not greater than deposited in a bare iron wire. Sparkover was believed to have limited both the peak power and energy deposited in the iron wire. Although the sample cell geometry will apparently confine the wire material for longer periods of time than wires exploded at atmospheric conditions, the sparkover problem must be eliminated for the sample cell geometry to be effective in obtaining high energy densities.

From the results of this study it has been found that additional work is needed before quantitative data for simulation of the chemical environment in a nuclear explosion can be obtained by exploding wire experiments. Considerations in this additional work should include:

- 1) The conditions which will produce the highest energy densities in the medium surrounding an exploding wire should be determined by a parameter study. Specific parameters of interest would include wire size, wire material, sample cell size, and material in the sample cell. Constraints on the system would include: (a) adequate sample cell design to prevent sparkover, and (b) the total material present in the cell would have to simulate the environment of a nuclear explosion. Prevention of sparkover was a major problem in sample cell design, particularly for wire explosions with high peak voltages and high peak powers. Therefore, it would be desirable to experimentally determine if a sample cell which alters the magnetic pressure on an exploding wire is significantly better than a sample holder simply made of an insulating material. If a sample cell incorporating the magnetic pinch is found to produce significantly higher experimental temperatures than a simple insulating sample holder, a sample cell with improved insulating characteristics will

be required.

2) A study of the upper limiting energy density that can be deposited in an exploding wire is required. Although the general qualitative effects (e.g., An increase in charging voltage of the capacitor bank increases the energy density in an exploding wire.) are known for fast explosions, practical limits may occur in explosive ablative type wire explosions. Thus, an analog computer model to simulate the mechanism of an exploding wire should be developed. Model design considerations would include: (a) an equation of state for the wire, (b) theoretical and experimental results describing the energy distribution in an exploding wire, (c) the skin effect, (d) the application of magnetic fields on an exploding wire, and (e) confinement of wire material by surrounding material. The Saha equation should be an adequate first approximation to calculate the amount of ionization of the material. Also, equations which describe the application of magnetic fields to plasmas for controlled fusion research should be applicable to exploding wires.

3) Direct experimental methods (such as spectrometry⁴¹ or calorimetry) for measuring the temperature or energy densities in the material of an exploding wire experiment should be used to check the accuracy of the voltage-current method. The voltage-current method of analysis may be limited by the following factors: (a) Only deposited energy was measured and one must rely on incomplete theoretical models to determine the energy transferred from the wire to the sample material, (b) Specific heat and latent heat data are incomplete for the high temperatures involved, and (c) The energy density or temperature distribution in the sample material can not be measured directly by the voltage-current method.

Spectrometry and calorimetry can measure more directly the temperature or the energy densities in the sample volume. The measurement of pressure in the sample volume would also be necessary to completely specify the thermodynamic conditions; if the temperature and pressure are reproducible the chemical effects should also be reproducible.

4) Since the chemical effects to be simulated in a nuclear explosion are far removed from generally known chemistry and since literature on chemical effects induced by exploding wires is very limited, it would be desirable to simulate known high temperature chemical processes with exploding wires. In this way experimental results with exploding wires could be verified and the consistency improved. The high temperature chemistry effects produced by shock tubes, plasma arcs, and laser beams have been studied. However, results with these methods are limited to low pressures and are also limited in the amount and type of chemical material present. Thus, exploding wires with high pressures and with the introduction of metal in the high temperature chemical environment are not completely analogous to the chemistry of shock tubes, plasma arcs, or laser beams. Therefore, some interpretation of results obtained by these methods in terms of the experimental conditions present in the exploding wire experiment will still be required to determine the experimental accuracy obtainable for chemical effects produced by exploding wires.

Acknowledgments

The author wishes to express his gratitude to Dr. Walter Meyer for his advice and constructive criticism during this study and to the Kansas State University Nuclear Engineering faculty and staff for their help. In particular thanks are due Mr. R. E. Hightower and Mr. R. L. Wild for their assistance in assembling the apparatus and their helpful suggestions concerning the operation of the apparatus. Thanks are also due Dr. Basil Curnutte, Jr., Department of Physics, for the loan of the capacitor bank and x-ray power supply unit. The use of the Department of Applied Mechanics' traveling microscope is also appreciated. The author wishes to express his sincere appreciation to both the Kansas State University Engineering Experiment Station and the National Science Foundation for their financial support.

LITERATURE CITED

1. W. G. Chace, "A Survey of Exploding Wire Progress," in Exploding Wires, Vol. 3, edited by W. G. Chace and H. K. Moore, pp. 1-7, Plenum Press, New York, (1964).
2. Plowshare Series: Report No. 2, Proceedings of the Second Plowshare Symposium (Held at San Francisco, May 13-15, 1959): Part I: Phenomenology of Underground Nuclear Explosions, UCRL-5675.
3. Plowshare Series: Report No. 2, Proceedings of the Second Plowshare Symposium (Held at San Francisco, May 13-15, 1959): Part II: Excavation, UCRL-5676.
4. Plowshare Series: Report No. 2, Proceedings of the Second Plowshare Symposium (Held at San Francisco, May 13-15, 1959): Part III: Recovery of Power and Isotopes from Contained Underground Nuclear Explosions, UCRL-5677.
5. Plowshare Series: Report No. 2, Proceedings of the Second Plowshare Symposium (Held at San Francisco, May 13-15, 1959): Part IV: Industrial Uses of Nuclear Explosives in the Fields of Water Resources, Mining, Chemical Production, and Petroleum Recovery, UCRL-5678.
6. Plowshare Series: Report No. 2, Proceedings of the Second Plowshare Symposium (Held at San Francisco, May 13-15, 1959): Part V: Scientific Applications of Nuclear Explosives in the Fields of Nuclear Physics, Seismology, Meteorology, and Space, UCRL-5679.
7. Proceedings of the Third Plowshare Symposium (Held at Lawrence Radiation Laboratories, April 21-23, 1964) Engineering with Nuclear Explosives, TID-7695.
8. Walter Meyer and F. G. Svensson, August Monthly Report, Chemical Engineering Division, Lawrence Radiation Laboratory, (1964).
9. W. G. Chace and E. M. Watson, "A Bibliography of Electrically Exploded Conductor Phenomenon," Optical Physics Laboratory Project 8608, Air Force Cambridge Research Laboratories, L. G. Hanscom Field, Mass., (1962).
10. W. H. Richardson, "Exploding Wire Phenomena," SCR-53, (1958).

11. R. C. Maninger, "Preburst Resistance and Temperature of Exploding Wires," in Exploding Wires, Vol. 3, edited by W. G. Chace and H. K. Moore, pp. 47-64, Plenum Press, New York, (1964).
12. Früngel, Frank B. A., High Speed Pulse Technology, Vol. 1, pp. 379-391, Academic Press, New York, (1965).
13. W. G. Chace and M. A. Levine, "Classification of Wire Explosions," J. Appl. Phys. 31, 1298 (1960).
14. F. H. Webb, H. H. Hilton, P. H. Levine, and A. V. Tollestrup, "The Electrical and Optical Properties of Rapidly Exploded Wires," in Exploding Wires, Vol. 2, edited by W. G. Chace and H. K. Moore, pp. 37-75, Plenum Press, New York, (1962).
15. F. D. Bennett and J. W. Marvin, "Current Measurement and Transient Skin Effects in Exploding Wire Circuits," Rev. Sci. Inst. 33, 1218-1226 (1962).
16. Jack Katzenstein, "The Pinch Effect in the Exploding Wire Phenomena," in Exploding Wires, Vol. 1, edited by W. G. Chace and H. K. Moore, pp. 135-144, Plenum Press, New York, (1959).
17. Jan Nasilowski, "Unduloids and Striated Disintegrations of Wires," in Exploding Wires, Vol. 3, edited by W. G. Chace and H. K. Moore, pp. 295-313, Plenum Press, New York, (1964).
18. F. D. Bennett, G. D. Kahl, and E. H. Wedemeyer, "Resistance Changes Caused by Vaporization Waves in Exploding Wires," in Exploding Wires, Vol. 3, edited by W. G. Chace and H. K. Moore, pp. 65-88, Plenum Press, New York, (1964).
19. T. J. Tucker and F. W. Neilson, "The Electrical Behavior of Fine Wires Exploded by a Coaxial Cable Discharge System," in Exploding Wires, Vol. 1, edited by W. G. Chace and H. K. Moore, pp. 73-82, Plenum Press, New York, (1959).
20. R. C. Maninger, "Effects of Transmission Lines in Applications of Exploding Wires," in Exploding Wires, Vol. 2, edited by W. G. Chace and H. K. Moore, pp. 109-126, Plenum Press, New York, (1962).

21. J. K. Trolan, F. M., Charbonnier, F. M. Collins, and A. H. Guenther, "A Versatile Ultrafast Pulsed Power System," in Exploding Wires, Vol. 3, edited by W. G. Chace and H. K. Moore, pp. 361-389, Plenum Press, New York, (1964).
22. R. Harvey and G. J. Yevick, "Quiet, Simple, Inexpensive Air-Gap Switch," Rev. Sci. Inst. 34, 1444-45 (1963).
23. H. S. Leopold, "Effect of Bridgewire Parameters on Explosive Initiation," in Exploding Wires, Vol. 3, edited by W. G. Chace and H. K. Moore, pp. 125-152, Plenum Press, New York, (1964).
24. C. P. Nash and C. W. Olsen, "Factors Affecting the Time to Burst in Exploding Wires," in Exploding Wires, Vol. 2, edited by W. G. Chace and H. K. Moore, pp. 5-13, Plenum Press, New York, (1962).
25. F. D. Bennett, H. S. Burden, and D. D. Shear, "Correlated Electrical and Optical Measurements of Exploding Wires," Phys. Fluids 5, 102-113 (1962).
26. O. H. Zinke, R. B. Owen, and C. K. Manka, "Translational Equilibrium of Wires Exploded in Vacuo," in Exploding Wires, Vol. 3, edited by W. G. Chace and H. K. Moore, pp. 103-113, Plenum Press, New York, (1964).
27. M. E. Meeker, "Solid and Solid-Liquid Phases in Wires at High Current Densities," SCTM 314-58(51), (1958).
28. V. V. Bondarenko, I. F., Kvartskhava, A. A. Pliutto, and A. A. Chernov, "Resistance of Metals at High Current Densities," JETP 1, 221-226 (1955).
29. R. J. Reithel and J. H. Blackburn, "A Hydrodynamic Explanation for the Anomalous Resistance of Exploding Wires," in Exploding Wires, Vol. 2, edited by W. G. Chace and H. K. Moore, pp. 21-31, Plenum Press, New York, (1962).
30. C. P. Nash, R. P. DeSieno, and C. W. Olsen, "Electrical and Emissive Properties of Exploded Confined Conductors," in Exploding Wires, Vol. 3, edited by W. G. Chace and H. K. Moore, pp. 231-246, Plenum Press, New York, (1964).

31. A. Sakurai and T. Takao, "Effect of Applied Axial Magnetic Field on the Exploding Wire Phenomenon," in Exploding Wires, Vol. 3, edited by W. G. Chace and H. K. Moore, pp. 247-256, Plenum Press, New York, (1964).
32. F. D. Bennett, "Energy Partition in Exploding Wire Phenomena," Phys. Fluids 1, 515-522 (1958).
33. Handbook of Chemistry and Physics, C. D. Hodgman, Editor in Chief, (Chemical Pub. Co., Cleveland, 1959), 40th ed., p. 3257.
34. V. E. Scherrer, "The NRL-AFSWP Exploded Wire Research Program," in Exploding Wires, Vol. 1, edited by W. G. Chace and H. K. Moore, pp. 118-134, Plenum Press, New York, (1959).
35. G. J. Dienes and G. H. Vineyard, Radiation Effects in Solids (Interscience Publishers, Inc., New York, 1957), Chap. 2, p. 35.
36. C. E. Moore, Atomic Energy Levels, U. S. National Bureau of Standards Circular, No. 467, Vol. III, Washington, (1958).
37. C. A. Rouse, "Ionization Equilibrium Equation of State," Astrophys. J. 134, 435-446 (1961).
38. K. G. Moses and T. Korneff, "Voltage Measurements in the Presence of Strong Fields," Rev. Sci. Inst. 34, 849-853 (1963).
39. Handbook of Chemistry and Physics, R. C. Weast, Editor in Chief, (Chemical Pub. Co., Cleveland, 1967), 48th ed., p. D-32.
40. K. L. Nielsen, Methods in Numerical Analysis (Macmillan Company, New York, 1964), 2nd ed., Chap. 4, p. 137.
41. R. Eastwood, R. Hysom, and R. Woodruff, "Determination of the Ion Density in an Exploding Wire Plasma by Spectroscopic Means," unpublished report Kansas State University Department of Physics.
42. L. Baker, Jr., R. L. Warchal, R. C. Vogel, and M. Kilpatrick, "Studies of Metal-Water Reactions at High Temperatures: I. The Condenser Discharge Experiment: Preliminary Results with Zircconium," ANL-6257, (May, 1961).

43. N. R. Draper and H. Smith, Applied Regression Analysis (John Wiley & Sons, Inc., New York, 1966), Chap. 2, pp. 77-81.
44. E. J. Kobetich, "Plotting Subprogram for use on the IBM-1410 Computer and the IBM-1403 Printer," unpublished report Kansas State University Department of Physics, (June 20, 1965).
45. J. D. Jackson, Classical Electrodynamics (John Wiley & Sons, Inc., New York, 1962), Chap. 10, pp. 320-322.

APPENDIX A

Measurement and Calibration of Circuit Parameters

In the calibration of the voltage measuring circuit calibrated voltage amplitudes up to 7 kilovolts were used; an analysis of the oscilloscope photographic records of voltage measurements showed that the accuracy of these measurements was limited by the reading of the records with a Leitz Coordinate Comparator with scale divisions of 10^{-5} inches. The precision of measured distances was limited by the ability to set the microscope cross hairs on the oscillogram traces. By measuring 55 distances 5 times each, the standard deviation of each reading was determined to be .00497 inches. After calibration of the voltage measuring circuit the static voltmeter was calibrated using the voltage measuring circuit; the fractional standard deviation of the static voltmeter was found to be .011 volts per volt.

Experimental data to determine the capacitance of the discharge circuit were obtained by discharging the capacitor bank through calibrated resistors (Tru-ohm). Voltage-time oscillogram records were obtained by measuring the voltage across 5×10^4 ohms resistance. The vertical position of each voltage trace was measured by the coordinate comparator at horizontal intervals of $\Delta t/R_{cal} = 10^{-6}$ sec/ohm. The vertical position of the zeroline reference was also measured for each oscilloscope record.

A weighted least squares fit in the logarithmic domain was used to calculate the capacitance (See Appendix B). Since the positions measured at a large number of time intervals after the initiation of

discharge through a calibrated resistor approached the zeroline reference position, a least-squares fit using too many points did not give accurate results. Switch effects were also significant when the voltage remaining on the capacitor bank was small. Therefore, least-square fitting of the data was accomplished using 3 to 11 data points and the F test number was used to determine the number of points which gave the best fit for each oscilloscope record.

Five oscillograms were photographed on each of five separate days for a capacitor bank discharge with 8 capacitors (Nominally 1 μ F each and initially charged to 8 kV) in parallel. The values of capacitance which gave the best fit (F test number) for each of the 25 oscillograms were averaged to obtain the capacitance of the capacitor bank. With 4 capacitors in parallel, 7 oscillogram records were obtained. The 7 records were obtained during two days. The same procedure was used to determine the capacitance which gave the best least-squares fit for each trace and the results of 7 traces were averaged. The variance of the capacitance calculated using equation (B-6) was the result of the variance in the fitting of one curve, but significant variation was expected to possibly occur between different discharges. Thus, the variance of the capacitance was estimated using

$$\sigma^2(\bar{C}) = \left(\frac{1}{N-1}\right) \left(\frac{1}{N}\right) \sum_{i=1}^N (\bar{C} - C_i)^2, \quad (A-1)$$

and also using equation (B-6) together with the propagation of variance formula. The hypothesis of no variation of the capacitance from day to day was accepted since the Student's t-test did not show differences greater than the 95% confidence range. Also, there was insufficient evidence to show that the variance calculated by equation (A-1) was sig-

nificantly (F test -- 95% confidence level) larger than the variance calculated by equation (B-6) and the propagation of variance formula. However, the estimated variance calculated by equation (A-1) was the value used to calculate the reported standard deviation for capacitance. The following values were calculated for the capacitance at an initial charging voltage of 8 kV:

<u>Number of Capacitors</u>	<u>Total Capacitance (microfarads)</u>
4	3.587 \pm .042
8	7.712 \pm .051

The capacitance was also determined for eight capacitors with an initial charging voltage of 11 kV; the calculated value of capacitance for each of these discharges was within the standard deviation of a single observation of the values reported above.

The current waveform was used to determine the extraneous circuit resistance and the inductance of the exploding wire circuit. The current in a circuit containing only resistance and inductance when a charged capacitor is connected to the circuit has the following form:⁴²

$$i = \frac{V_o}{\sqrt{(L/C) - (R^2/4)}} [\exp (-Rt/2L)] [\sin \sqrt{(1/LC) - R^2/4L^2} \quad t] \quad (A-2)$$

for the underdamped case of $R^2 < 4L/C$

where:

i is the current in kA,

V_o is the charging voltage in kV,

R is the total circuit resistance in ohms,

L is the total circuit inductance in henries,

C is the capacitance in farads, and

t is the time in seconds.

For the case of $R^2 \ll 4L/C$ equation (A-2) can be expressed approximately as follows:

$$i \cong K[\exp(-Bt)][\sin(\omega t)] \quad (A-3)$$

where:

$$K = V_o (C/L)^{1/2} ,$$

$$B = R/2L , \text{ and}$$

$$\omega = (1/LC)^{1/2} .$$

For the exploding wire circuit used in this study the total circuit resistance was the sum of the wire resistance and the extraneous circuit resistance. With a shorting bar substituted for the wire, the total circuit resistance was the extraneous circuit resistance and R^2 was much less than $4L/C$. Thus, the period of the oscillation was

$$\tau = 2\pi(LC)^{1/2} . \quad (A-4)$$

Fifty-seven oscillogram records were used to measure the period with the capacitance of $7.712 \pm .051$ microfarads. The arithmetic average of the measured periods was $20.11 \pm .03$ microseconds. (The error limit reported is the estimated standard deviation.) The variance of the period of the circuit with the shorting bar in place was estimated using

$$\sigma^2(\bar{\tau}) = \left(\frac{1}{N-1}\right) \left(\frac{1}{N}\right) \sum_{i=1}^N (\tau_i - \bar{\tau})^2 \quad . \quad (\text{A-5})$$

where:

$$N = 57$$

$\bar{\tau}$ = arithmetic average of the measured periods (20.11 μsec).

The circuit inductance was calculated from the measured values of the period and the previously determined value of capacitance using

$$L = (\tau/2\pi)^2 (1/C) \quad . \quad (\text{A-6})$$

The variance of the circuit inductance was determined using the propagation of variance formula:

$$\sigma^2(F) = \left(\frac{\partial F}{\partial x_1}\right)^2 \sigma^2(x_1) + \left(\frac{\partial F}{\partial x_2}\right)^2 \sigma^2(x_2) + \dots + \left(\frac{\partial F}{\partial x_m}\right)^2 \sigma^2(x_m) \quad . \quad (\text{A-7})$$

where:

$$F = F(x_1, x_2, \dots, x_m), \text{ and}$$

x_i ; $i = 1, 2, \dots, m$ are independent variables.

Applying equation (A-7) to (A-6) and carrying out the partial differentiation yields

$$\sigma^2(\bar{L}) = (\tau/2\pi^2 C)^2 \sigma^2(\tau) + (\tau/2\pi C)^4 \sigma^2(C) \quad . \quad (\text{A-8})$$

Thus, the calculated value of inductance is $1.33 \pm .01 \mu\text{H}$.

The peak values of current are when $t = \tau(2n - 1)/4$ where n is a positive integer. The value of the current at the n^{th} peak is given by

$$i_n = (-1)^{n+1} K[\exp(B\tau)]^{-(2n-1)/4} \quad (A-9)$$

Therefore, if A_n is the absolute value of the current at the n^{th} peak and is measured on the oscilloscope photographic record using distance units, then

$$X_n = \frac{A_n + A_{n+1}}{A_{n+2} + A_{n+3}} = \exp(B\tau) = \exp(2\pi^2 RC/\tau) \quad (A-10)$$

The effective circuit resistance from peak n to peak $n+3$ was calculated from the following equation:

$$R_n = (\tau/2\pi^2 C) \ln X_n \quad (A-11)$$

for values of $n = 1, 2, \dots, 7$ for each recorded oscillogram. The variance of the circuit resistance was calculated using the propagation of variance formula:

$$\sigma^2(R_n) = (R_n/C)^2 \sigma^2(C) + (R_n/\tau)^2 \sigma^2(\tau) + (R_n/X_n \ln X_n)^2 \sigma^2(X_n) \quad (A-12)$$

where:

$$\sigma^2(X_n) = (1 + X_n^2)/(A_{n+2} + A_{n+3})^2 \sigma^2(A), \text{ and}$$

$$\sigma^2(A) = (.00497 \text{ in})^2 \text{ is the reading variation.}$$

The computer program described in Appendix C was used to calculate values from equations (A-11) and (A-12) and the output of the computer program was used to calculate a weighted average resistance for each discharge using

$$R_i = \frac{\sum_{n=1}^7 w_n R_n}{\sum_{n=1}^7 w_n} \quad (A-13)$$

where:

$$w_n = (1/\sigma^2(R_n)) .$$

Fifteen oscillograms, obtained from discharges of the capacitor bank through a shorting bar, were measured for current amplitudes at the current peaks. Results for each oscillogram were calculated as described above and the results of the fifteen oscillograms were averaged to determine the extraneous circuit resistance;

$\bar{R}_e = .0351 \pm .0006$ ohms. The standard deviation reported is the square root of the variance which was calculated using

$$\sigma^2(\bar{R}_e) = \left(\frac{1}{N-1}\right) \left(\frac{1}{N}\right) \sum_{i=1}^N (\bar{R}_e - R_i)^2 \quad (A-14)$$

where:

$N = 15$, and

\bar{R}_e is the arithmetic average of the extraneous circuit resistance of fifteen oscillograms. The variance, $\sigma^2(\bar{R}_e)$, was also calculated by applying the propagation of variance formula to equation (A-13) and to the averaging of the fifteen oscillograms. The F test showed that the variance calculated using equation (A-14) was significantly larger than the variance calculated by the propagation of variance formula. This indicates that significant variation of the measured current occurred between different discharges.

The output of the current measuring circuit was calibrated using the same oscillogram measurements which were used to calculate the circuit inductance and the extraneous circuit resistance. Equation (A-9) yields

$$i_n - i_{n+1} = K(-1)^{n+1} \{ [\exp(B\tau)]^{-(2n-1)/4} + [\exp(B\tau)]^{-(2n+1)/4} \} . \quad (\text{A-15})$$

Substituting from (A-10) yields

$$i_n - i_{n+1} = K (-1)^{n+1} [X^{-(2n-1)/4} + X^{-(2n+1)/4}] . \quad (\text{A-16})$$

The measured value on the photographs which corresponded to the current, $(i_n - i_{n+1})$, was the distance $(A_n + A_{n+1})$ which was the vertical distance between peaks n and $n + 1$ on the photographic records. Thus, the vertical scale of the current waveform was calculated using

$$I_n \text{ (kA/division)} = \left(\frac{K}{A_n + A_{n+1}} \right) [X^{-(2n-1)/4} + X^{-(2n+1)/4}] . \quad (\text{A-17})$$

for $n = 1, 2, \dots, 7$. The computer program described in Appendix C used equation (A-17) and the propagation of variance formula applied to equation (A-17) to calculate values of I_n and $\sigma^2(I_n)$ for $n = 1, 2, \dots, 7$.

The output of the computer program described in Appendix C was used to calculate a weighted average for each oscilloscope trace using

$$I_i \text{ (kA/division)} = \frac{\sum_{n=1}^7 w_n I_n}{\sum_{n=1}^7 w_n} \quad (\text{A-18})$$

where:

$$w_n = \frac{1}{\sigma^2(I_n)} .$$

Results for each oscillogram were calculated as described above and the results of the fifteen oscillograms were averaged. From these calculations the vertical scale of the current waveforms was determined to be $I = 19.44 \pm .65$ kA/photo division for the following circuit parameters; $R_{int} = 5$ kohm, $C_{int} = .001$ μ F, and switch setting of amplifier $L_s = 20$ volts/cm.

The standard deviation of a single observation for the current measuring circuit was calculated by the propagation of variance formula and by the following equation:

$$\sigma^2(I) = \left(\frac{1}{N-1}\right) \sum_{i=1}^{15} (\bar{I} - I_i)^2, \quad (A-19)$$

where:

$N = 15$, and

\bar{I} is the arithmetic average of the current scale which was calculated from fifteen oscillograms. Since the standard deviation of each current measurement was of interest, the standard deviation of a single observation, $\sigma^2(I)$, was determined instead of the standard deviation of the mean, $\sigma^2(\bar{I})$. Similar to the results of the extraneous circuit resistance the F test showed that the variances calculated by the two methods differed significantly. The variance calculated using equation (A-19) gave larger variance and was the value used to calculate the reported estimate of the standard deviation of a single observation.

The vertical scale for other integrating circuit parameters was given by

$$I' \text{ (kA/photo division)} = (10 R_{int} C_{int} V_{L_s}) I \quad (A-20)$$

where:

R_{int} is the resistance of the integrating circuit (kohm),
 C_{int} is the capacitance of the integrating circuit (μF), and
 V_{L_s} is the switch setting of amplifier L_s on the current measuring circuit.

The time derivative of the current in an RLC circuit for the underdamped case has the following form:

$$(di/dt) = \frac{1}{\sqrt{1 - \frac{R^2 C}{4L}}} (V_o/L) [\exp -(Rt/2L)] [\cos \sqrt{\frac{1}{LC} - \frac{R^2}{4L^2}} t]. \quad (A-21)$$

where the notation is the same as in equation (A-2). For the case of $R^2 \ll 4L/C$ equation (A-21) can be expressed approximately as follows:

$$(di/dt) = (V_o/L) [\exp (-Rt/2L)] [\cos (\omega t)] . \quad (A-22)$$

An analogous procedure was used to calibrate the (di/dt) waveform as was used to calibrate the current. The time derivative of the current at the m^{th} peak is given by

$$(di/dt)_m = (-1)^{m-1} (V_o/L) [\exp -(m-1)B\tau/2] . \quad (A-23)$$

The quantity Y_m was defined by

$$Y_m = \frac{D_m + D_{m+1}}{D_{m+2} + D_{m+3}} \quad (A-24)$$

where D_m is the absolute value of the current derivative at the m^{th} peak and is measured on the oscilloscope record using divisions on the photograph as units. The vertical scale of the (di/dt) waveform was determined using the following equation:

$$(dI/dt)_m \text{ (kA} \cdot \text{sec}^{-1}/\text{division)} = \frac{V_o}{L(D_m + D_{m+1})} [Y^{-(m-1)/2} + Y^{-m/2}] \quad . \quad (\text{A-25})$$

for $m = 1, 2, \dots, 7$. A weighted average of the vertical scale of the current derivative on each oscilloscope record was calculated using

$$(dI/dt)_i \text{ (kA} \cdot \text{sec}^{-1}/\text{division)} = \frac{\sum_{m=1}^7 w_m (dI/dt)_m}{\sum_{m=1}^7 w_m} \quad (\text{A-26})$$

where:

$$w_m = \frac{1}{\sigma^2 (dI/dt)_m} \quad .$$

The computer program described in Appendix D was used for calculations in calibrating the circuit for measuring the time derivative of current. Equations (A-24), (A-25), and (A-26) were used in the computer program described in Appendix D. The propagation of variance formula was also applied to the above equations and programmed in the computer code. Results for each oscillogram were calculated as described above and the results of ten oscillograms were averaged. The estimated variance of a single observation was calculated by the propagation of variance and also by using

$$\sigma^2(dI/dt) = \left(\frac{1}{N-1}\right) \sum_{i=1}^{10} [\overline{(dI/dt)} - (dI/dt)_i]^2 \quad . \quad (\text{A-27})$$

where:

$N = 10$, and

$\overline{(dI/dt)}$ is the arithmetic average of the current derivative scale of ten oscillograms.

The F test showed that the variance calculated using equation (A-27) was significantly larger than the variance calculated by the propagation of variance formula. The results of the calibration of the current derivative measuring circuit were:

$dI/dt = (5.42 \pm .12) \times 10^9 \text{ A}\cdot\text{sec}^{-1}/\text{photo division}$, which were valid for the following amplifier settings; $V_{L_p} = 20 \text{ V/cm}$, and $V_{L_s} = 1 \text{ V/cm}$.

The vertical scale for other time derivative circuit parameters for the measuring circuit was given by

$$(dI'/dt) = (V_{L_p} V_{L_s} / 20) (dI/dt) \text{ A}\cdot\text{sec}^{-1}/\text{photo division.} \quad (\text{A-28})$$

APPENDIX B

Description and Explanation of IBM-1410 Computer Program for
Calculating Capacitance of Discharge Circuit

The free response of an overdamped resistance-capacitance network has the form

$$V_R(t) = V_0 \exp(-t/RC) \quad (B-1)$$

Transforming to the natural logarithmic domain gives

$$z = z_0 + (t/R) a \quad (B-2)$$

where the quantities are defined as;

$$z = \ln V(t) , \text{ and}$$

$$a = -(1/RC) .$$

Written in matrix form, the weighted least squares fit of data to equation (B-2) is⁴³

$$b = (T^T W T)^{-1} T^T W z, \quad (B-3)$$

where

$$b = \begin{Bmatrix} z_0 \\ a \end{Bmatrix}, \quad z = \begin{Bmatrix} z_1 \\ z_2 \\ \vdots \\ z_n \end{Bmatrix},$$

$$T = \begin{Bmatrix} 1 & t_1/R \\ 1 & t_2/R \\ \vdots & \vdots \\ 1 & t_n/R \end{Bmatrix}, \text{ and} \quad W = \begin{Bmatrix} w_1 & 0 & 0 & \dots & 0 \\ 0 & w_2 & 0 & \dots & 0 \\ \vdots & & \cdot & & \vdots \\ 0 & \cdot & \cdot & & w_n \end{Bmatrix}.$$

The variance of the estimate is⁴³

$$\sigma_{\text{est}}^2 = \frac{z^T W z - b^T (T^T W) z}{\# \text{ of degrees of freedom}} \quad . \quad (\text{B-4})$$

The weights of z used in the calculations were

$$w_i = (1/\sigma^2(z_i)) = \frac{v_i^2}{\sigma^2(V_i)} \quad . \quad (\text{B-5})$$

The variance of the voltage, $\sigma^2(V_i)$, was determined by the variance of measuring distances on the photographs with the traveling microscope (See Appendix A).

The variance of the capacitance for the least-squares fit was calculated from⁴³

$$\sigma^2(C) = C^4 A_{22} \sigma_{\text{est}}^2 \quad , \quad (\text{B-6})$$

where

$$(T^T W T)^{-1} = \begin{pmatrix} A_{11} & A_{12} \\ A_{21} & A_{22} \end{pmatrix} \quad .$$

The above equations were programmed in FORTRAN IV language for the IBM 1410 computer. The source program is listed and the logic diagram is shown in this appendix. Table B-1 defines important symbols used in the program.

The input to the program was arranged as follows:

TIME DATA: FORMAT(8F10.0)

T(J): Time parameter data (actual time from the start of the oscilloscope trace divided by the calibrated resistance in the circuit) at which voltage measurements were obtained. Data were read in with eight values per card.

Table B-1: Symbols used in the IBM-1410 computer program for calculating capacitance of discharge circuit

Symbol	Explanation
CAP	Least squares fit value of capacitance
F	F test number
I	I th time the photograph was measured
J	J th position on the photograph
K	Number to identify photograph (data set for sub-run)
SIGC	Estimated standard deviation of capacitance from least squares fit
SIGV	Estimated standard deviation of initial voltage on capacitor bank from least -squares fit
SUMPC	Estimated variance removed by the correlation
T(J)	Time/calibrated resistance in circuit
V(I,J)	Voltage on photograph at time T(J) for measurement # I
VARES	Variance of the estimate
VO(I)	Zero voltage reference for the I th measurement
VZERO	Least squares value of initial voltage
WW	Weight of voltage at time T(J)
X	Reading variance of voltages
Z	Natural logarithm of voltage V(J)

CARDS USED FOR SUB-RUNS

FIRST CARD: FORMAT(2I2)

IX: Number of times photograph was measured.

JX: Number of data points taken on each photograph.

SECOND CARD: FORMAT(5F10.0)

VO(I): Position of zero line for I^{th} measurement of the photograph.

REMAINING CARDS: FORMAT(5F10.0)

V(I,J): Measured position of voltage at time corresponding to T(J) for I^{th} reading. The position of the voltage at T(1) for five measurements was punched on the first card. The following cards had positions of voltage at T(J) consecutively for $J = 2, 3, \dots, 11$. Each card had five punched values for five measurements of photograph.

(Data for multiple sub-runs were fed in order with one set of cards for each of the sub-runs. JX for each sub-run must be less than or equal to the number of points read in for the time data.)

The output of the program was in printed form. Values printed were: K, J(number of points used in least squares fit), CAP, SIGC, VZERO, SIGV, and F.


```

C      THIS PROGRAM COMPUTES THE CAPACITANCE AND THE INITIAL VOLTAGE OF
C      AN OVERDAMPED RESISTANCE-CAPACITANCE NETWORK
      MONTE      JOB  CAPAC
      MONTE      CONT OLIVER BLOCK,NUC.ENGG.,15XIN.,10PAGES
      MONTE      ASGN MJB,12
      MONTE      ASGN MGO,16
      MONTE      MODE GO,TEST
      MONTE      EXEQ FORTRAN,,,,,,CAPAC
      DIMENSION V(5,11),T(11),VO(5)
90  FORMAT(5F10.0)
91  FORMAT(8F10.0)
92  FORMAT(1H ,I4,3X,I4,5X,F12.5,5X,F10.5,10X,F12.5,5X,F12.8)
93  FORMAT(27H VARIANCE MATRIX,   A(1,1)=,F12.8,5X,8H A(1,2)=,
      2F12.8,5X,8H A(2,1)=,F12.8,5X,8H A(2,2)=,F12.8)
94  FORMAT(3H K=,I2,5X,3H J=,I2,5X,19H MEASURED VARIANCE=,F12.8)
95  FORMAT(14H F TEST NUMBER,5X,F10.5)
96  FORMAT(2I2)
97  FORMAT(1HL,3X,1HK,5X,1HJ,6X,11HCAPACITANCE,10X,3HDEV,16X,4HVOLT,9X
      J,2HDEV)
      READ(1,91)(T(J),J=1,11)
      DO12K=23,100
      WRITE(3,97)
      READ(1,96) IX,JX
      READ(1,91)(VO(I),I=1,IX)
      READ(1,91)((V(I,J),I=1,IX),J=1,JY)
      DO15I=1,IX
      DO15J=1,JX
13  V(I,J)=V(I,J)-VO(I)
      BA=0.0
      BB=0.0
      BC=0.0
      BT=0.0
      BTT=0.0
      Y1=0.0
      Y2=0.0
      Y3=0.0
      DO12J=1,JX
      JJ=J-1
      XI=IX
      AV=0.0
      DO14I=1,IX
14  AV=V(I,J)+AV
      AV=AV/XI
      XI=IX-1
      X=0.0000247
      WW=AV*AV/X
      Z=ALOG(AV)
      Y1=WW*7+Y1
      Y2=WW*7*T(J)+Y2
      Y3=Z*7*WW+Y3

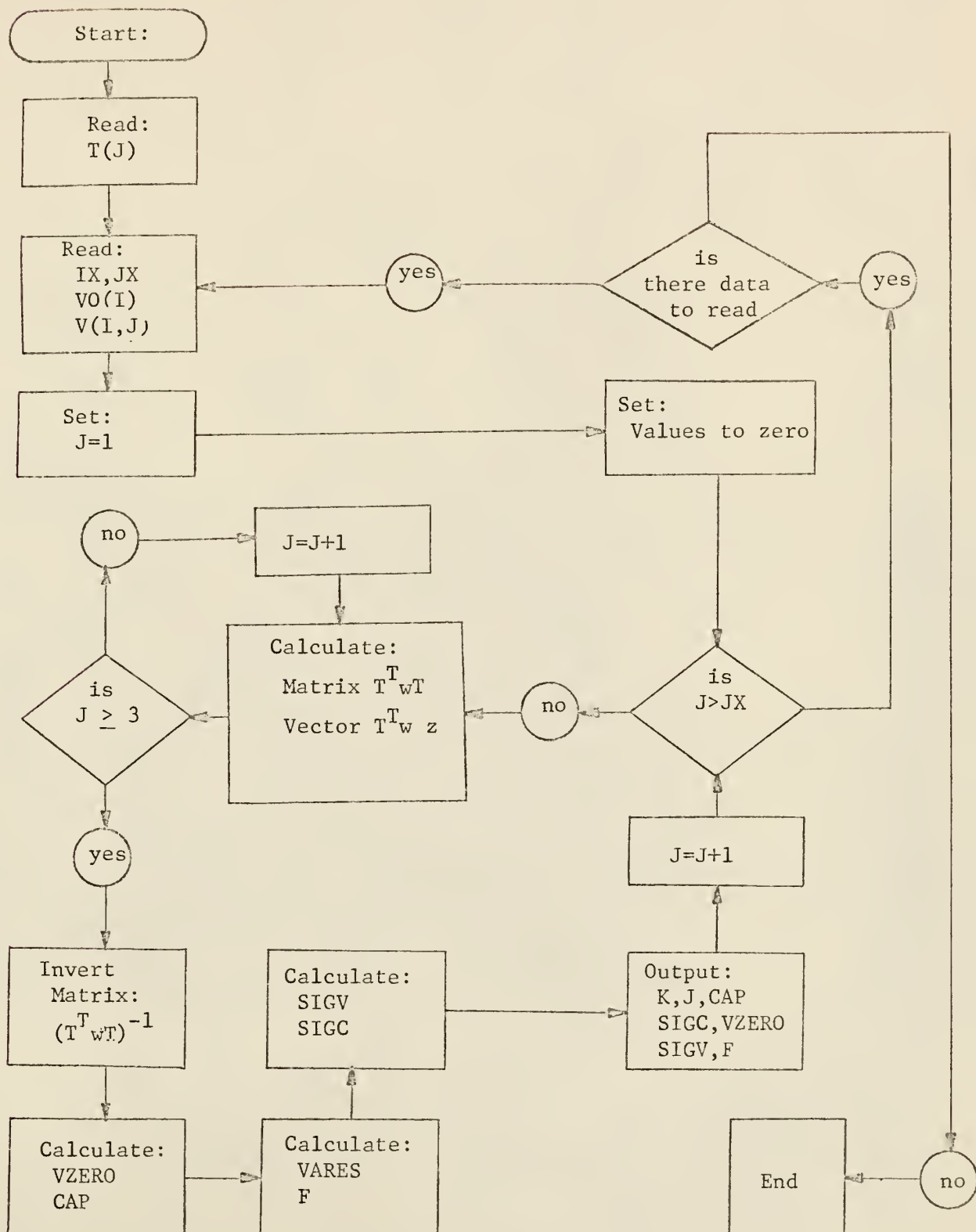
```

```

ET=T(I)*T(J)+PT
BTT=T(J)+BTT
BA=WW+BA
F=WW*T(J)+BE
BC=WW*T(J)*T(J)+BC
A(1,1)=RA
A(1,2)=RB
A(2,1)=RR
A(2,2)=RC
IF(JJ)12,12,12
12 CONTINUE
DET=A(1,1)*A(2,2)-A(1,2)*A(2,1)
W=A(1,1)
A(1,1)=A(2,2)/DET
A(1,2)=-A(1,2)/DET
A(2,1)=-A(2,1)/DET
A(2,2)=W/DET
VV=A(1,1)*Y1+A(1,2)*Y2
VZFRC=EXP(VV)
CAP=(1.0/(A(2,1)*Y1+A(2,2)*Y2))
XJ=J
XJJ=J+1
VARES=(Y3-VV*Y1-(Y2/CAP))/XJJ
F=SQRT(A(1,1)*VARES)
D=SQRT(A(2,2)*VARES)
SUMPC=(BT-(BTT*BTT/XJ))/(CAP*CAP)
F=SUMPC/VARES
SIGV=VV*VZFRC*B
SIGC=CAP*CAP*D
WRITE(3,92)K,J,CAP,SIGC,VZFRC,SIGV
WRITE(3,95)F
12 CONTINUE
STOP
END
MON$      EXEC LINKLOAD
          CALL CAPAC
MON$      EXEC CAPAC,MJR
MON$      JOB  ACT$SOLIVER BLOCK          NUC ENGG  0237C40412

```

Figure 37. Logic diagram for capacitance of discharge circuit computer program.



APPENDIX C

Description and Explanation of IBM-1410 Computer Program for
Calculating Extraneous Circuit Resistance and for
Calculating the Calibration of the Current Measuring Circuit

This computer program was written to calculate the extraneous circuit resistance of the discharge circuit and to calculate the calibration of the current measuring circuit. The experimental procedure used to obtain the data is discussed in Section 4.2, and the equations used in the calculations are discussed in Appendix A. Equations used in the calculations include (A-17), (A-10), (A-11), and (A-12). These equations were programmed in FORTRAN IV language for the IBM-1410 computer. The source program is listed and the logic diagram is shown in this appendix.

Table C-1 defines important symbols used in the program.

The input to the program was arranged as follows:

FIRST CARD: FORMAT(8F10.0)

1) T: Period of oscillation, 2) C: Capacitance of capacitor bank,
3) V0: Initial charging voltage on capacitor bank, 4) VART:
Estimated variance of measured capacitance, 6) VARV: Estimated
variance of static voltmeter measurements, &) VARA: Estimated
reading variance of photograph measurements, and 8) F: Conversion
factor from measuring units to photograph units.

CARDS USED FOR SUB-RUNS

INITIAL CARD FOR EACH SUB-RUN: FORMAT(2I2)

1) L: Number of first current peak entered as data, and
2) N: Number of last current peak entered as data.

Table C-1: Symbols used in the IBM-1410 computer program for calculating the extraneous circuit resistance and for calculating the calibration of the current measuring circuit.

Symbol	Explanation
A(I)	Vertical position of 1 th current peak as measured by the traveling microscope
AMIC	Current per microscope division
APH	Current per photo division
C	Capacitance of capacitor bank
DEVD	Estimated standard deviation of DN
DEVM	Estimated standard deviation of AMIC
DEVP	Estimated standard deviation of APH
DEVR	Estimated standard deviation of RE
DN	Difference in value of current between peaks I and I+1
F	Conversion factor (.363 microscope divisions per photo division)
I	Number to identify current peaks of current waveform
J	Number to identify photograph (data set for sub-run)
L	Number of first current peak entered as data
N	Number of last current peak entered as data
RE	Effective extraneous circuit resistance from peak I to peak I+3 for SB # J
T	Period of discharge circuit with shorting bar
VARA	Estimated reading variance of photograph measurements
VARC	Estimated variance of capacitance
VARD	Estimated variance of DN
VARR	Estimated variance of RE
VART	Estimated variance of period of discharge circuit
VARV	Estimated variance of static voltmeter measurements
VO	Initial charging voltage on capacitor bank

REMAINING CARDS FOR EACH SUB-RUN: FORMAT(8F10.0)

A(I): Measured vertical position of I^{th} current peak as measured by the traveling microscope. (Data for multiple sub-runs were fed in order with one set of cards for each of the sub-runs.)

The output of the program is set up for printed form. Values printed were: RE, DEVR, VARR, DN, DEVD, VARD, AMIC, DEVM, APH, and DEVP. Some of these values were used for further calculations as described in Appendix A.


```

C      THIS PROGRAM COMPUTES THE CURRENT CALIBRATION OF THE CURRENT
C      MEASURING NETWORK AND THE RESISTANCE OF AN UNDERDAMPED
C      PLC NETWORK
      MON$1      JOB CURCAL
      MON$5      COMT OLIVER BLOCK,NUC. ENCL. 15 MIN., 10 PAGES
      MON$5      ASGN MJR. 12
      MON$1      ASGN MGC, 16
      MON$5      MODE GC, TEST
      MON$5      EXEC FORTRAN,,,,,,CURCAL
      DIMENSION A(20)
90  FORMAT(8F10.0)
91  FORMAT(2I2)
99  FORMAT(1HL,10X,32HSHORTING BAR CURRENT CALIBRATION,10X,
      219HPHOTO. NUMREP SB,I2)
100 FORMAT(1HK,I2,5X,22HRESISTANCE OF CIRCUIT=,F12.7,5X,4HDEV=,
      2F12.8,5X,4HVAR=,F12.8)
101 FORMAT(1X,I2,6X,21HPEAK TO PEAK CURRENT=,F12.7,5X,4HDEV=,F12.8,
      25X,4HVAR=,F12.8)
102 FORMAT(1X,I2,27HCURRENT PER MICRO DIVISION=,F12.7,5X,4HDEV=,F12.8)
103 FORMAT(1X,I2,27HCURRENT PER PHOTO DIVISION=,F12.7,5X,4HDEV=,F12.8)
      READ(1,90) T,C,VC,VART,VARC,VARV,VARA,F
      DO10J=1,100
      READ(1,91) L,N
      READ(1,90)(A(I),I=L,N)
      NM=N-2
      PI=3.1415926536
      PS=PI*PI
      DO10I=L,NM
      I1=I+1
      I2=I+2
      I3=I+3
      XNUM=A(I)-A(I1)
      XDEN=A(I2)-A(I3)
      X=XNUM/XDEN
      XX=ALOG(X)
      RE=(T*XX)/(2.*PS*C)
      VARX=(VARA+(X*X*VARA))/(XDEN*XDEN)
      VARR=((VARC/(C*C))+(VART/(T*T))+(VARX/(XX*XX*XX)))*(PE*RE)
      DEVV=SQRT(VARR)
      VK=2.*PI*VC*C/T
      XI=I
      PA=-((XI/2.0)-.25)
      PE=X**PA
      PC=X***(PA-0.5)
      PD=X***(PA-1.0)
      PE=X***(PA-1.5)
      DN=XV*(PS+PC)
      VARK=((4.*PS*C*VARV)/(T*T))+((4.*PS*VC*VC*VARC)/(T*T))
      2+((4.*PS*VU*VC*C*VART)/(T*4.))

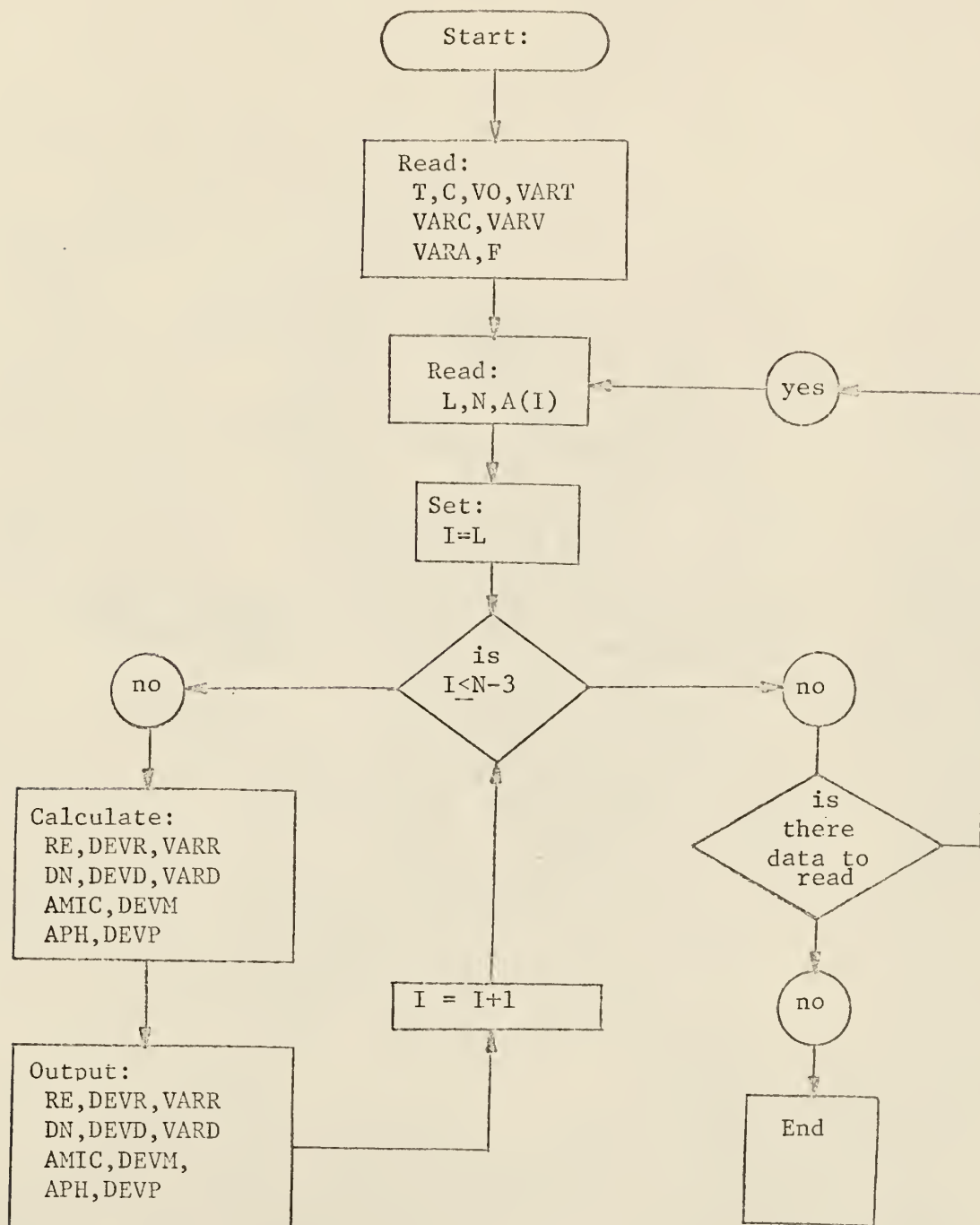
```

```

VARD=(VARK*(PD+PC)*(PD+PC))+(VARXXX*XX*((PA*PD)+((PA-0.5)*PF))
2*((PA*PD)+((PA-0.5)*PF)))
AMIC=DI/XNUM
APH=AMIC*F
DEVQ=SQRT(VARD)
DEVW=DEVQ/XNUM
DEVP=DEVW*F
WRITE(3,99)J
WRITE(3,100)I,RE,DEVP,VARR
WRITE(3,101)I,DN,DEVQ,VARD
WRITE(3,102)I,AMIC,DEVW
WRITE(3,103)I,APH,DEVP
10 CONTINUE
STOP
END
MON$1      EXEC LINKLOAD
            CALL CURCAL
MON$1      EXEC CURCAL,MJR
MON$1      JOB ACT$SOLIVER BLOCK          NUC ENGG 0237C40412

```

Figure 38. Logic diagram for extraneous circuit resistance and current calibration computer program.



APPENDIX D

Description and Explanation of IBM-1410 Computer Program for
Calibration of the Current Derivative Measuring Circuit

This computer program was written to calibrate the current derivative measuring circuit. The experimental procedure used to obtain the data is discussed in Section 4.2, and the equations used in the calculations are discussed in Appendix A. Equations used in the calculations include; (A-24), (A-25), and the propagation of variance formula. These equations were programmed in FORTRAN IV language for the IBM-1410 computer. The source program is listed and the logic diagram is shown in this appendix. Table D-1 defines important symbols used in the program.

The program described in this appendix and the program described in Appendix C have nearly the same form; the main difference is the interchange of statements so that equations for the current derivative calibration are used in this program and equations for the current calibration and extraneous circuit resistance are used in the program described in Appendix C. (Note also that the program described in this appendix included the calculation of the weighted average, equation (A-26), for each oscilloscope trace. The weighted average was calculated using a hand calculator for the current calibration.)

The input to the program was arranged as follows:

FIRST CARD: FORMAT(8F10.0)

1) T: Period of oscillation, 2) C: Capacitance of
capacitor bank, 3) V0: Initial charging voltage on capacitor bank, 4) VART: Estimated variance of measured period,

Table D-1: Symbols used in the IBM-1410 computer program for calculating the calibration of the current derivative measuring circuit.

Symbol	Explanation
A(I)	Vertical position of I^{th} current derivative peak as measured by the traveling microscope
AMIC	Current derivative per microscope division
APH	Current derivative per photo division
B	Weighted average of current derivative per photo division as calculated from Equation (A-26) for each trace
BB	Estimated standard deviation of B which was calculated using the propagation of variance formula
C	Capacitance of capacitor bank
DEVD	Estimated standard deviation of DN
DEVM	Estimated standard deviation of AMIC
DEVP	Estimated standard deviation of APH
DN	Difference in value of current derivative between peaks I and I+1
F	Conversion factor (.363 microscope divisions per photo division)
I	Number to identify peaks of current derivative waveform
J	Number to identify photograph (data set for sub-run)
L	Number of first current derivative peak entered as data
N	Number of last current derivative peak entered as data
T	Period of discharge circuit with shorting bar
VARA	Reading variance of photograph measurements
VARC	Estimated variance of capacitance
VARD	Estimated variance of DN
VART	Estimated variance of period of discharge circuit
VARV	Estimated variance of static voltmeter measurements
VO	Initial charging voltage on capacitor bank

5) VARC: Estimated variance of measured capacitance, 6) VARV: Estimated variance of static voltmeter measurements, 7) VARA: Estimated reading variance of photograph measurements, and 8) F: Conversion factor from measuring units to photograph units.

CARDS USED FOR SUB-RUNS

INITIAL CARD FOR EACH SUB-RUN: FORMAT(2I2)

1) L: Number of first current derivative peak entered as data, and 2) N: Number of last current derivative peak entered as data.

REMAINING CARDS FOR EACH SUB-RUN: FORMAT(8F10.0)

A(I): Measured vertical position of I^{th} current derivative peak as measured by the traveling microscope. (Data for multiple sub-runs were fed in order with one set of cards for each of the sub-runs.)

The output of the program is set up for printed form.

Values printed were: DN, DEVD, VARD, AMIC, DEVM, APH, DEVP, B, AND BB. Some of these values were used for further calculations as described in Appendix A.


```

C      THIS PROGRAM COMPUTES THE CURRENT DERIVATIVE CALIBRATION OF THE
C      CURRENT DERIVATIVE MEASURING NETWORK
MON1$      JOB CURCAL DERIVATIVE
MON1$      CONT OLIVER BLOCK, MDC.ENG0.15XIN0.,10PAGES
MON1$      ASGN MJR,12
MON1$      ASGN MGO,16
MON1$      MODE GO,TEST
MON1$      EXEQ FORTRAN,.,.,.,.,CURCAL
      DIMENSION A(20)
80 FORMAT(8F10.0)
91 FORMAT(2I2)
99 FORMAT(1HL,10X,57HSHORTING BAR CURRENT DERIVATIVE CALIBRATION (AMP
2/SEC*G-9),10X,19HPHOTO. NUMBER DI,13)
101 FORMAT(1X,12,6X,32HPEAK TO PEAK CURRENT DERIVATIVE=,F12.7,5X,4HDEV
2=,F12.8,5X,4HVAR=,F12.8)
102 FORMAT(1X,12,38HCURRENT DERIVATIVE PER MICRO DIVISION=,F12.7,5X,4H
2DEV=,F12.8)
103 FORMAT(1X,12,38HCURRENT DERIVATIVE PER PHOTO DIVISION=,F12.7,5X,4H
2DEV=,F12.8)
104 FORMAT(18H WEIGHTED AVERAGE=,F12.7,5X,4HDEV=,F12.8)
      READ(1,20) T,C,VO,VART,VARC,VARV,VARA,F
      DO10 J=32,48
      R=0.0
      BR=0.0
      READ(1,91) L,N
      READ(1,91) (A(I),I=L,N)
      NM=N-2
      PI=3.1415926536
      PS=PI*PI
      DO11 I=1,NM
      I1=I+1
      I2=I+2
      I3=I+3
      XNUM=A(I)-A(I1)
      XDEN=A(I2)-A(I3)
      X=XNUM/XDEN
      VARX=(VARA+(X*X*VARA))/(XDEN*XDEN)
      XK=4.*PS*C*VO/(T*T)
      XI=I
      PA=-((XI/2.)-.5)
      PR=X**PA
      PC=X***(PA-0.5)
      PD=X***(PA-1.0)
      PE=X***(PA-1.5)
      DM=XK*(PR+PC)
      VARX=X.*XK*XK*VART/(T*T)+XK*XK*VARC/(C*C)+XK*XK*VARV/(VO*VO)
      VARD=(VARX*(PR+PC)*(PR+PC))+(VARX*XK*XK*((PA*PD)+((PA-0.5)*PE))
2*((PA*PD)+((PA-0.5)*PE)))
      AMIC=DM/XNUM
      APH=AMIC*F

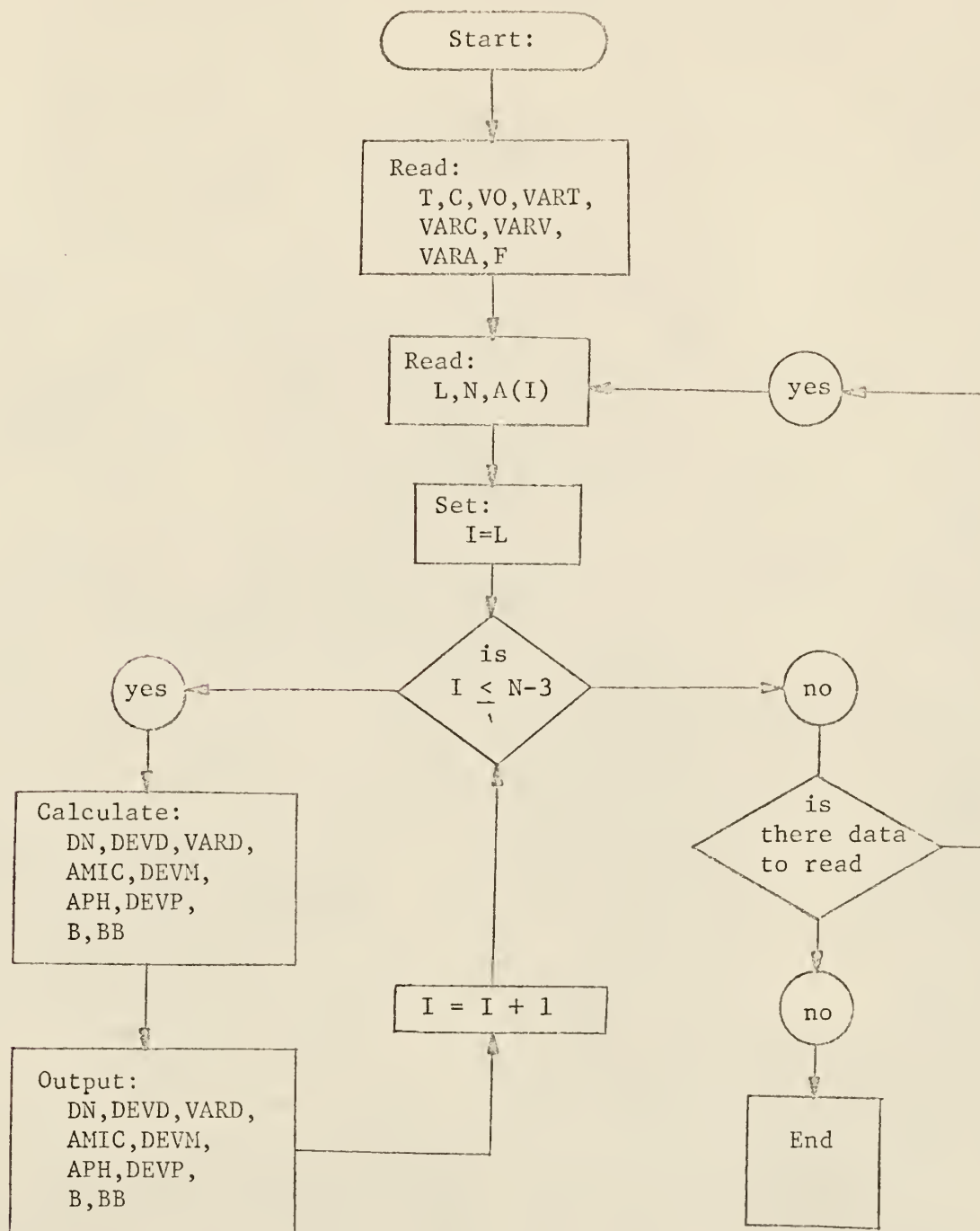
```

```

DEVD=SQRT(VARD)
DEVM=DEVD/YNUM
DEVP=DEVM*F
Z=Z+ABS(APH/(DEVP*DEVP))
ZZ=ZZ+(1./(DEVP*DEVP))
B=Z/ZZ
BH=SQRT(1./ZZ)
WRITE(3,99)J
WRITE(3,101)I,DN,DEVD,VARD
WRITE(3,102)I,AMIC,DEVM
WRITE(3,103)I,APH,DEVP
WRITE(3,104)B,BH
10 CONTINUE
STOP
END
MON$S - EXEC LINKLOAD
        CALL CURCAL
MON$S  EXEC CURCAL,MJR
MON$S  JOB ACT$SOLIVER BLOCK          NUC INGO 0237C40412

```

Figure 39. Logic diagram for current derivative calibration computer program.



APPENDIX E

Description and Explanation of IBM 360/50 Computer Program for Calculating Physical Quantities Associated with an Exploding Wire

This program was written to calculate the resistance of an exploding wire, the power input to an exploding wire, the energy deposited in an exploding wire, the action integral of an exploding wire, the voltage across an exploding wire, and the current through an exploding wire. Measured distances on photographic records of voltage, current, and current derivative curves versus time were used as data for the calculations. The theoretical equations used in the calculations were discussed in Section 3.0 with the exception of the action integral. The action integral, defined as the integral of the current squared over the time interval of interest, has been used in correlating results in exploding wire studies.¹⁹ However, in this study the current was not uniquely determined during the initial portion of the wire explosion; thus the action integral did not give meaningful results. The equations used for the calculations were algebraic except for the calculation of the energy deposited and the action integral. Simpson's rule was used for the numerical integrations and the estimated integration error was estimated as discussed in Section 5.2.

The propagation of variance formula (equation A-7) was applied (to equations used to calculate the resistance and power) to obtain an estimate of the variance of the resistance and power due to propagation of variance in the experimentally determined quantities (voltage, current, and current derivative). The propagation of variance formula was applied to the summation of terms in the numerical integration by Simpson's rule

to determine the variance of energy and action due to the propagation of variance of the experimentally measured quantities.

These equations were programmed in FORTRAN IV language for the IBM 360/50 computer. The source program is listed and the logic diagram is shown in this appendix. Table E-1 defines important symbols used in the program.

The input to the computer program was arranged as follows:

FIRST CARD: FORMAT(5I2)

1) N: Number of horizontal positions entered (must be odd integer), 2) IA: Month of year, 3) IB: Date of month, 4) IC: Photograph number, and 5) ID: Trace number.

(IA, IB, IC, and ID were used to identify data and relate data to photographs and results.)

VOLTAGE DATA: FORMAT(8F10.0)

V(J): Voltage parameter data which were entered as the vertical position of the voltage curve as measured by the traveling microscope. Data were read in eight values per card for values of $J = 1, 2, \dots, N$.

CURRENT DATA: FORMAT(8F10.0)

A(J): Current parameter data which were entered as the vertical position of the current curve as measured by the traveling microscope. Data were read in eight values per card for values of $J = 1, 2, \dots, N$.

CURRENT DERIVATIVE DATA: FORMAT(8F10.0)

Y(J): Current derivative parameter data which were entered as the vertical position of the current derivative curve as measured by the traveling microscope. Data were read in eight values per card

Table E-1: Symbols used in the IBM 360/50 computer program for calculating physical quantities associated with an exploding wire.

Symbol	Explanation
AA	Vertical position of current zero line reference
ACON	Conversion factor on oscilloscope record of current curve (kA/photo division)
ACZERO	Action integral from initiation of discharge to TZERO
A(J)	Value associated with current at horizontal position J
AMAX	Estimated maximum action (Used in scaling for PLOT)
CMAX	Estimated maximum current (Used in scaling for PLOT)
CONF	Conversion factor (.363 microscope divisions/photo division)
DELT	Horizontal distance between successive points measured on photograph (inches)
DEVA(J)	Estimated standard deviation of current at J th horizontal position
DEVV(J)	Estimated standard deviation of voltage at J th horizontal position
EMAX	Estimated maximum energy (Used in scaling for PLOT)
ERROR	Estimated integration error (See Section 5.2)
EZERO	Energy deposited from initiation of discharge to TZERO
IA, IB, IC, ID }	Numbers to identify data and relate to photograph and results
J	Number used to designate horizontal position at which curves were measured
N	Number of horizontal positions used to measure vertical positions of voltage, current, and current derivative curves
PMAX	Estimated maximum power (Used in scaling for PLOT)
RMAX	Estimated maximum resistance (Used in scaling for PLOT)
TCON	Conversion factor of horizontal scale of oscilloscope record (μ sec/ photo division)

Table E-1: Symbols used in IBM 360/50 computer program for calculating physical quantities associated with an exploding wire (continued)

Symbol	Explanation
TMAX	Estimated maximum time (Used in scaling for PLOT)
TZERO	Time after initiation of discharge for initial data point T(1)
VCON	Conversion factor on oscilloscope record of voltage curve (kV/photo division)
V(J)	Value associated with voltage at horizontal position J
VMAX	Estimated maximum voltage (Used in scaling for PLOT)
VV	Vertical position of voltage zeroline reference
WL	Inductance of wire (microhenries)
YCON	Conversion factor on oscilloscope record of current derivative curve (kA/ μ sec/photo division)
Y(J)	Value associated with current derivative at horizontal position J
YY	Vertical position of current derivative zeroline reference

for values of $J = 1, 2, \dots, N$.

CONVERSION FACTORS DATA: FORMAT(8F10.0)

1) DELT: Horizontal distance between successive data points measured with the traveling microscope, 2) TCON: Conversion factor of horizontal scale of oscilloscope record, 3) VCON: Conversion factor of vertical scale of voltage curve, 4) ACON: Conversion factor of vertical scale of current curve, 5) CONF: Conversion factor from microscope divisions to photograph divisions, 6) AA: Vertical position of current zeroline reference, 7) VV: Vertical position of voltage zeroline reference, 8) YY: Vertical position of current derivative zeroline reference, 9) WL: Inductance of the wire, and 10) YCON: Conversion factor of vertical scale of current derivative curve. Data were read in with eight values on the first card after the current derivative data and two values on the second card after the current derivative data.)

REFERENCE POSITION OF INITIAL DATA POINT: FORMAT(8F10.0)

1) TZERO: Time after initiation of discharge for initial data point, 2) EZERO: Energy deposited from initiation of discharge to TZERO, and 3) ACZERO: Action integral from initiation of discharge to TZERO.

SCALE FACTORS FOR SUBROUTINE PLOT: FORMAT(8F10.0)

1) TMAX: Estimated maximum value of time - used to scale horizontal axis of plots, 2) RMAX: Estimated maximum value of resistance calculated - used to scale vertical axis of resistance versus time plot, 3) PMAX: Estimated maximum value of power, 4) EMAX: Estimated maximum value of energy, 5) AMAX: Estimated maximum

value of action, 6) VMAX: Estimated maximum value of voltage, and 7) CMAX: Estimated maximum value of current.

TITLE AND AXIS LABELS FOR SUBROUTINE PLOT:

CARD 1: Title card for graphs, and CARDS 2-7: Axis label cards for vertical and horizontal axis. The horizontal axis for each plot was time. The vertical axis were in the following order: resistance, power, energy, action, voltage, and current. More detailed information of the content of title and axis label cards can be found with write up for subroutine PLOT.⁴⁴

The output of the program was obtained both in printed form and graphs. The subroutine PLOT, available for use with the 360/50 computer, was used to plot the results in graphical form. The printed form for resistance, power, and energy was arranged in columns as follows: J, T(J), physical quantity (neglecting the induced voltage across wire), estimated standard deviation, estimated deviation due to measurement of the photographs, and corrected physical quantity (corrected to include the induced voltage drop across the wire). The printed form of the action integral was as follows: J, T(J), action, estimated standard deviation, and estimated standard deviation due to measurement of the photographs. The printed form of the voltage and current was arranged as follows: T, T(J), voltage or current, and estimated standard deviation. The printed values of resistance, power, energy, voltage, and current as functions of time were used to plot the results shown in Figs. 8-33.

```

C      THIS PROGRAM COMPUTES FROM MEASUREMENTS ON PHOTOGRAPHS OF
C      EXPLODING WIRE DATA THE FOLLOWING: (1) RESISTANCE, (2) POWER,
C      (3) ENERGY, (4) ACTION, (5) VOLTAGE, (6) CURRENT.
//HREF=      (JOB)=35404120002,13,14,0*,FLOCK,ASGLVE=1
//          EXEC FTGCLGKS
//EORT,SYSIN DD *
      DIMENSION V(100),A(100),T(100),DEVA(100),DEVV(100)
      DIMENSION X(100),VAR(100),DEV(100),Y(100),RDEV(100)
80 FORMAT(8F10.0)
91 FORMAT(5I2)
101 FORMAT(1H1,15X,40HCURRENT THROUGH WIRE AS FUNCTION OF TIME,5X,I2,1
2H-,I2,1H-,I2,1H-,I2)
102 FORMAT(1H1,15X,39HVOLTAGE ACROSS WIRE AS FUNCTION OF TIME,5X,I2,1H
2H-,I2,1H,I2,1H-,I2)
103 FORMAT(1H1,15X,35HAIRE RESISTANCE AS FUNCTION OF TIME,5X,I2,1H-,I2
2,1H-,I2,1H-,I2)
104 FORMAT(1H1,15X,44HENERGY DEPOSITED IN WIRE AS FUNCTION OF TIME,5X,
2I2,1H-,I2,1H-,I2,1H-,I2)
105 FORMAT(1H1,15X,35HACTION INTEGRAL AS FUNCTION OF TIME,5X,I2,1H-,I2
2,1H-,I2,1H-,I2)
106 FORMAT(2HLJ,5X,14HTIME(MICROSEC),5X,16HRESISTANCE(OHMS),5X,9HDEVIAT
ION,5X,8HREAD DEV,5X,21HRESISTANCE(CORRECTED))
107 FORMAT(2HLJ,5X,14HTIME(MICROSEC),5X,16HENERGY(JOULES),5X,9HDEVIAT
ION,5X,8HREAD DEV,5X,17HENERGY(CORRECTED))
108 FORMAT(2HLJ,5X,14HTIME(MICROSEC),5X,16HACTION(COUL-AMP),5X,9HDEVIAT
ION,5X,8HREAD DEV)
109 FORMAT(1H,14,4X,F10.5,8X,F14.6,4X,F12.8,4X,F12.8)
110 FORMAT(1H,14,4X,F10.5,8X,F14.6,4X,F12.8,4X,F12.8,4X,F14.6)
111 FORMAT(1H1,15X,25HPOWER AS FUNCTION OF TIME,5X,I2,1H-,I2,1H-,I2,1H
2H-,I2)
112 FORMAT(2HLJ,5X,14HTIME(MICROSEC),5X,21HPOWER(MECAJOULES/SEC),3X,9H
2DEVIATION,5X,8HREAD DEV,5X,16HPOWER(CORRECTED))
113 FORMAT(2HLJ,5X,14HTIME(MICROSEC),5X,15HVOLTAGE(KVOLTS),5X,9HDEVIAT
ION)
114 FORMAT(1H,14,F10.5,8X,F14.6,4X,F12.8)
115 FORMAT(2HLJ,5X,14HTIME(MICROSEC),7X,14HCURRENT(KANPS),5X,9HDEVIAT
ION)
116 FORMAT(7,18HINTEGRATION ERROR=F14.8)
      DO30K=1,100
      READ(1,91)N,IA,IR,IC,ID
      READ(1,90)(V(J),J=1,N)
      READ(1,90)(A(J),J=1,N)
      READ(1,90)(Y(J),J=1,N)
      READ(1,90)DELT,TCOM,VCOM,ACOM,CONF,AA,VV,YY,PL,YCOM
      READ(1,90)TZERO,EZERO,ACZERO
      READ(1,90)TMAX,RMAX,PVMAX,EMAX,IMAX,VMAX,CMAX
      WRITE(2,103)IA,IR,IC,ID
      WRITE(3,106)

```

```

NN=N-1
RVARV= .0049* .0049*VCON*VCON/(CONF*CONF)
RVARA= .0049* .0049*ACON*ACON/(CONF*CONF)
DELT=(DELT*TCOM)/CONF
DO10J=1,N
XJ=J-1
T(J)=DELT*XJ+ZERO
TP(J)=T(J)
A(J)=ABS((AA-A(J))*ACON/CONF)
Y(J)=ABS(((VV-V(J))*VCON-(YY-Y(J))*YCON*PL)/(CONF*A(J)))
YP(J)=Y(J)
V(J)=ABS((VV-V(J))*VCON/CONF)
DEVV(J)=.0049*VCON/CONF
DEVA(J)=SQRT(.0049*.0049*ACON*ACON/(CONF*CONF)+.0332*.0332*A(J)*A(
2J))
X(J)=V(J)/A(J)
RDEV(J)=SQRT((RVARV+(RVARA*V(J)*V(J))/(A(J)*A(J)))/(A(J)*A(J)))
VAR(J)=(DEVV(J)*DEVV(J)+(DEVA(J)*DEVA(J)*V(J)*V(J))/(A(J)*A(J)))/(
1A(J)*A(J))
10 DEV(J)=SQRT(VAR(J))
TPMAX=TPMAX
WRITE(3,111)(J,T(J),X(J),DEV(J),RDEV(J),Y(J),J=1,N)
CALL PLOT(TP,1.,TPMAX,0,YP,1.,RMAX,0,0.,0.,0.,0,N,1,2,0)
WRITE(3,111)IA,IP,IC,ID
WRITE(3,112)
DO13J=1,N
TP(J)=T(J)
X(J)=A(J)*V(J)
RDEV(J)=SQRT(RVARV*A(J)*A(J)+RVARA*V(J)*V(J))
VAR(J)=DEVV(J)*DEVV(J)*A(J)*A(J)+DEVA(J)*DEVA(J)*V(J)*V(J)
DEV(J)=SQRT(VAR(J))
Y(J)=V(J)*A(J)*A(J)
YP(J)=Y(J)
12 CONTINUE
TPMAX=TPMAX
WRITE(3,111)(J,T(J),X(J),DEV(J),RDEV(J),Y(J),J=1,N)
CALL PLOT(TP,1.,TPMAX,0,YP,1.,RMAX,0,0.,0.,0.,0,N,1,2,0)
WRITE(3,114)IA,IP,IC,ID
WRITE(3,107)
X(1)=ZERO
RVARV=-(2.*DELT*DELT/9.)*(A(1)*A(1)*RVARV+V(1)*V(1)*RVARA)
VAR(1)=-(2.*DELT*DELT/9.)*(A(1)*A(1)*DEVV(1)*DEVV(1)+V(1)*V(1)*DEV
1A(1)*DEVA(1))
ERROR=(4.*(Y(1)-Y(N))+(Y(2)+Y(N)))*(DELT/90.)
NPTS=(N-1)/2
DO11J=3,N,2
JJ=J-1
JJJ=J-2
JP=(J-1)/2
ERROR=ERROR+(8.*DELT/90.)*(Y(J)-Y(JJ))

```

```

Y(J)=(DELT/3.)*(A(JJJ)*V(JJJ)+4.*A(JJ)*V(JJ)+A(J)*V(J))+X(JJJ)
Y(J)=Y(J)-(0.5*PI*A(J)*A(J))
YP(JP)=Y(J)
TP(JP)=T(J)
RDEV(J)=SQRT((DELT*DELT/9.)*((3.*A(JJJ)*A(JJJ)*RVARV+3.*V(JJJ)*V(J
JJ)*RVARA)+(16.*A(JJ)*A(JJ)*RVARV+16.*V(JJ)*V(JJ)*RVARA)+(A(J)*A(J
3)*RVARV+V(J)*V(J)*RVARA))+RVAR)
RRVAR=RDEV(J)*RDEV(J)
VAR(J)=(DELT*DELT/9.)*((3.*A(JJJ)*A(JJJ)*DEVV(JJJ)*DEVV(JJJ)+3.*V(
1JJJ)*V(JJJ)*DEVA(JJJ)*DEVA(JJJ)+(16.*A(JJ)*A(JJ)*DEVV(JJ)*DEVV(JJ
2)+16.*V(JJ)*V(JJ)*DEVA(JJ)*DEVA(JJ)+(A(J)*A(J)*DEVV(J)*DEVV(J)+V(
3J)*V(J)*DEVA(J)*DEVA(J)))+VAR(JJJ)
11 DEV(J)=SQRT(VAR(J))
DO21J=3,N,2
WRITE(3,111)(J,T(J),X(J),DEV(J),RDEV(J),Y(J))
20 CONTINUE
WRITE(3,116)ERROR
TPMAX=TMAX
CALL PLOT(TP,.,TPMAX,0,YP,0.,EMAX,0.,0.,0.,0.,0,N,1,2,0)
WRITE(3,115)IA,IB,IC,ID
WRITE(3,108)
X(1)=ACZERO
NPTS=(N-1)/2
RRVAR=-(8.*DELT*DELT/9.)*A(1)*A(1)*RVARA)
VAR(1)=-(8.*DELT*DELT/9.)*(A(1)*A(1)*DEVA(1)*DEVA(1))
ERROR=(DELT/9.)*(4.*(A(1)-A(N))+A(2)+A(NN))
DO12J=3,N,2
JJ=J-1
JJJ=J-2
JP=(J-1)/2
TP(JP)=T(J)
ERROR=ERROR+(8.*DELT/90.)*(A(J)-A(JJ))
X(J)=(DELT/3.)*(A(JJJ)*A(JJJ)+4.*A(JJ)*A(JJ)+A(J)*A(J))+X(JJJ)
YP(JP)=X(J)
RDEV(J)=SQRT((4.*RVARA*DELT*DELT/9.)*(3.*A(JJJ)*A(JJJ)+16.*A(JJ)*A
2(JJ)+A(J)*A(J))+RRVAR)
RRVAR=RDEV(J)*RDEV(J)
VAR(J)=(4.*DELT*DELT/9.)*(2.*A(JJJ)*A(JJJ)*DEVA(JJJ)*DEVA(JJJ)+16.
1*A(JJ)*A(JJ)*DEVA(JJ)*DEVA(JJ)+A(J)*A(J)*DEVA(J)*DEVA(J))+VAR(JJJ)
12 DEV(J)=SQRT(VAR(J))
DO21J=3,N,2
WRITE(3,119)(J,T(J),X(J),DEV(J),RDEV(J))
21 CONTINUE
WRITE(3,116)ERROR
TPMAX=TMAX
CALL PLOT(TP,.,TPMAX,0,YP,0.,AMAX,0.,0.,0.,0.,0,NPTS,1,2,0)
WRITE(3,102)IA,IB,IC,ID
WRITE(3,113)

```



```

DO22J=1,N
22 TP(J)=T(J)
   TPVAX=TPVAX
   WRITE(3,114)(J,T(J),V(J),DEVV(J),J=1,N)
   CALL PLOT(TP,1,TPVAX,0,V,0,VMAX,0,0,1,0,0,N,1,2,0)
DO23J=1,N
23 TP(J)=T(J)
   TPVAX=TPVAX
   WRITE(3,111)IA,IB,IC,ID
   WRITE(3,115)
   WRITE(3,114)(J,T(J),A(J),DEVA(J),J=1,N)
   CALL PLOT(TP,1,TPVAX,0,A,0,CMAX,0,0,0,0,0,N,1,2,0)
20 CONTINUE
   STOP
   END

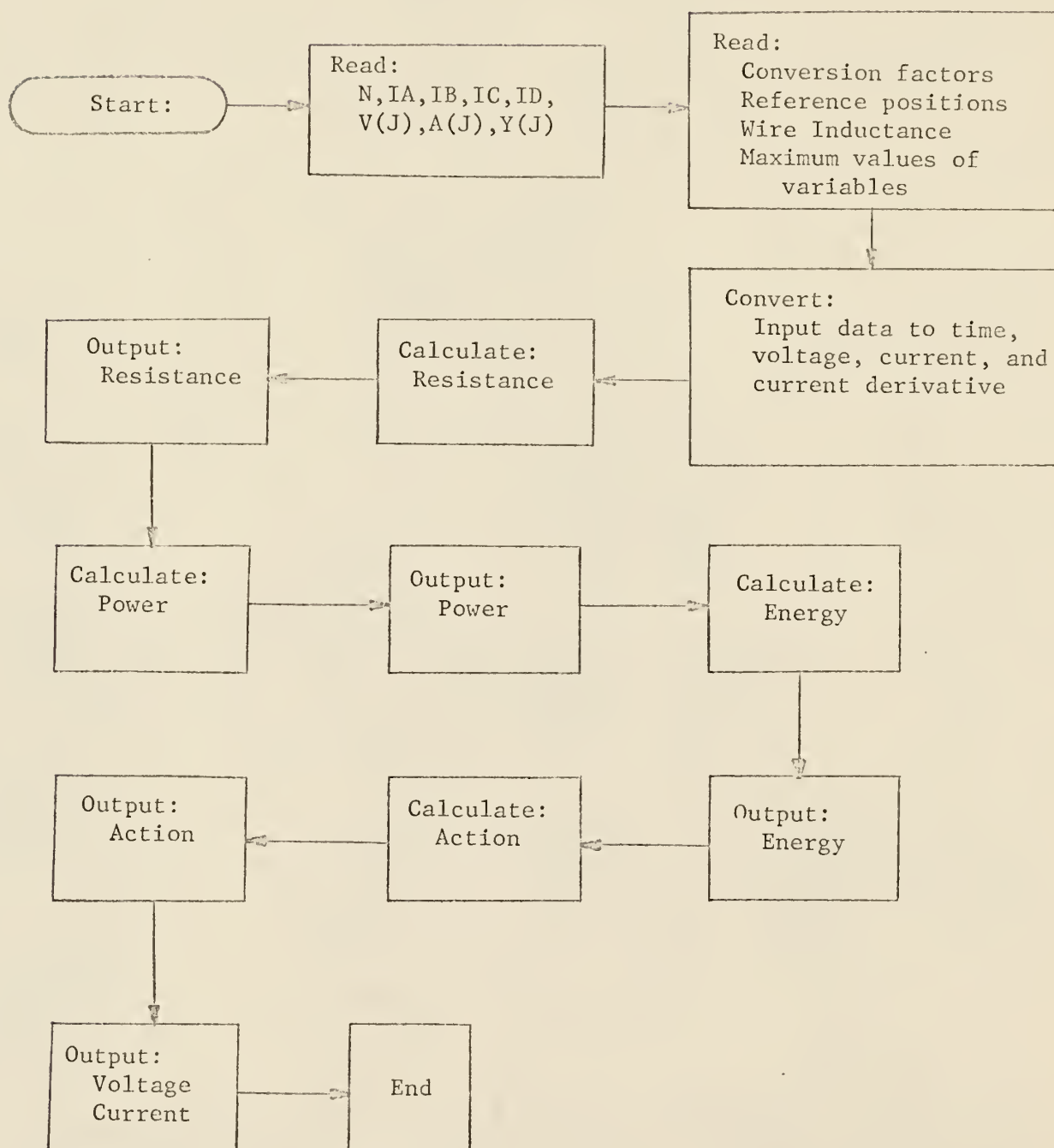
```

```

/*
//GC.SYSIN DD *

```

Figure 40. Logic diagram for physical quantities of an exploding wire computer program.



APPENDIX F

Energy Losses by Conduction and Convection from Exploding Wires

An upper limit of the heat losses by conduction and convection from an exploding wire can be obtained as described below. Since the wire length is much greater than the diameter, the heat losses through the ends may be neglected and the wire considered as an infinitely long cylinder. Assuming there is a step change in temperature from ambient conditions to the maximum temperature (T_{\max}) and further assuming the wire surface temperature (T_{∞}) is equal to the temperature of the ambient medium gives an upper limiting value for heat losses due to conduction and convection for the time interval from when the wire initially begins to be heated until the wire explosion.

The transient temperature distribution in the wire is obtained by solving the heat diffusion equation,

$$\left(\frac{\partial T}{\partial t} \right) = \alpha \nabla^2 T \quad (F-1)$$

where:

$T = T(r, t)$ is the time dependent temperature distribution,

α is the thermal diffusivity, and

r_0 is the initial wire radius;

with the boundary conditions

$$T(r, \infty) = T_{\infty},$$

$$T(r_0, t) = T_{\infty},$$

$$T(r, 0) = T_{\max}, \text{ and}$$

$$T(0, t) - \text{finite.}$$

Introducing a change of variables such that

$$\theta(r,t) = T(r,t) - T_{\infty}, \quad (F-2)$$

and substituting equation (F-2) into equation (F-1) gives

$$\frac{\partial \theta(r,t)}{\partial t} = \alpha \left[\frac{1}{r} \frac{\partial}{\partial r} \left(r \frac{\partial \theta}{\partial r} \right) \right]. \quad (F-3)$$

The boundary conditions are

$$\theta(r, \infty) = 0, \quad (F-3a)$$

$$\theta(r_0, t) = 0, \quad (F-3b)$$

$$\theta(r, 0) = T(r, 0) - T_{\infty} = \theta_0, \text{ and} \quad (F-3c)$$

$$\theta(0, t) = \text{finite}. \quad (F-3d)$$

Equation (F-3) can be solved by separation of variables using the substitution

$$\theta(r,t) = R(r)\tau(t). \quad (F-4)$$

Substituting equation (F-4) into equation (F-3) and separating the variables gives the following differential equations:

$$\frac{d\tau(t)}{dt} + \alpha\lambda^2\tau(t) = 0, \text{ and} \quad (F-5)$$

$$\frac{1}{r} \frac{\partial}{\partial r} \left[r \frac{\partial R(r)}{\partial r} \right] + \lambda^2 R(r) = 0. \quad (F-6)$$

Equation (F-6) is Bessel's equation of order zero with parameter λ .

With the boundary condition (F-3d) the solution of equation (F-6) is

$$R(r) = \sum_{n=1}^{\infty} b_n J_0(\lambda_n r) \quad (F-7)$$

where:

$J_0(\lambda_n r)$ is the Bessel function of the first kind of order zero.

The solution of equation (F-5) is

$$\tau(t) = a_n \exp(-\alpha \lambda_n^2 t) \quad (F-8)$$

where the boundary condition (F-3a) has been used. By substituting equation (F-7) and (F-8) into equation (F-4) gives

$$\theta(r,t) = \sum_{n=1}^{\infty} K_n \exp(-\alpha \lambda_n^2 t) J_0(\lambda_n r) \quad (F-9)$$

Applying boundary condition (F-3b) gives that λ_n is the n^{th} root of $J_0(\lambda_n r_o) = 0$. To evaluate the constants K_n the solution is written at time $t = 0$ (Using F-3c).

$$\theta(r,0) = \theta_o = \sum_{n=1}^{\infty} K_n J_0(\lambda_n r) \quad (F-10)$$

From the orthogonality relations the constants K_n are given by

$$K_n = \frac{2\theta_o}{\lambda_n r_o J_1(\lambda_n r_o)} \quad (F-11)$$

where $J_1(\lambda_n r_o)$ is the Bessel function of the first kind of order one.

The temperature distribution is given by

$$\theta(r,t) = \sum_{n=1}^{\infty} \left[\frac{2\theta_o}{\lambda_n r_o J_1(\lambda_n r_o)} \right] J_0(\lambda_n r) \exp(-\alpha \lambda_n^2 t) \quad (F-12)$$

The average temperature rise of the wire above ambient conditions at time t is given by

$$\bar{\theta}(t) = \frac{\int_0^{r_o} \theta(r,t) r dr}{\int_0^{r_o} r dr} \quad (F-13)$$

By substitution and integration we obtain

$$\bar{\theta}(t) = \sum_{n=1}^{\infty} \frac{4\theta_o}{\lambda_n^2 r_o^2} \exp(-\alpha \lambda_n^2 t) , \quad (F-14)$$

which is the average temperature rise above ambient conditions at time t .

The ratio of $\bar{\theta}(t)$ to θ_o gives an estimate of the maximum energy loss by conduction and convection at time t for an exploding wire. Representative values of $\bar{\theta}(t_m)/\theta_o$ are given in Table F-1, where t_m is the maximum time interval of interest during a wire explosion. For wires which exploded on the first current pulse, t_m was taken to be the time of burst. For wires which exploded on the second current pulse, t_m was taken to be the time from when the voltage crosses the zeroline to the time of burst.

Table F-1: Estimates of maximum energy losses from exploding wires by conduction and convection.

Wire Material	Wire Radius (in.)	α (in. ² /sec)	t_m (μ sec)	$\bar{\theta}(t_m)/\theta_o$
Aluminum	.0160	.232	10	.79
Copper	.005	.189	2.5	.71
Copper	.010	.189	3.0	.84
Iron	.007	.0328	2.5	.91

APPENDIX G

Skin Effect and Magnetic Pressure

Since the time to burst of an exploding wire is characterized by times in the microsecond range or less and by high currents which may change rapidly, the skin effect may be important and must be considered. The application of a step function increase in current to a cylindrical wire has been considered to obtain a measure of the transient skin effect.²⁷ The ratio of the current at the wire center to the steady state current (the current in the wire when a uniform density of current is reached) is given by

$$\phi = \frac{i_z(r=0)}{i_\infty} = 1 + \frac{\exp(-\alpha_n^2 t / r_0^2 \sigma \mu)}{J_0(\alpha_n)} \quad , \quad (G-1)$$

where:

α_n is the n^{th} root of $J_1(\alpha) = 0$,

σ is the electrical conductivity,

μ is the permeability ($4\pi \times 10^{-7}$ H/m), and

r_0 is the wire radius.

Equation (G-1) was used to calculate time intervals at which the skin effect would be important; the calculated results for wires of interest in this investigation are given in Table G-1. Time intervals longer than the reported values would have $\phi > .95$. Since the times to burst for wire explosions in this study were greater than the time intervals in Table G-1, consideration of the skin effect was not necessary in this study.

Table G-1: Time intervals at which the ratio of the current at a wire center to the steady state current equals .95 for wires used in this study.

Wire Material	Wire Radius (m x 10 ⁴)	σ (mho·m ⁻¹ x 10 ⁻⁷)	t (μsec)
Aluminum	4.06	3.8	2.09
Copper	1.27	5.8	.31
Copper	2.54	5.8	1.25
Iron	1.78	1.0	.11

At high current densities it is expected that magnetic pressure will have a significant effect on a wire explosion. If the self-magnetic field is to compress a wire without ejecting it from the circuit, it is necessary that the return current be symmetrical about the wire.¹⁶ Figure 41 shows an enlarged drawing of the sample cell used in this study. Since the return current was symmetrical about the wire the magnetic force was directed towards the center of the wire and the magnetic pressure would tend to confine the wire material.

When the current flowing in the wire is uniform throughout the wire, the forces on the moving charges result in a pressure distribution (dyne/cm²) through the cross section of the wire given by.⁴⁵

$$p(r) = \frac{I^2}{\pi c^2 r_o^2} \left(1 - \frac{r^2}{r_o^2} \right) \quad (G-2)$$

where:

I is the current flowing in the wire (statamps),

c is the velocity of light (cm/sec), and

r is the distance from the center of the wire to the point where the pressure is evaluated (cm).

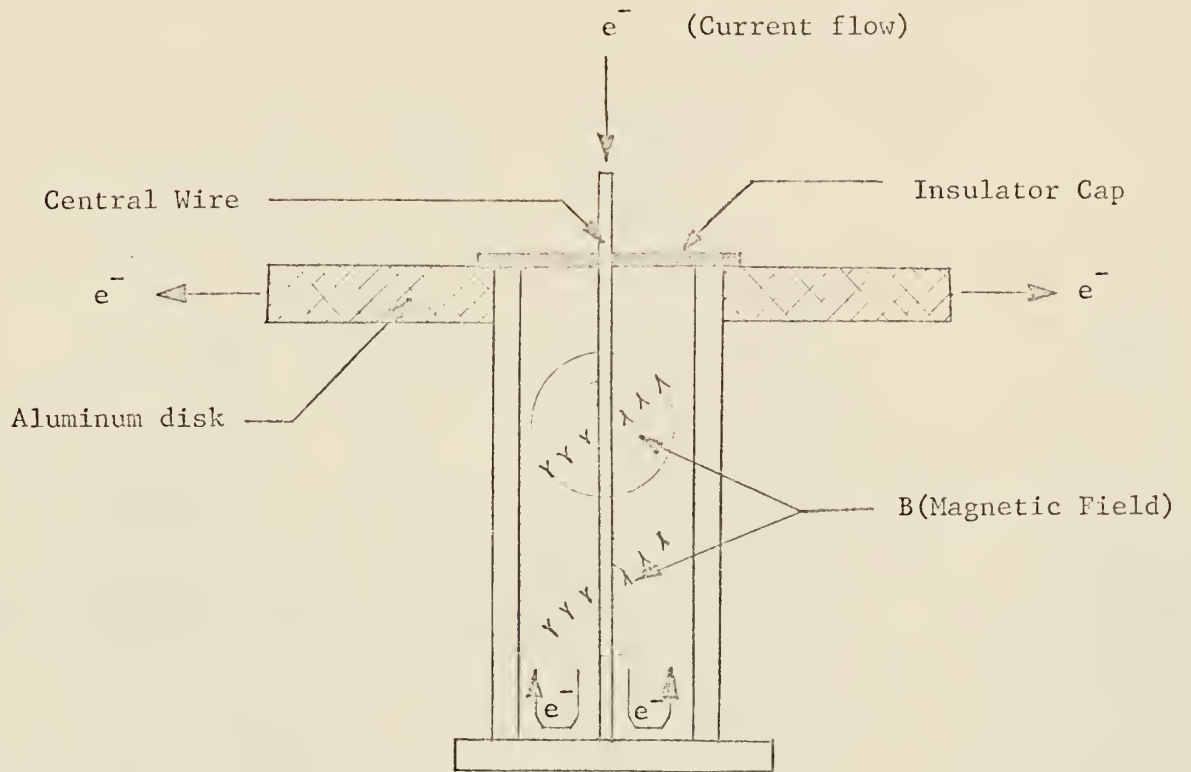


Figure 41. Sketch of Magnetic Pinch Sample Cell

If the current is limited to a very thin layer on the surface of the wire, i.e., skin effects dominate, the pressure is constant inside the cylinder and equal to⁴⁵

$$p = (I^2 / 2\pi r_o^2 c^2) . \quad (G-3)$$

Note that the pressure calculated by equation (G-3) is one half the pressure calculated for an axial position of the wire using equation (G-2).

Calculating the pressure for a 10 mil diameter wire ($r_o = 5$ mils) at the axial position using equation (G-2) gives the following results.

Current Density (A/cm ²)	Pressure (atm)
10^8	50,000
10^7	500
10^6	5

SIMULATION OF THE CHEMICAL ENVIRONMENT
OF A NUCLEAR EXPLOSION BY
EXPLODING WIRE TECHNIQUES

by

OLIVER ULFERT JOHN BLOCK
B.S., University of Nebraska 1965

AN ABSTRACT OF A MASTER'S THESIS

submitted in partial fulfillment of the
requirements for the degree

MASTER OF SCIENCE

Department of Nuclear Engineering
KANSAS STATE UNIVERSITY
Manhattan, Kansas

1969

Abstract

Exploding wire experimental results are given in terms of voltage, current, resistance, power, and deposited energy as a function of time after the initiation of an explosion. Voltage and current measurements were made for wires at atmospheric conditions as well as wires exploded in a sample cell; this cell tended to confine the wire material and to increase energy deposit by employing the magnetic pinch principle. Circuit parameters varied included capacitance (4 and 8 microfarad capacitor banks were used), and charging voltage (8, 11, and 15 kilovolt charging voltages were studied). Wire parameters varied included wire material (aluminum, copper, iron, and nickel-chromium wires were exploded), wire diameter (10-32 mil diameters were used), and wire length (1/2 - 3 inch wires were studied). Experimental results show that rapid matching of wire parameters to circuit parameters (to obtain the most energetic wire explosions) is possible knowing the qualitative effects of the wire parameters on the deposited energy. It has been shown experimentally that about six times the desired energy deposit must actually be stored in the capacitor bank to produce the temperatures or energy densities predicted by the theoretical design method presented. Further work required to simulate the chemical environment of a nuclear explosion by exploding wire techniques is discussed.